

NANOCARBON BASED CHEMIRERESISTIVE WATER
QUALITY SENSORS

NANOCARBON BASED CHEMIRESENSITIVE WATER QUALITY SENSORS

By ANA ZUBIARRAIN LASERNA, B.Sc.

*A Thesis Submitted to the School of Graduate Studies in Partial
Fulfilment of the Requirements for the Degree of Master of Science in
Chemistry*

McMaster University

© Copyright by Ana Zubiarrain Laserna, August 2019

McMaster University

MASTER OF SCIENCE (2019)

Hamilton, Ontario (Chemistry & Chemical Biology)

TITLE: Nanocarbon Based Chemiresistive Water Quality Sensors

AUTHOR: Ana Zubiarrain Laserna, B.Sc. (University of the Basque Country)

SUPERVISOR: Dr. Peter Kruse

NUMBER OF PAGES: xvii, 114

ABSTRACT

Failure to monitor the quality of drinking water can have devastating consequences. The development and implementation of sensing technology can be a crucial aspect of water quality control strategies. Chemiresistive sensors can be installed at any point of the distribution system and can provide real-time data on the levels of different water quality parameters. These sensors work by detecting changes in the conducting properties of a transducing element, induced by interactions with the analyte. Nanocarbon films have attracted interest as possible transducing materials because of their similarities to graphene, a two-dimensional material known for its exceptional electron transport properties. This thesis explores the fabrication and sensing performance of few layer graphene (FLG) and graphene-like carbon (GLC) films. The FLG sensors were used to detect copper ions in water, while the GLC sensors were used to monitor the concentration of free chlorine. The films were functionalized to improve selectivity and showed noticeable changes in their conducting properties as a result of charge transfer between them and the analyte. These changes were quantified by probing the sensors with a constant voltage and they were found to be dependent on the concentration of the analyte over a wide dynamic range. Overall, the work presented in this thesis suggests that, by tuning the selectivity of the films, nanocarbon based chemiresistive sensors can be a universal solution to water quality monitoring.

ACKNOWLEDGEMENTS

First and foremost, I would like to thank Dr. Peter Kruse for giving me the opportunity to pursue research under his supervision. I am grateful for his guidance, patience, and dedication. I would also like to thank Dr. Ravi Selvaganapathy for his advice on the engineering aspects of the project, Dr. David Emslie for his input on strategies for the functionalization of the sensors, Dr. Ranjith Divigalpitiya and 3M for providing me with graphene-like carbon, and Dr. Mark Biesinger for performing the XPS analysis of my samples. I would like to recognize Chris Butcher at the CCEM for training me on how to use the FESEM, the Adronov Group for letting me use some of their equipment (especially James Bodnaryk for teaching me how to use it), and Karen Newmann and Trisha Martin for letting me borrow chemicals and equipment. Finally, I would like to show my appreciation to every staff member at the Chem Office for their help and to Dr. Randall Dumont for being the Chair at my defence.

I would like to acknowledge my fellow lab members for making long days of research go by a little bit faster. Special thanks go to Amir and Dipankar, who put up with me when I was the only other person in the lab. I am grateful for the graduate community at the Chemistry Department, I will miss Yummy Wednesdays. I would also like to thank my housemates at #38 for making the house feel like home, and the great community at Alchemy CrossFit, who has kept me sane throughout these years.

Last but not least, I would like to thank each and every member of my family. Thank you all for your unconditional love and support. But special thanks to my mom. These years have been really hard at times, but you helped me make it through. Thank you for your endless patience. Thank you for always being on the other end of the phone. Thank you for jumping on a plane without hesitation. Thank you.

TABLE OF CONTENTS

CHAPTER 1 — INTRODUCTION	- 1 -
1.1. GLOBAL WATER SECURITY.....	- 1 -
1.2. WATER QUALITY PARAMETERS	- 3 -
1.3. CHEMIREISTIVE WATER QUALITY SENSORS	- 6 -
1.3.1. <i>Tuning analyte selectivity through film functionalization.....</i>	<i>- 6 -</i>
1.3.2. <i>Graphene-like transducing films.....</i>	<i>- 7 -</i>
1.4. MOTIVATION BEHIND THE PRESENTED WORK	- 10 -
1.4.1. <i>Quantification of copper(II) cations in water</i>	<i>- 11 -</i>
1.4.2. <i>Monitoring of free chlorine in water</i>	<i>- 13 -</i>
1.5. STRUCTURE OF THE THESIS.....	- 16 -
CHAPTER 2 — EXPERIMENTAL.....	- 17 -
2.1. FUNDAMENTALS OF THE EXPERIMENTAL TECHNIQUES	- 17 -
2.1.1. <i>Raman spectroscopy</i>	<i>- 17 -</i>
2.1.1.1. Interpretation of spectral features in graphene samples	- 19 -
2.1.2. <i>X-ray Photoelectron Spectroscopy and X-ray induced Auger Electron Spectroscopy^{133,134}</i>	<i>- 22 -</i>
2.1.3. <i>The DPD method</i>	<i>- 25 -</i>
2.1.4. <i>Chemiresistive sensor testing.....</i>	<i>- 26 -</i>
2.2. SENSOR FABRICATION	- 27 -
2.2.1. <i>SOP for the fabrication of carbon nanotube flow sensors</i>	<i>- 28 -</i>

2.2.1.1. Materials	- 28 -
2.2.1.2. List of precautions	- 29 -
2.2.1.3. Production of channels	- 30 -
2.2.1.4. Production of substrates.....	- 30 -
2.2.1.5. Sensor assembly.....	- 33 -
2.2.1.6. Waste disposal	- 34 -
2.2.2. <i>Choice of materials for the transducing film</i>	- 35 -
2.2.2.1. Exfoliated graphite	- 35 -
2.2.2.2. Graphene-like carbon	- 39 -
2.2.3. <i>Choice of substrate: glass slides or PET</i>	- 40 -
2.2.4. <i>Choice of sensor geometry: flow sensors or dip sensors</i>	- 42 -
2.3. ANALYTE STABILITY	- 43 -
2.3.1. <i>pH of the solutions</i>	- 43 -
2.3.2. <i>Free chlorine degradation</i>	- 45 -
2.4. SUMMARY	- 46 -
CHAPTER 3 — COPPER SENSORS	- 48 -
3.1. INTRODUCTION	- 48 -
3.2. EXPERIMENTAL DETAILS	- 48 -
3.2.1. <i>Data acquisition</i>	- 48 -
3.2.2. <i>Data quality</i>	- 49 -
3.2.3. <i>Immersion mode: static or stirring and minimum</i> <i>concentration</i>	- 50 -
3.3. COMPOSITION OF THE WATER.....	- 52 -

3.3.1. <i>NaCl to control the ionic strength</i>	- 53 -
3.3.2. <i>NaHCO₃ to control the pH</i>	- 55 -
3.4. INTERFERENCES	- 57 -
3.5. CALIBRATION CURVES.....	- 60 -
3.6. RESETTING	- 66 -
3.7. CHARACTERIZATION OF THE SENSORS USING XPS	- 69 -
3.8. SUMMARY	- 75 -
CHAPTER 4 — FREE CHLORINE SENSORS.....	- 77 -
4.1. INTRODUCTION	- 77 -
4.2. EXPERIMENTAL DETAILS	- 78 -
4.2.1. <i>Data acquisition</i>	- 78 -
4.2.2. <i>Data quality</i>	- 79 -
4.2.3. <i>Composition of the water</i>	- 80 -
4.2.4. <i>Determining the concentration of the solutions</i>	- 81 -
4.3. PERFORMANCE AT DIFFERENT CONCENTRATION RANGES.....	- 82 -
4.3.1. <i>Low range: detecting breaches in a chlorine filter</i>	- 83 -
4.3.2. <i>Middle range: detecting fluctuations in the concentration</i>	- 85 -
4.3.3. <i>High range: quantifying free chlorine in unknown samples</i>	- 86 -
4.4. INTERFERENCES	- 89 -
4.5. FOULING RESISTANCE	- 91 -
4.6. SUMMARY	- 93 -
CHAPTER 5 — CONCLUSION	- 94 -

5.1. SUMMARY	- 94 -
5.2. LESSONS LEARNT AS A CHEMISTRY GRADUATE STUDENT.....	- 96 -
5.3. FUTURE WORK	- 97 -

LIST OF FIGURES

Figure 1.1. Bernal (ABA) and rhombohedral (ABC) stacking of graphene layers.	10 -
Figure 2.1. Depiction of the different excitation-relaxation mechanisms that can happen during a Raman spectroscopy experiment.	18 -
Figure 2.2. a) Raman spectra of graphite and graphene. Reprinted with permission from Ref. [124] Copyright 2006 by The American Physical Society. b) Evolution of the Raman spectra of FLG as the number of layers increases. Reprinted with permission from Ref. [132] Copyright 2012 by WILEY-VCH. c) Raman spectrum of an exfoliated graphite transducing film. The peaks have been identified (the red colour indicates defects).	22 -
Figure 2.3. a) Simulation of the doublet arising from the spin-orbit coupling for Si 2p. b) Diagram of the electronic transitions involved in XPS and X-AES. The resulting peaks would be labeled as 1s (XPS) and KL_1L_2 (X-AES).	25 -
Figure 2.4. Reaction between free chlorine and DPD. The intensity of the colour is proportional to the concentration.	26 -
Figure 2.5. Second fraction in different alcohol-water mixtures (vials from left to right: ETA, IPA, TBA) sonicated for different lengths of time (pictures from left to right: 1 hour, 3 hours, 5 hours).	37 -
Figure 2.6. a – b) FESEM images of the FLG film at different magnifications: a) $\times 4,300$ and b) $\times 33,000$. c) Raman spectrum of the FLG film. The peaks labeled in black are characteristic of FLG, while the peaks labeled in red indicate the presence of defects.	38 -
Figure 2.7. Side-by-side comparison of the performance of two FLG sensors with different substrate materials: a) PET and b) glass slide.	41 -
Figure 2.8. Improvement in performance of a PET sensor after switching to silver contact reinforcements. a) PET sensor with silver contact reinforcements. b) Glass sensor with pencil contact reinforcements.	42 -
Figure 2.9. Sensing performance of two different sensing geometries: a) flow sensor and b) dip sensor. Insets: pictures of each type of device.	43 -

Figure 2.10. Long-term pH stability of ultrapure water when left in an open beaker. The temperature has no effect in the pH of the solution. - 45 -

Figure 2.11. Long term stability of the concentration of free chlorine solutions using **a)** dip sensors and **b)** flow sensors. The time and amount of PDMS in contact with the solution affects the degradation of the solutions. - 46 -

Figure 3.1. Doping-sensing sequence of a copper sensor (inset: structure of DAP). - 49 -

Figure 3.2. Effect of adding a 200 ppm NaCl background concentration on the resetting efficacy. **a)** Response of three sensors to 1 ppm of copper pre-reset and post-reset in the absence of NaCl (pink) and with 200 ppm of NaCl (green). **b)** Resetting efficacy given as the signal recovery (post-reset signal change to pre-reset signal change ratio). - 55 -

Figure 3.3. Interference study. **a)** Response of two doped dip sensors to the presence of cations commonly found in drinking water. The concentration of the cations is 50 ppm and copper is 100 ppb. All ions were added cumulatively. **b)** Response of three flow sensors to the presence of some cations and trace metals. The concentration of magnesium is 58 ppm, calcium is 96 ppm, and the trace metals including copper is 20 μ M (approximately 1 ppm). The devices were exposed to each ion in sequence. Sensors G2 and G3 were run as blanks while G10 was functionalized. The solutions contained no NaHCO_3 or NaCl background. - 59 -

Figure 3.4. Calibration curves obtained with the copper sensors. Sensors G49, G50, and G51 were doped with DAP while G52 was run blank. **a)** Raw data collected with sensor G49. **b)** Curve fittings: Langmuir adsorption isotherm, Freundlich adsorption isotherm, and exponential decay. - 61 -

Figure 3.5. Linearized Langmuir adsorption isotherms of the copper sensors. - 65 -

Figure 3.6. Reset-sense cycles. **a)** Raw data from two reset-sense cycles, the first one at pH 3 and the second one at pH 7.5. **b)** Resetting efficacy on four sensors given as the signal recovery (post-reset signal change to pre-reset signal change ratio). Each set of colours represents a different pH of the resetting solution. - 68 -

Figure 3.7. Scheme of what solutions the sensors were exposed to before XPS analysis. - 69 -

Figure 3.8. High resolution XPS spectra of copper and carbon. Only the spectra collected on the blank sensor are shown, but the results are consistent on all four sensors. **a)** Cu 2p spectrum. The 2p_{3/2} shake-up line indicates the presence of Cu(2+). **b)** Auger LMM line. Its position and shape confirms the presence of Cu(2+). **c)** C 1s spectrum (inset: colour code of the different types of carbon). **d)** Percentage area of the different types of carbon. The values shown are the average over all four sensors. - 73 -

Figure 3.9. **a)** High-resolution spectra of nitrogen for the ligand and the sensors. **b)** Breakdown of the percentage area of the two nitrogens. - 75 -

Figure 4.1. Reduction-oxidation reaction of PCAT. Exposure to free chlorine pushes the equilibrium towards the pernigraniline base. - 78 -

Figure 4.2. Doping-sensing sequence of a free chlorine sensor. - 79 -

Figure 4.3. Raw data showcasing the negative effect of a 200 ppm NaCl background concentration on the performance of **a)** free chlorine sensors and **b)** permanganate sensors. - 81 -

Figure 4.4. **a)** Curve fittings obtained for the low range concentrations (0.01 – 0.2 ppm). The curves shown are a Langmuir adsorption isotherm, a Freundlich adsorption isotherm, and an exponential decay. **b)** Raw data showing the response of sensor GLCFS14 to the lowest concentrations. - 84 -

Figure 4.5. Detection of fluctuations in free chlorine concentration (0.2 – 0.5 ppm). - 86 -

Figure 4.6. Three calibration curve replicates obtained with the same set of free chlorine sensors. Only the Langmuir adsorption isotherm curve fitting is shown. - 89 -

Figure 4.7. Interference study. Signal change of two doped sensors (blue) and two blank sensors (orange) when exposed to ions commonly found in drinking water. Inset: magnified portion of the graph. **a)** Response to anions. **b)** Response to cations. - 91 -

Figure 4.8. Signal loss due to exposure to 2 ppm of humic acid. The effect was studied on two doped sensors (blue) and two blank sensors (orange). - 92 -

LIST OF TABLES

Table 1.1. Small selection of the regulations and health concerns pertaining to inorganic chemical parameters. The Canadian and European values are Maximum Allowable Concentrations (MAC) unless otherwise stated, as opposed to guideline values in the case of the WHO. Concentrations are given in ppb ($\mu\text{g/L}$) and ppm (mg/L). ... - 4 -

Table 3.1. Changes in the ionic strength of increasing concentration copper solutions before and after the addition of sodium chloride. - 54 -

Table 3.2. pH of 42 ppm sodium bicarbonate and 53 ppm sodium carbonate solutions (fresh and overnight), and pH of different tap water samples. - 56 -

Table 3.3. Constants and coefficients of determination for the calibration curves. - 63 -

Table 3.4. Equation parameters for the linearized Langmuir adsorption isotherm. - 65 -

Table 3.5. Elemental composition of the ligand and the transducing films. Obtained through XPS analysis and given as atomic percentage. - 71 -

Table 4.1. Parameters of the curves that describe the response of the sensors to the low range concentrations. - 84 -

Table 4.2. Calibration curve parameters for the three replicates performed at the high concentration range. GLCFS14 and GLCFS18 were functionalized with PCAT, while GLCFS16 and GLCFS17 were run as blanks. - 87 -

LIST OF EQUATIONS

Equation 3.1	- 54 -
Equation 3.2	- 54 -
Equation 3.3	- 54 -
Equation 3.4	- 63 -
Equation 3.5	- 63 -
Equation 3.6	- 63 -
Equation 3.7	- 64 -

LIST OF ABBREVIATIONS AND SYMBOLS

2D	2-Dimensional
3D	3-Dimensional
ABTS	2,2-azino-bis(3-ethylbenzothiazoline)-6-sulfonic acid-diammonium salt
ALARA	As Low As Reasonably Achievable
AO	Aesthetic Objective
CNT	Carbon Nanotube
DAP	2,3-diaminophenazine
DPD	<i>N,N</i> -diethyl- <i>p</i> -phenylenediamine
EDTA	Ethylenediaminetetraacetic acid
EPA	United States Environmental Protection Agency
ETA	Ethanol
FAAS	Flame Absorption Atomic Spectroscopy
FESEM	Field Emission Scanning Electron Microscopy
FET	Field Effect Transistor
FLG	Few Layer Graphene
GLC	Graphene-Like Carbon
HOMO	Highest Occupied Molecular Orbital
HOPG	Highly Ordered Pyrolytic Graphite
ICP-AES	Inductively Coupled Plasma Atomic Emission Spectroscopy
ICP-MS	Inductively Coupled Plasma Mass Spectrometry
IPA	Isopropanol

ISE	Ion Selective Electrode
ISO	International Organization for Standardization
LUMO	Lowest Unoccupied Molecular Orbital
MAC	Maximum Allowable Concentration
MeOH	Methanol
PCAT	Phenyl-Capped Aniline Tetramer
PDMS	Polydimethylsiloxane
PET	Polyethylene Terephthalate
ppb	$\mu\text{g/L}$
ppm	mg/L
RCF	Relative Centrifugal Force
SDS	Safety Data Sheet
SOP	Standard Operation Procedure
SWCNT	Single Walled Carbon Nanotube
TBA	<i>Tert</i> -butanol
TOC	Total Organic Carbon
VOC	Volatile Organic Compound
WHO	World Health Organization
X-AES	X-ray induced Auger Electron Spectroscopy
XPS	X-ray Photoelectron Spectroscopy
Z	Atomic Number

DECLARATION OF ACADEMIC ACHIEVEMENT

The PCAT used in CHAPTER 4 was synthesized by Omar Sharif. The XPS analysis was performed by Dr. Mark Biesinger at the University of Western. The rest of the work was performed by the author.

CHAPTER 1 — INTRODUCTION

1.1. Global water security

Access to safe and clean drinking water has been recognised as a human right for almost two decades.¹ However, as of 2015 over 2 billion people (29% of the global population) lacked access to safely managed drinking water services.² Consumption of dirty water led to 502,000 diarrhoeal deaths in 2012,³ a number that ascends to 3.4 million if one considers all water-related diseases, such as cholera and arsenicosis.⁴ There are many steps that need to be taken in order to lower those numbers, one of them being implementing proper monitoring of the chemical quality of drinking water throughout its life cycle. But this is not an easy task. The availability of adequate testing facilities, the cost of analyses, the integrity of the samples, and the points and frequency of sampling are some of the numerous factors that need to be considered,⁵⁻⁷ which can hinder progress. It is important to highlight that certain populations are particularly vulnerable, such as those living in developing countries and indigenous communities.^{4,8} Thus, emphasis should be placed on making monitoring strategies accessible and cost effective. Chemiresistive sensors are cheap devices that can provide continuous and real-time monitoring at any point of the water distribution system. Hence, they could be the perfect ally in the quest to safe and clean drinking water.

The availability of more advanced sensing technology could have helped prevent a number of tragedies, highlighting the importance of research on water quality sensors. In the year 2000, 7 people died and 2,300 others got sick within a two-week time span during the Walkerton Tragedy (Canada). Improper operating practices led to insufficient chlorine in drinking water, which resulted in a fatal *E. coli* outbreak.^{9,10} The Flint Water Crisis (USA) is a great example of how complex water chemistry can be. In 2014, soon after the town switched from buying pretreated water from Lake Huron to taking water from Flint River and treating it at the Flint Water Service Centre, residents noticed an apparent decline in color, taste, and odour of their tap water. The treatment plant had never been prepared for full-time operation, which led to very poor control of the pH, alkalinity, hardness, corrosivity, chlorination, and fluoridation of the water. The main consequence was the destruction of the passivation layers inside water pipes, which resulted in leaching of iron and dangerous amounts of lead. In addition, the incident was linked to deathly *E. coli* and *Legionella* outbreaks. Even though the plant was shut down in 2015, high levels of lead can still be found in the water.¹¹⁻¹⁴ This example is particularly relevant for Hamilton, as 20,000 homes still have lead water pipes. However, steps have already been taken to minimize risks and in 2015 the Council approved the addition of orthophosphate, a corrosion inhibitor, to the water system.¹⁵

1.2. Water quality parameters

Water quality parameters are commonly divided into physical, chemical (inorganic and organic), and biological parameters. Some physical parameters include colour, temperature, conductivity, and total dissolved solids. Examples of inorganic chemical parameters include pH, hardness, disinfectants, nitrogen content, and micronutrients. Organic contaminants are very diverse and are often classified as *total organic carbon* (TOC). Lastly, algae and human pathogens are some examples of biological parameters. References [5] and [16] contain comprehensive lists of the aforementioned water quality parameters. Here we will focus on inorganic chemical parameters, with an emphasis on copper and free chlorine.

In order to ensure water safety, the concentration of hazardous chemical parameters needs to be regulated. Since 1983, the World Health Organization (WHO) has been constantly developing and updating guideline values for all water quality parameters. These serve as a basis for national and regional governing bodies when drafting water quality legislation. The values suggested by the WHO take into account that some chemicals might be consumed through other sources (e.g. inhalation and food) and allow for a safe lifetime of consumption. However, these values might differ from local targets due to sociocultural, economic, and environmental factors (e.g. amount of water consumed daily or high background concentrations).⁵ Table 1.1 gathers some inorganic chemical parameters and compares the guideline values set by the WHO with the

maximum concentrations allowed in Canada and Europe. The health concerns associated with high levels of such contaminants are also summarized.

Table 1.1. Small selection of the regulations and health concerns pertaining to inorganic chemical parameters. The Canadian and European values are Maximum Allowable Concentrations (MAC) unless otherwise stated, as opposed to guideline values in the case of the WHO. Concentrations are given in ppb ($\mu\text{g/L}$) and ppm (mg/L).

Parameter	WHO ⁵	Canada ¹⁷	Europe ¹⁸	Health concerns ^{5,17}
Arsenic	10 ppb	10 ppb (ALARA) ⁽¹⁾	10 ppb	Carcinogenic, dermal lesions, peripheral neuropathy, vascular disease.
Antimony	20 ppb	6 ppb	5 ppb	Potentially carcinogenic.
Chlorine	5 ppm	—	—	None. Guideline value for effective disinfection.
Copper	2 ppm	1 ppm (AO) ⁽²⁾	2 ppm	Gastrointestinal effects.
Fluoride	1.5 ppm	1.5 ppm	1.5 ppm	Dental and skeletal fluorosis.
Lead	10 ppb	10 ppb	10 ppb	Neurodevelopmental effects, cardiovascular disease, impaired renal function, impaired fertility, central nervous system effects.
Mercury	6 ppb (inorganic)	1 ppb (all forms)	1 ppb	Haemorrhagic gastritis and colitis, kidney damage, neurological symptoms.
Monochloramine	3 ppm	3 ppm	—	Potentially mutagenic, reduced body weight gain, immunotoxicity.
Nitrate	50 ppm	45 ppm	50 ppm	Methemoglobinemia and thyroid effects in bottle-fed infants (most sensitive).
Nitrite	3 ppm	3 ppm	0.5 ppm	Methemoglobinemia and thyroid effects in bottle-fed infants (most sensitive).

Selenium	40 ppb	50 ppb	10 ppb	Gastrointestinal disturbances, discoloration of the skin, tooth decay, hair loss, weakened nails, changes in peripheral nerves.
Uranium	30 ppb	20 ppb	—	Nephritis.

⁽¹⁾ ALARA – As Low As Reasonably Achievable.

⁽²⁾ AO – Aesthetic Objective (staining of laundry and plumbing, bitter taste, colour).

In extreme cases where those values are exceeded and the consumption of tap water poses an acute health risk (either by ingestion, inhalation or dermal contact), it may be necessary to issue a water avoidance advisory.^{5,19} This is a rather unusual occurrence, but might be required after a chemical spill or a natural disaster. In order to efficiently and effectively manage pollutant levels in drinking water it is important to understand where they are being introduced into the system (i.e. water source, treatment or distribution). When their concentration needs to be measured, including during routine monitoring, standard methods are used. They are important to ensure that the results of the tests are reliable and comparable.²⁰ References [21–24] compile many of the standard methods available for the analysis of water. Some of the methods require complex and long sample treatment, as well as expensive and specialized equipment. This entails an economic burden and can result in water testing protocols being neglected. The enforcement of sensor technology could help alleviate this problem.

1.3. Chemiresistive water quality sensors

A chemiresistive sensor is a device capable of detecting a chemical process through quantifiable changes in the conducting properties of a transducing element. The transducing element is usually a metal oxide, a semiconductor, a conductive polymer or a nanocarbon material.²⁵ By probing the sensor with a small constant voltage, the changes in resistance caused by the modification of the conducting properties can be monitored in real time. Because sensing of gases entails less challenges than sensing in liquid media, such as avoiding short circuits and easy resetting of the device, most of the exploratory work was done using analytes in the gas phase.^{26–31} However, the push for developing water quality sensors has driven research and some liquid-phase chemiresistors have been reported.^{32–35}

1.3.1. Tuning analyte selectivity through film functionalization

A common sensing mechanism is the adsorption of the analyte onto the surface of the transducing film, but it can be functionalized in order to enhance selectivity and enable new sensing strategies, such as catalytic reactions, protonation and complexation.²⁵ Previous work in our group involved the use of chemiresistive sensors to measure the levels of free chlorine in water.^{36–38} This was done by doping single walled carbon nanotubes (SWCNTs) or a pencil film with a phenyl-capped aniline tetramer (PCAT), which is readily oxidized by chlorine. The change in the

oxidation state of the dopant modifies the resistance of the transducing film. This was found to be proportional to the logarithmic scale of concentration. The devices can be reset both electrochemically and using methanol, which returns the PCAT to its original reduced state.

In principle, any kind of chemiresistive sensor might be built provided that the interaction of the analyte with the dopant leads to a measurable change in electron transport. This is likely to happen if the electronic structure of the doping molecule significantly changes after interacting with the analyte. Functionalization of the transducing films with chelating agents is a potential gateway to cation detection. Dyes fall under this category and have the following desirable properties: they are selective, minimizing the likelihood of interferences from other ions; they have big and easily tunable HOMO-LUMO gaps, which should maximize electronic changes; they are aromatic, which should favour non-covalent interactions with nanocarbon films; and they are usually commercially available or can be easily synthesized, making the devices suitable for mass production. The idea of using complexation reactions to detect both cations and anions has been successfully explored in our group.^{39–41} For the reasons mentioned earlier, dyes were targeted as potential molecules to dope the films.^{42,43}

1.3.2. Graphene-like transducing films

The use of carbon nanotubes (CNTs) or pencil as materials for the transducing films can be detrimental to the performance of the sensors for

a couple of reasons. The first one is the presence of redox-active impurities that can interfere with the measurements due to their highly susceptible oxidation states. The manufacturing process of CNTs involves the use of transition metal catalysts, such as molybdenum, iron, cobalt, and nickel.^{44–47} In the case of pencil, it is the presence of clay and its structural iron that acts as an impurity.⁴⁸ Even though the amount of clay can be minimized by choosing a soft pencil (high graphite to clay ratio), there will always be a small amount of clay present.⁴⁹ On top of that, the lead contains wax, which can interfere with the conduction of electricity.⁴⁹ The second drawback arises from the numerous voids present in the films, which potentially slow down the sensor response and hinder resetting due to the fact that those crevices are harder to reach. The voids in CNTs are a consequence of the random network they form, and clay has a high cation exchange capacity.⁵⁰ Additionally, CNTs often come as somewhat ill-defined mixtures of tubes with different properties, which depend on the synthesis and purification processes.^{51,52} To overcome these issues, the possibility of using graphene-like materials is proposed. These materials are closely related to highly ordered pyrolytic graphite (HOPG), which has the advantage of being a highly defined and commercially available substrate on which further characterization can be performed, such as the study of the interactions between the dopants and the film or the analytes and the dopants.^{53–55}

Graphene is a perfectly flat monolayer of sp^2 hybridized carbon atoms arranged in a honeycomb lattice that features 1.42 Å bonds and 120°

angles.⁵⁶ This ideal 2D material has outstanding electronic properties, which arise from the symmetry of the lattice.⁵⁶ It is a zero-gap semiconductor or zero-overlap semimetal.⁵⁷ Electrons in graphene have the ability to travel submicrometer distances without scattering. This is known as ballistic transport (i.e. transport without electric resistivity).⁵⁸ The electronic properties can be tuned via doping.^{59–64} There are many ways to do this, which can be classified as growth on different substrates, adsorption of atoms/molecules, substitution or heteroatom doping, creation of vacancies, and size confinement.⁶⁵

The parent material is graphite, which consists of graphene layers stacked on top of each other with an interlayer spacing of 3.354 Å.⁶⁶ It is a semimetal with a 41 meV band overlap.⁵⁷ There are two main ways in which the layers can be stacked (depicted in Figure 1.1), with only 6% of the graphite having a disordered structure. The allotrope with ABA stacking is known as Bernal graphite, and it makes up 80% of the graphite found in nature. Rhombohedral graphite shows an ABC stacking and it can be found in 14% of the naturally occurring material.⁶⁷ These structural differences are reflected in the electronic properties of the material, with Bernal graphite being a semimetal with an electrically tunable band overlap and rhombohedral graphite being a semiconductor with an electrically tunable band gap.⁶⁸

Few layer graphene (FLG) is easier to isolate than its 2D counterpart and shows a good compromise between the properties of graphene and

graphite. It has sparked interest because many applications do not need to go as thin as a monolayer for good performance. Strictly speaking, a two-dimensional material is an ordered structure consisting of a single layer of atoms. However, the threshold between monolayer and bulk is not so clear if one looks at the properties. If graphene layers are stacked on top of each other, the electronic structure evolves until it converges into that of bulk graphite. The magnitude of the band overlap is a good indicator of said evolution and can help us determine the boundary between 2D- and 3D-like behaviour. For samples with 11 or more layers the overlap is only 10% different to graphite, so the threshold between few layer graphene and graphite has been suggested to be at 10 layers.⁵⁷

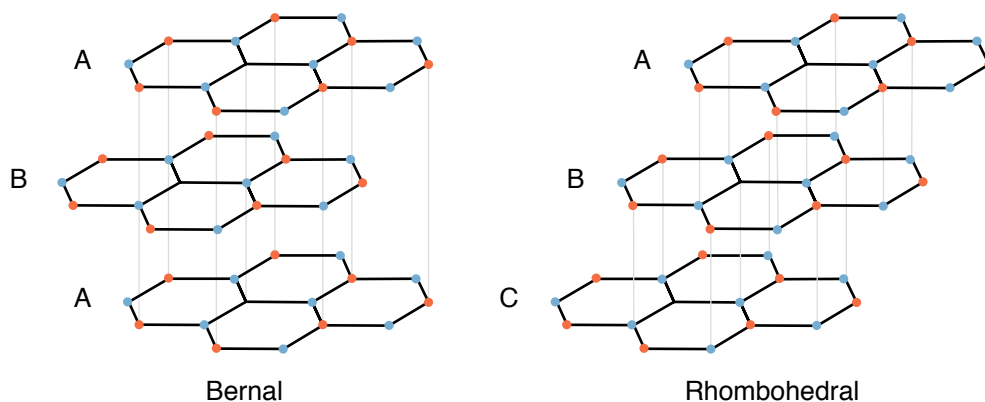


Figure 1.1. Bernal (ABA) and rhombohedral (ABC) stacking of graphene layers.

1.4. Motivation behind the presented work

The idea of detecting ions with chemiresistive sensors had been explored in the group using copper as a model system.^{40,41} However, the experiments needed to be polished and repeated. In addition, all the exploratory work had been carried out on SWCNTs and pencil, so the use of graphene-like

materials wanted to be explored. The free chlorine monitoring project was more mature,^{36–38} but there were some aspects that needed to be improved, such as switching to graphene-like materials, overcoming issues with sensor design and fabrication, and the degradation of the solutions.

1.4.1. Quantification of copper(II) cations in water

It is important to monitor copper because, although it is an essential trace element, it can be toxic and even deadly both for humans and animals if ingested at high concentrations, as well as being able to interrupt microbial activity in soil.^{69,70} The World Health Organization has a guideline value of 2 mg/L in drinking water, which leaves a reasonable margin for other sources of copper without exceeding the tolerable upper intake level of 10 mg/day.^{5,71} However, Health Canada has an aesthetic objective of 1 mg/L in order to avoid staining of laundry and sanitaryware.⁷² The main source in drinking water is corrosion of copper piping,^{5,73} but it can originate from many other sources,⁷⁴ such as mining,⁷⁵ leaching from antifouling paints used in ship maintenance,⁷⁶ leaching from wood preservatives,⁷⁷ and leaching from incinerator bottom ash used in landfill storage.⁷⁸

There are numerous well-established analytical methods that can be used to determine the concentration of copper in water samples with high accuracy and low limits of detection,⁷¹ such as flame atomic absorption spectroscopy (FAAS),⁷⁹ inductively coupled plasma atomic emission spectroscopy (ICP-AES),⁸⁰ and inductively coupled plasma mass

spectrometry (ICP-MS).⁸¹ Simpler commercially available techniques include ion selective electrodes (ISEs),⁸² spectrophotometric methods,⁸³ and stripping voltammetry.⁸⁴ Because of the importance of monitoring copper, research on the development of new quantification strategies has always been active. That being said, there has been a noticeable spike in the number of publications in recent years.⁸⁵ Most of the reported techniques are solution based spectrophotometric assays, where the development of colour takes place through copper catalyzed reactions⁸⁶ or the use of selective dyes.^{87–89} Another possibility is fluorescence quenching, which can be achieved using polyelectrolytes,⁹⁰ quantum dots,⁹¹ or noble metal nanoclusters.⁹² Finally, solid state sensors are an alternative to solution based analysis. Examples of the sensing strategies include but are not limited to square wave anodic stripping voltammetry⁹³ and field effect transistors (FETs).^{94,95}

However, the aforementioned methods have some weaknesses.⁸⁵ Big instrumental techniques are expensive, require well trained personnel, and must be used in a laboratory setting, which delays sample analysis. Spectroscopic methods have better portability, but they need additional reagents or complex syntheses, and are limited to discontinuous testing. ISEs can be used for continuous on-site monitoring, but they suffer from interferences and need regular calibration. Solid state sensors have the potential to overcome these limitations. Here we report a chemiresistive sensor for the continuous monitoring of copper(II) cations in water samples.

The devices use FLG suspensions to fabricate the transducing films, which are functionalized with commercially available 2,3-diaminophenazine. The response of the sensors is related to concentration in the tested range (10 $\mu\text{g/L}$ to 3 mg/L). They can be reset by lowering the pH, which was verified through XPS analysis. Further testing on interferences from ions commonly present in water remains to be done, as well as experimenting with the measurement of copper(II) in real water samples. Overall, these devices have demonstrated that a chemiresistive sensor can be built for any ion monitoring needs provided that the right dopant is selected to functionalize the films.

1.4.2. Monitoring of free chlorine in water

One of the biggest health concerns related to the consumption of drinking-water is the presence of pathogens (e.g. bacteria and viruses). This is because an isolated exposure can lead to infection and have fatal consequences.⁹⁶⁻⁹⁸ Additionally, monitoring their presence and concentration in water is not straightforward.⁹⁹ As a consequence, successful treatment of contaminated water is crucial. It involves many steps, such as coagulation, filtration, and disinfection.¹⁰⁰ In the pH range of drinking water the addition of commercial chlorine disinfectants (e.g. chlorine gas) results in the equilibrium between hypochlorous acid (HOCl) and hypochlorite (OCl^-). Together they are known as free chlorine.¹⁶ It is the most commonly used disinfectant and it works by interfering with cell membrane functions.¹⁰¹ It is added to the water during primary disinfection

(to remove pathogens) and during secondary disinfection (to avoid proliferation in the distribution system). The World Health Organization recommends that a concentration of 0.5 – 5 mg/L of free chlorine is maintained in the distribution system and that a minimum of 0.2 mg/L is kept at the point of delivery.⁵ Failure to maintain adequate free chlorine levels can have catastrophic results, as was the case during the Walkerton Tragedy (Canada), when an *E. Coli* outbreak killed 7 people and infected 2,300 others.^{9,10}

There are five EPA (United States Environmental Protection Agency) approved methods for the determination of free chlorine in water.²³ They use amperometry, titration, and colorimetry.^{102,103} The International Organization for Standardization (ISO) has three approved methods, which rely on titrimetry and colorimetry.¹⁰⁴ Oxidation of *N,N*-diethyl-*p*-phenylenediamine (DPD) to generate a magenta solution followed by measurement of the absorbance is the most popular approach to determine the concentration of free chlorine in water.^{105–107} However, because of the extensive use of free chlorine as a disinfectant, many other quantification strategies have been reported.⁸⁵ Examples of other reagents for colorimetric detection include ABTS,¹⁰⁸ Michler's thioketone,¹⁰⁹ and syringaldazine.¹¹⁰ Chemiluminescence^{111–113} and fluorescence^{114,115} are also successful optical sensing strategies. Multiple electrochemical sensors have also been developed, based on the principles of cyclic voltammetry^{116,117} and amperometry^{118–120}. The cited cyclic voltammetry techniques rely on the

measurement of reaction products to improve sensor performance (e.g. selectivity and limit of detection), while the amperometric methods do so by using functionalized working electrodes.

The aforementioned methods have some weaknesses that hinder their application as continuous on-line monitoring devices. The batch-like nature of the reactions involved in the spectroscopic techniques limits them to discontinuous testing, and the consumption of reagents is a drawback. Electrochemical sensors overcome these limitations but are susceptible to hysteresis and fouling. Thus, it is imperative to develop sensing technology that will overcome these limitations. The reported free chlorine chemiresistive sensors have some features than can be improved. The need for an external reset impedes the detection of fluctuations in the concentration of free chlorine. Certain applications require a lower limit of detection and the fabrication process was not suitable for mass production. On top of that, the nanotube and pencil films could be interfering with the measurements. Here we report a chemiresistive sensor for the continuous monitoring of free chlorine that uses a PCAT doped graphene-like carbon (GLC) sheet as the transducing element. The magnitude of the response of the devices was related to the concentration of the analyte over the tested range (10 ppb – 1 ppm). Reducing the concentration of free chlorine resets the devices, which allows for the detection of concentration fluctuations. Interferences by other ions commonly present in water were found to be negligible, but the devices showed some tendency to biofouling. Overall,

the devices are suited for continuous on-line monitoring of free chlorine in water and the production could be easily upscaled.

1.5. Structure of the thesis

In this chapter the concept of water safety has been introduced and chemiresistive sensors have been suggested as an appealing solution to water quality monitoring needs. After listing guideline values for common contaminants, copper and free chlorine have been presented as the focus of this thesis. In CHAPTER 2 the fundamentals of the experimental techniques used throughout the thesis are described (namely Raman, XPS and X-AES, the DPD colorimetric method, and conductance measurements). The fabrication of different types of sensors and the stability of the analyte solutions are also discussed. CHAPTER 3 presents the results obtained with the copper sensors, which include deciding on a composition of the background water, studying the selectivity of the devices, getting calibrations curves, optimizing the resetting procedure, and characterizing the devices with XPS. CHAPTER 4 covers similar aspects in relation to the free chlorine sensors. Finally, CHAPTER 5 summarizes the findings of this thesis and outlines future work.

CHAPTER 2 — EXPERIMENTAL

2.1. Fundamentals of the experimental techniques

2.1.1. Raman spectroscopy

Raman spectroscopy can be used to observe phonon modes in a solid, which provides a spectral fingerprint of the material. A laser is used to irradiate the sample at ambient conditions, increasing its energy. In most cases, the new energy does not match that of a stationary state, so the system is said to be in a virtual level. However, by tuning the energy of the incident radiation, the excitation can be matched to a specific stationary state. This process is known as Resonant Raman and it leads to an enhancement of the signal. The increase in energy leaves the system in an excited state, and it can relax by scattering the incoming radiation. The type of scattering depends on the excitation-relaxation mechanism.^{121,122} They are depicted in Figure 2.1 for easier visualization.

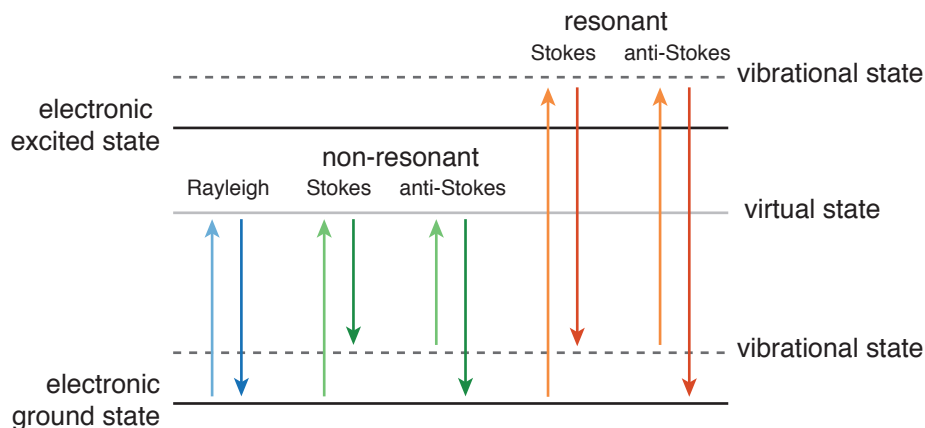


Figure 2.1. Depiction of the different excitation-relaxation mechanisms that can happen during a Raman spectroscopy experiment.

Rayleigh scattering happens when the photon is elastically scattered. It is the most probable type of scattering. In the field of graphene it has been successfully used to count the number of layers and to assess structural and chemical modifications after its preparation.¹²³ Conversely, Raman scattering is the result of the inelastic scattering of photons by phonons. If the photon transfers some of its energy to the system, it is known as Stokes scattering. If, on the other hand, the photon encounters the sample in an already excited vibrational state and returns it to the ground state by absorbing energy, it is known as Anti-Stokes scattering.¹²² The probability is much smaller due to the fact that the population of an excited vibrational state is much smaller than the ground state (according to the Maxwell-Boltzmann distribution).¹²¹ Consequently, the majority of Raman spectra correspond to Stokes scattering. They are plotted as the intensity of the scattered light against the photon energy loss (known as Raman shift – units of cm^{-1}). For a vibration to be Raman active it must lead to a change in the

polarizability of the material.¹²¹ Since electronic excitations are often the intermediate state in the scattering process, the spectral features contain information about both the atomic structure and the electronic properties of the material.¹²²

Raman spectroscopy is one of the most popular characterization techniques for graphene because it is user-friendly, non-destructive and extremely versatile. Due to their different electronic fingerprints, it can be used to count the number of layers,^{124,125} distinguish the type of stacking,⁶⁸ identify the type of doping,^{64,126–128} and detect defects.^{129–131} Raman scattering in graphene is always resonant due to its zero-gap electronic dispersion.¹²³ However, the spectra can be challenging to interpret owing to the fact that all carbon-based materials show only a few and very similar features. The following section is a brief discussion on how to obtain information about graphene samples from small subtleties in the shape, intensity and position of the peaks. Figure 2.2c features a Raman spectrum of a transducing film fabricated with a suspension of exfoliated graphite for which the peaks have been identified (both a description of the fabrication of the film and a detailed discussion of the spectrum can be found in section 2.2.2.1).

2.1.1.1. Interpretation of spectral features in graphene samples

The most intense features in pristine graphene are a G peak at $\sim 1580\text{ cm}^{-1}$ and a 2D band at $\sim 2700\text{ cm}^{-1}$ (formerly known as G'). The 2D band is about four times more intense than the G peak, but as the number of layers

increases it becomes broader, more up-shifted, and less intense.^{124,132} After five layers it becomes indistinguishable from the 2D band in bulk graphite, for which it consists of components 2D₁ and 2D₂, ¼ and ½ the height of the G peak respectively.¹²⁴ These details can be appreciated in Figure 2.2a and Figure 2.2b. The symmetry or lack of thereof in the 2D band contains information about the type of stacking, with the Bernal allotrope being more symmetric than the rhombohedral.⁶⁸

Graphene can be doped in a controlled manner using an FET geometry and applying a gate voltage. The G peak stiffens (i.e. increased phonon energy, bigger Raman shift) and sharpens as a consequence of both hole and electron doping, while the 2D band stiffens for hole doping and softens (i.e. decreased phonon energy, smaller Raman shift) for electron doping. The intensity of these features is also doping dependent, with I(2D)/I(G) decreasing as the sample is increasingly doped.¹²⁷ The same evolution of the G and 2D peaks is observed when graphene is doped through adsorption of aromatic molecules. Those with electron-withdrawing groups p-dope the material, while those with electron-donating groups n-dope it.^{64,126} The same trend is observed for metal adatoms, where the type of doping depends on the metal's work function.¹²⁸

The aforesaid adsorption events lead to symmetry breaking, which introduces a D peak at $\sim 1350\text{ cm}^{-1}$.^{64,126,128} The D' band at $\sim 1620\text{ cm}^{-1}$ is another important defect activated Raman mode. At low levels of defects one can look at the I(D)/I(D') ratio in order to identify their nature. A

maximum of ~ 13 is achieved for sp^3 -defects, ~ 7 for vacancy-like defects, and a minimum of ~ 3.5 corresponds to boundaries in polycrystalline graphite. At high concentrations there is no clear dependence.¹²⁹ On top of that, $I(D)/I(G)$ can be used to determine the density of point defects at a specific excitation wavelength.¹³¹ Edges behave like defects. Both the armchair and zigzag structures show a D' band, but only the armchair is accompanied by a D peak.¹³⁰ Note that the D and 2D bands are excitation energy dependent, while the G peak is not.¹²⁵ Finally, other common but less intense features that can be seen in the Raman spectra of pristine graphene are $D+D''$ at ~ 2450 and $2D'$ at ~ 3250 cm^{-1} . Defected samples can also show D'' at ~ 1100 cm^{-1} and $D+D'$ at ~ 2950 cm^{-1} .^{122,123}

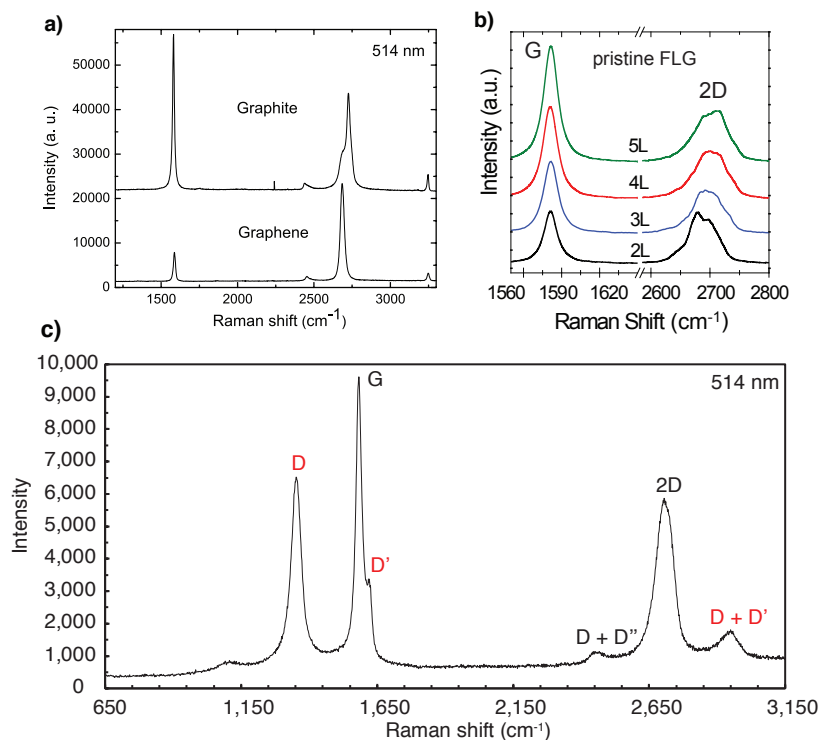


Figure 2.2. **a)** Raman spectra of graphite and graphene. Reprinted with permission from Ref. [124] Copyright 2006 by The American Physical Society. **b)** Evolution of the Raman spectra of FLG as the number of layers increases. Reprinted with permission from Ref. [132] Copyright 2012 by WILEY-VCH. **c)** Raman spectrum of an exfoliated graphite transducing film. The peaks have been identified (the red colour indicates defects).

2.1.2. X-ray Photoelectron Spectroscopy and X-ray induced Auger Electron Spectroscopy^{133,134}

X-ray Photoelectron Spectroscopy (XPS) is a surface analysis technique that can be used to obtain information about the chemical composition of the surface. It is based on the photoelectric effect: the sample is irradiated with monochromatic X-rays, which causes the ejection of core electrons if the energy of the radiation is higher than the binding energy of the electrons and the work function of the spectrometer. The excess energy is transferred to the electrons as kinetic energy. On the spectra, the count of emitted

photoelectrons is plotted against their kinetic energy. The notation used to describe them uses quantum numbers according to the scheme nl_j , where n is the principal quantum number, l is the orbital angular momentum quantum number and j is the total angular momentum quantum number ($j = |l \pm s|$, where s is the spin angular momentum quantum number). The latter is relevant for orbitals with $l > 0$ and causes the peak to split into two. Their relative intensities are related to their degeneracy ($2j + 1$). Thus, one would expect to see a doublet with relative intensities of 1:2 for the $2p_{1/2}$ and $2p_{3/2}$ peaks respectively. This can be clearly seen in the high-resolution spectrum of Si 2p in Figure 2.3a.

An XPS experiment starts by collecting a survey spectrum to identify the elements present. This is followed by acquiring high-resolution spectra of the peaks of interest in order to get a better understanding of the chemical composition. Each element has characteristic binding energies, and the position and separation of the peaks contain information about their chemical state. The peak area is proportional to the concentration of each chemical species. These values are all tabulated. The surface sensitivity of the technique arises from the small mean free path of electrons in a solid. Only electrons elastically emitted contribute to the peaks, and they can only travel tens of angstroms. XPS must be performed at high vacuum to facilitate transmission of photoelectrons to the analyzer and to minimize surface contamination.

The emission of a photoelectron leaves the atom ionized. The main relaxation mechanism for elements with low atomic number is the emission of an Auger electron (for elements with $Z > 35$ fluorescence becomes more likely).¹³⁵ The first step of the process is filling the core hole with an electron from a higher level. Next, in order to conserve the energy of the system, a second electron is ejected. This is the Auger electron, and the process is known as X-ray induced Auger Electron Spectroscopy (X-AES). Auger peaks are labeled following the X-ray notation. For instance, a KL_1L_2 peak represents a 1s hole that was filled with a 2s electron followed by emission of a 2p Auger electron. For simplicity it is often abbreviated as KLL. The kinetic energy of Auger electrons is approximately the difference between the energy of the initial ion and the doubly charged final ion, so it has a fixed value. XPS and Auger peaks can be discriminated using a dual anode spectrometer or synchrotron radiation. The kinetic energy of the XPS electrons is a function of the energy of the incoming radiation, whereas the energy of Auger electrons is not. Figure 2.3b shows the electronic transitions involved in XPS and X-AES.

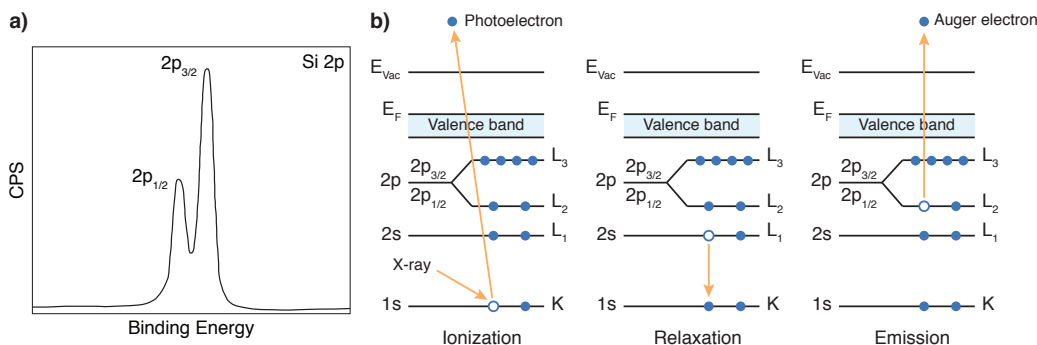


Figure 2.3. **a)** Simulation of the doublet arising from the spin-orbit coupling for Si 2p. **b)** Diagram of the electronic transitions involved in XPS and X-AES. The resulting peaks would be labeled as 1s (XPS) and KL_1L_2 (X-AES).

2.1.3. The DPD method

The DPD method is a colorimetric test used to quantify free chlorine in water samples. It was first reported by Arthur Palin in 1957 and has since been adopted as one of the standard methods for chlorine monitoring.^{103–105} The amines in *N,N*-diethyl-*p*-phenylenediamine (DPD) get oxidized by free chlorine to give two possible products: a magenta coloured free radical known as *Würster dye* and a colourless imine (Figure 2.4). At a near neutral pH the dye is the main oxidation product. It has two absorption maxima (512 and 535 nm) that allow for its quantification. The method can be easily modified to measure total chlorine (free chlorine + chloramines) by adding small amounts of iodide. The latter reacts with chloramine to give triiodide, which then reacts with DPD to produce the magenta colour. The method is commercially available, including mono-doses that contain all the reagents required to properly measure chlorine. These reagents consist of the indicator (DPD oxalate or sulfate), a buffer to keep the pH within the optimal range (commonly phosphate), a sequestering agent to minimize

metal-catalyzed oxidation (EDTA) and potassium iodide for total chlorine measurement (optional).¹³⁶ In order to avoid faulty results, it is important to know that manganese is the main interfering species and that too much chlorine or waiting before measuring the absorbance will lead to fading of the solution as the production of the imine is favoured. Permanganate solutions can be used to calibrate the method.^{105,136}

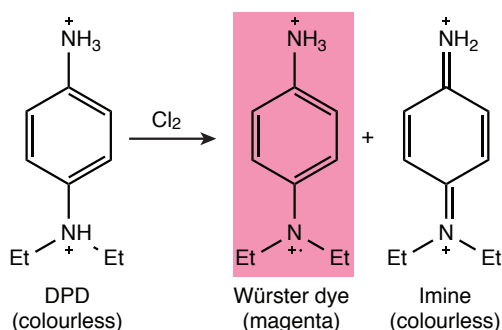


Figure 2.4. Reaction between free chlorine and DPD. The intensity of the colour is proportional to the concentration.

2.1.4. Chemiresistive sensor testing

In order to test the performance of the sensors, their conductance over time was measured by applying a small constant voltage. An eDAQ Quad Multi-Function isoPod™ (“eDAQ”) was used, which allows for the simultaneous measurement of up to four sensors. If needed, two eDAQs can be used in parallel, enabling the recording of eight signals at the same time. The eDAQ was set to the *Biosensor* function, with a data acquisition rate of 30/min and the maximum number of decimal places possible. To maximize resolution, the sampling range was chosen such that it was twice the amplitude of the biggest signal expected. The sample averaging period

was set to 1.0 s to improve the signal-to-noise ratio. To simplify the graphing process and minimize data loss due to overloading of the software, a new file was saved for each sample. First, the run was started, and the date and time were noted down. Next, data acquisition was stopped and saved. Then, a new file was open, and the run was initiated. Only after the software had started recording was the sample changed. This method minimizes information loss and events in the data can be easily traced back to the day and time. More specific details about the parameters used for the copper and free chlorine sensors will be provided in their respective chapters.

2.2. Sensor fabrication

The design of the original devices included sputtered gold electrodes in order to probe the sensor with a small voltage and a channel made out of PDMS (polydimethylsiloxane) to flow the solution through and prevent it from touching the electrodes. They also used SWCNTs or pencil for the transducing films. One of the main goals of this thesis was to develop a new generation of sensors. This section provides details about the optimization process and describes how to fabricate the devices. First, we report an SOP for the fabrication of SWCNT sensors. In this design, the sputtered gold electrodes have been substituted for copper tape in order to lower the cost of the devices and to make the fabrication process simpler. Next, we discuss the choice of transducing material, substrate, and sensor geometry.

2.2.1. SOP for the fabrication of carbon nanotube flow sensors

2.2.1.1. Materials


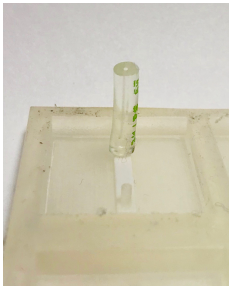
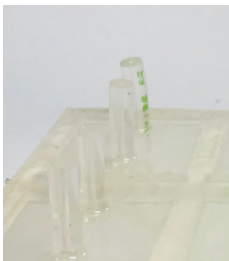
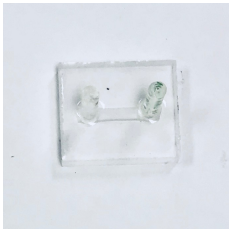
- Oven (optional)
- Ultrasonic bath (optional)
- Hot plate
- Balance
- Ohmmeter
- Wood stick applicators
- Small plastic containers
- Scalpel
- Pasteur pipette with bulb
- Kimwipes® Delicate Task Wipes
- Permanent marker
- Channel mould
- Sylgard® 184 Silicone Elastomer Kit from Dow Corning
- Masterflex® Tygon® Chemical Tubing L/S 13
- VWR Goldline frosted glass slides (#CA48323-185)
- 3M™ Copper Foil Tape 1181 1/4 inch
- Derwent Graphic 9B Pencil
- Single walled carbon nanotubes from Sigma-Aldrich (#773735)
- Methanol

2.2.1.2. List of precautions

Disclaimer: this is just a selection of the hazards and precautions associated with each of the substances featured in this SOP. Check SDS files for more information.

Substance	Hazards	Precautions	Other
Sylgard® 184 base	Flammable (Category 1)	Wear protective gloves/ eye protection	
Sylgard® 184 curing agent	Flammable (Category 1) Contact with water liberates highly flammable gases	Wear eye protection	Extinguishing media: DO NOT use dry chemical
Single walled carbon nanotubes	Eye irritation (Category 2A) Specific target organ toxicity - single exposure (Category 3), Respiratory system May cause genetic defects May cause cancer	Avoid breathing dust/ fume/ gas/ mist/ vapours/ spray Wear eye protection/ face protection	
Methanol	Flammable (Category 2) Acute toxicity, Oral (Category 3) Acute toxicity, Inhalation (Category 3) Acute toxicity, Dermal (Category 3) Specific target organ toxicity – single exposure (Category 1)	Keep away from heat, hot surfaces, sparks, open flames and other ignition sources Use only outdoors or in a well-ventilated area Wear protective gloves/ eye protection/ face protection	Extinguishing media: DO NOT use water jet
Copper foil tape	May be harmful if inhaled May be harmful if swallowed May be harmful if absorbed through skin May cause respiratory tract/ skin/ eye irritation Very toxic to aquatic life	Wear protective gloves/ eye protection	

2.2.1.3. Production of channels

Step	Description	Figure
1	Cut Masterflex® tubing in pieces of 1.5 cm long. Two pieces per sensor are required.	
2	Place tubing pieces on the sticks of the mould.	
3	Prepare Sylgard® 184 Silicone Elastomer (PDMS). Mix the base and the curing agent at a 10:1 ratio. 2.5 g are required per sensor. Blend thoroughly with a wood stick.	
4	Slowly pour the PDMS in the mould. Be careful not to cover any of the tube holes. Let the mixture stand still until the air bubbles disappear (approximately 30 min). Removal of air bubbles can be sped up by tapping the mould against a flat surface.	
5	Cure the PDMS. To do so, leave it at room temperature for 48 hours or introduce it in the oven for shorter curing times (approximately 40 min at 80 °C to avoid melting the mould).	
6	Use a scalpel to cut around the mould and remove the PDMS channel.	

2.2.1.4. Production of substrates

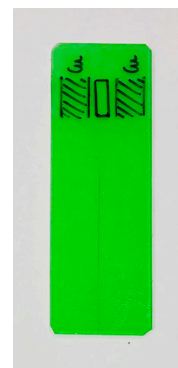
Step	Description	Figure
1	Clean a glass slide with a Kimwipe® drenched in methanol.	

- 2 Label the glass slide.



- 3 Clean the tip of the 9B pencil with a Kimwipe® and some methanol.

- 4 Always use a template in order to get a consistent sensor design. The template can be made using the PDMS channel as a guideline to know where to deposit the carbon nanotubes. The outline is on the frosted side of the slide.



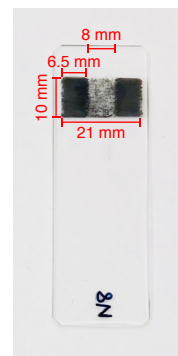
- 5 Draw on the sides using the 9B pencil, pressing hard on both directions. These reinforcements ensure a good contact between the copper tape and the CNTs.



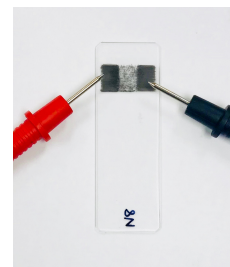
- 6 Use a suspension of CNTs in methanol to drop cast a film between the pencil reinforcements. Make sure that the CNTs overlap with the pencil reinforcements. If the suspension is freshly prepared, it must be sonicated first to break up the bundles (30 minutes followed by a 1 hour resting period). Let the methanol evaporate and keep adding drops until a homogeneous film is obtained.





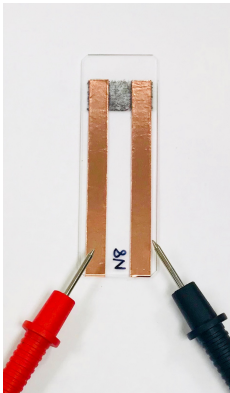

- 7 Let the film stand for at least 10 minutes so that the CNTs stick to the glass slide.
- 8 Take a Kimwipe® slightly dampened with methanol and gently wipe the surface of the CNTs until a thin film of around 10 k Ω is obtained. Towards the end, a dry Kimwipe® can be used in order to remove thinner layers of CNTs and approach the target resistance slower. The dimensions of the film are shown in the picture.



- 9 Measure the resistance of the film and write it down for future reference.
Note: if the substrates are left outside for prolonged periods of time, the resistance value could change. This is due to the fact that CNTs are able to sense the moisture of the environment.



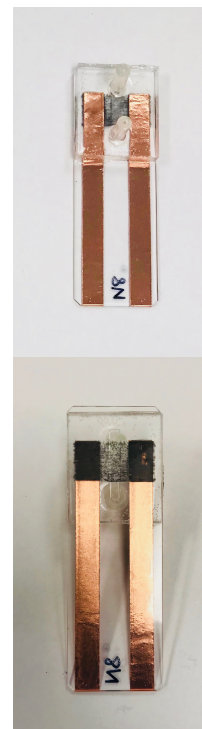
2.2.1.5. Sensor assembly

Step	Description	Figure
1	Cut the copper tape in 6.5 cm long pieces. Two bits are needed per sensor.	
2	Paste the tape on the glass slide and smooth it down using a Kimwipe®. Other objects can be too harsh and lead to decreased stability of the measurements.	
3	Measure the resistance. Write it down for future reference.	
4	Spread a small amount of PDMS on the glass slide using a wood stick applicator. Apply the polymer making a rectangular shape, leaving a gap slightly bigger than the liquid channel in the centre. Place a PDMS channel on top and gently press on it using a wood stick to get rid of air bubbles. If any areas start to unglue, carefully remove the channel and add some PDMS. <u>Note:</u> do not use too much PDMS nor press too hard, as it could lead to clogged inlets/outlets or partial covering of the CNTs in the sensing area. If that were to happen, discard the sensor.	

- 5 Cure the PDMS by placing the sensor on a hotplate at 80 °C for about 10 min.



- 6 Double check for clogs or covering of the CNT channel. If that is the case, discard the sensor. The width of the PDMS channel is 3 mm.



- 7 Measure the resistance of the sensor and write it down for future reference.

2.2.1.6. Waste disposal

Material	Waste container
PDMS channels and contaminated materials (gloves, applicators, wipes...)	Solid waste
Uncured PDMS	Solid waste (let it cure first)
CNTs and contaminated materials (gloves, wipes...)	Solid waste
Pipette used for drop casting CNTs	Broken glass container
Methanol	Organic solvents liquid waste

Copper foil tape	Solid waste
Copper foil tape peals	Regular trash
Full sensors	Solid waste

2.2.2. Choice of materials for the transducing film

Different nanocarbon materials were explored for the fabrication of the transducing films: carbon nanotubes, pencil lead, exfoliated graphite, and graphene-like carbon. The device fabrication was similar in all cases. The SOP in section 2.2.1 was used as a guideline with minor variations. To make pencil sensors a patch was drawn using horizontal strokes. The film is an extension of the pencil reinforcements, but it is thinner. These sensors had a resistance in the 15 k Ω range (same film dimensions as the CNT sensors), which was very easy to hit consistently for different devices. Neither the SWCNT sensors nor the pencil sensors were used for the experiments reported in in this thesis, but they were used by other researchers in the group.

2.2.2.1. Exfoliated graphite

Big efforts have been made towards exfoliating graphite in solution in order to obtain graphene suspensions. Having graphene in a liquid media enables new techniques, such as drop-casting on any substrate,³³ printing with graphene inks,¹³⁷ and carrying out reactions.¹³⁸ The first successful attempts at exfoliating graphite involved the use of highly toxic solvents or difficult to remove surfactants.^{139–141} The recent emphasis on a greener and more sustainable chemistry has sparked research to find alternative

routes.¹⁴² Here we adopted a recent method that works by sonicating graphite in a cosolvent mixture of alcohol and water at a critical concentration.¹⁴³ Alcohols behave very much like surfactants, so beyond that critical concentration they create micelles that can intercalate between the graphene sheets and stabilize the suspension. Using centrifugation, a size selection of the flakes can be performed.¹⁴⁴

Graphite powder (Sigma Aldrich #282863) was added to solutions of the following alcohols in Millipore water: 50 w% ethanol (ETA – Commercial Alcohols #P016EAAN), 30 w% isopropanol (IPA – Caledon #8601-7-40), and 10 w% *tert*-butanol (TBA – Fisher Scientific #A401). Three samples were prepared for each of the mixtures and different sonication times were tested (1, 3 and 5 hours). The samples were sonicated in an Elmasonic P30H Ultrasonic Cleaner at 80 kHz on Sweep Mode, and the temperature of the water bath was kept at 30 °C. Next, the samples were centrifuged at a relative centrifugal force (RCF) of 14100 g in an Eppendorf MiniSpin® plus centrifuge for 5 minutes. Then, the supernatant was collected and centrifuged for 15 more minutes. The second supernatant was discarded, and the precipitate was resuspended in a small amount of solvent (“second fraction”). This size selection approach was taken because it has been suggested that flakes with body defects are more stable towards sedimentation.¹⁴⁰ Thus, it is likely that the second supernatant has a higher concentration of defected flakes. The best exfoliation yield was obtained with IPA (Figure 2.5), so it was chosen as the cosolvent mixture to exfoliate

graphite. During routine production of graphitic suspensions, the sonication time was not controlled very strictly. This appears to have no significant effect on the number of defects, it only impacts the exfoliation yield.¹⁴⁰

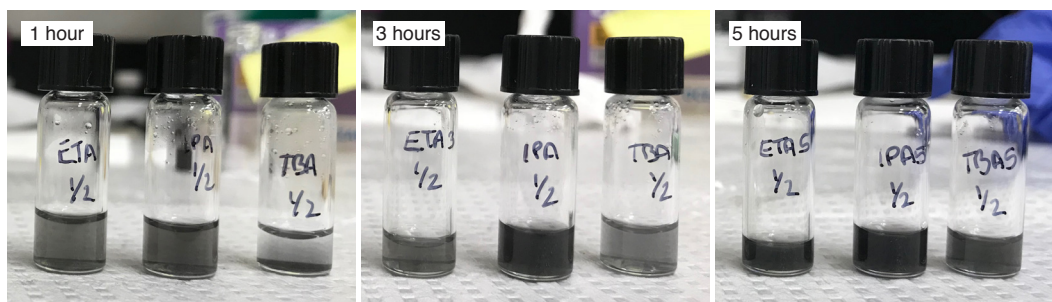


Figure 2.5. Second fraction in different alcohol-water mixtures (vials from left to right: ETA, IPA, TBA) sonicated for different lengths of time (pictures from left to right: 1 hour, 3 hours, 5 hours).

Slight modifications were made to the sensor fabrication SOP. The graphitic suspension was drop casted on a hotplate at 60 °C to accelerate evaporation of the solvent, which has a high water content. Before applying the PDMS it was left to thicken at room temperature for approximately 6 hours. This makes application easier and reduces the likelihood of it spreading over the channel. Alternatively, fresh PDMS can be placed on a hotplate at 60 °C for 10-15 minutes to achieve the desired consistency. The final cure was done at 60 °C instead of 80 °C owing to concerns about thermally and/or mechanically stressing the films. The resistance of the sensors was in the 10 – 20 k Ω range (overall film size 21 \times 18 mm: bare FLG 8 \times 18 mm, pencil reinforcements 6.5 \times 18 mm). Images of the films were obtained with FESEM (Figure 2.6a and Figure 2.6b), which show a network

of FLG platelets arranged in a parallel fashion with respect to the glass slide. This suggests that the undesirable voids present in CNT films have been minimized. Raman spectroscopy was also used to study the quality of the graphitic films (Figure 2.6c). The spectrum shows peaks characteristic of graphitic materials (namely the G, 2D and D + D'' bands). The absence of a shoulder in the 2D band suggests that the films consist of few layer graphene and not graphite, for which it should split into 2D₁ and 2D₂ components.¹²⁴ Finally, the D, D' and D + D' bands indicate that defects have been introduced in the flakes during processing. Some of these defects could be related to the size of the platelets (i.e. edge defects).¹³⁰

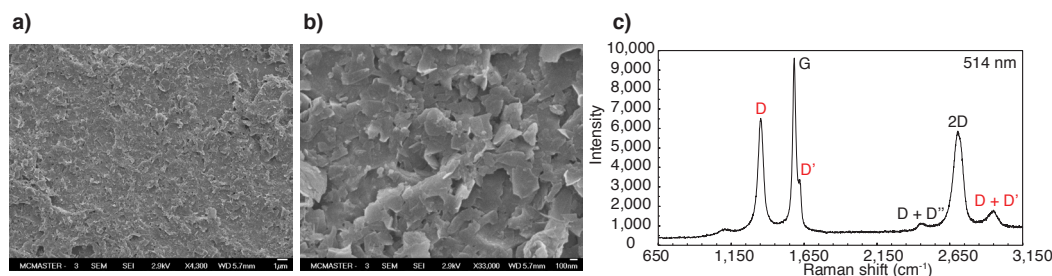


Figure 2.6. a – b) FESEM images of the FLG film at different magnifications: a) $\times 4,300$ and b) $\times 33,000$. c) Raman spectrum of the FLG film. The peaks labeled in black are characteristic of FLG, while the peaks labeled in red indicate the presence of defects.

Airbrushing the suspensions is an alternative to drop casting. To do so, adhesive tape was used to delimit the size of the films and the suspension was airbrushed using 20 psi of N₂. The airbrush used was the NEO for Iwata CN Gravity Feed Dual Action Brush (#N4500). The gas flow slows down evaporation of the solvent because it cools the surface of the sensors. Consequently, the hotplate was set to 100 °C. The resistance of the sensors was in the range of 20 k Ω and was easy to hit consistently (overall film size

21 × 18 mm: bare FLG 8 × 18 mm, pencil reinforcements 6.5 × 18 mm). Although this method yields more uniform films, it is time consuming and uses large amounts of the suspension. As a consequence, drop casting was adopted as the standard procedure.

2.2.2.2. Graphene-like carbon

Graphene-like carbon was obtained from the company 3M Canada Co. It consists of FLG platelets a few micrometres in size with some thicker nanocrystalline graphene embedded. It is manufactured in the absence of a binder and the platelets are deposited in a parallel fashion onto a PET substrate following a proprietary process. The GLC used to produce the sensors was 12 nm thick and had a sheet resistance bigger than 200 MΩ/sq.^{145,146} In order to attach the sheets to the glass slides double sided Kapton tape was used. It was cut to the desired dimensions and one of the adhesive sides was exposed. It was carefully placed on the non-conducting side of a GLC sheet, trying to avoid the formation of wrinkles and/or bubbles. Using a sharp blade, the GLC was cut around the Kapton tape. The other adhesive side was exposed, and it was pasted on the glass slide. Before pressing down to make sure that it was properly adhered, a piece of PET was placed over it to protect it. Next, a Kimwipe® was run back and forth over the surface. This type of sensor used silver paint instead of pencil for the contact reinforcements. Two patches were painted on the GLC with PELCO® Conductive Silver Paint (#16062), and they were cured on a hotplate at 60 °C for 20 minutes. The wet bonding process to attach the

PDMS channels was modified slightly. Using pre-thickened PDMS, a thin layer was spread on the areas where the channel would be placed later. The glass slide was placed on a hotplate at 80 °C for 4 minutes to partially cure the PDMS. Then, the PDMS channel was placed on top and the curing was finalized on the hotplate. This modification was introduced because it is more efficient at minimizing the chances of getting polymer in the channel. Since the thermal and mechanical stability of the GLC were not a concern, 80 °C were used to speed up the process. The resistance of the sensors fabricated following this method was in the range of 70 – 110 kΩ (overall film size 22 × 24 mm: bare GLC 8 × 24 mm, silver reinforcements 6.5 × 24 mm).

2.2.3. Choice of substrate: glass slides or PET

The glass slides had been suspected of contributing to the slow response and poor resetting of some sensors due to the presence of voids in its silicate structure. PET was tested as a possible alternative. PET with a thickness of 0.50 mm was purchased from Goodfellow (ES301485/8) and the sheets were cut down to glass slide size. The adhesion of the FLG to the plastic was very poor. This issue was overcome by sanding the surface, which introduced irregularities that allowed the flakes to stick. The performance of the sensors was studied by doping the films with PCAT and running solutions of potassium permanganate. Figure 2.7 compares the response of a PET sensor with the response of a glass sensor. The performance of the former was noticeable worse, with a very low signal-to noise ratio.

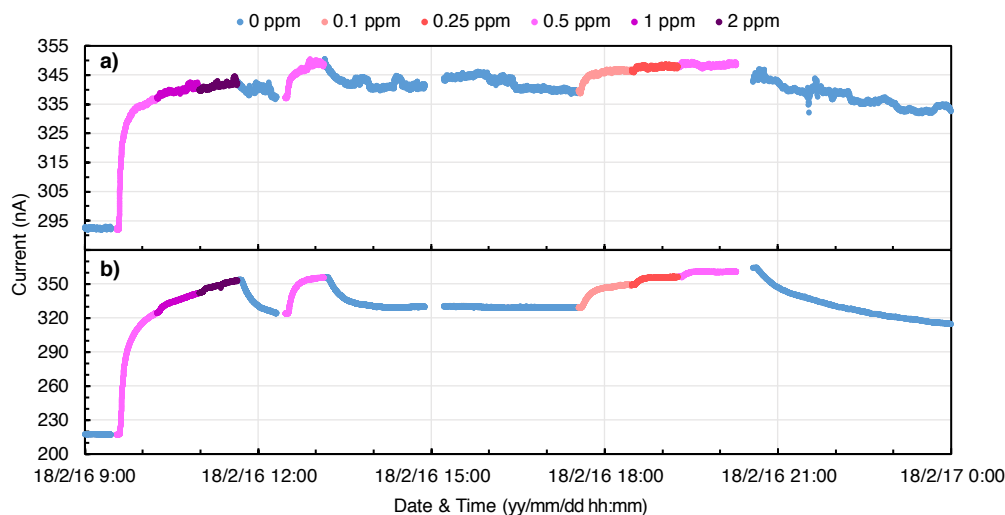


Figure 2.7. Side-by-side comparison of the performance of two FLG sensors with different substrate materials: **a)** PET and **b)** glass slide.

One of the reasons why a sensor could exhibit a very noisy signal is poor contact between the copper tape and the transducing film. In fact, it was hard to draw the pencil reinforcements on the PET surface. Thus, a second set of experiments was run where silver paint was used as the contact reinforcement for the PET sensor and pencil was used for the glass sensor. As it can be seen in Figure 2.8, the quality of the signal improved immensely. However, there are no significant differences between the two sensors. As a consequence, it was decided to keep using glass slides for the sensor fabrication. This is preferred because it eliminates the need for silver paint, which is toxic and could lead to interferences if any particles or the solvent contaminated the channel area. In addition, having to sand the surface of the plastic introduces a lot of variability amongst sensors.

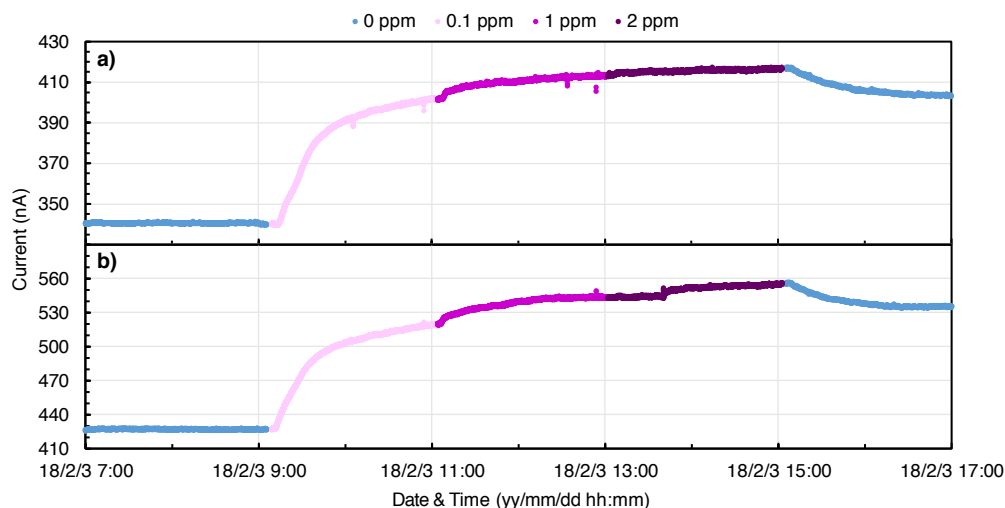


Figure 2.8. Improvement in performance of a PET sensor after switching to silver contact reinforcements. **a)** PET sensor with silver contact reinforcements. **b)** Glass sensor with pencil contact reinforcements.

2.2.4. Choice of sensor geometry: flow sensors or dip sensors

All the sensors described so far use a PDMS channel to bring the solutions into contact with the transducing film. However, the channel has been suspected of contributing to the slow response and poor resetting of the devices, due to the fact that solutes can stick to the walls.¹⁴⁷ A dip sensor geometry (Figure 2.9b - inset) could solve this problem. This design has some added advantages, such as avoiding the need for tubing (which could also have solute stick to their walls) and having a bigger sensing area. This type of sensor is run by introducing the transducing film in a vessel containing the solution. In order to avoid short circuits, the contacts must be masked with a dielectric. PDMS itself has a low dielectric constant,¹⁴⁸ so it was used to mask the copper tape by applying a thin layer of thickened polymer and curing it on a hotplate at 60 °C. After applying the PDMS, the

width of the film exposed to the solution was 6 mm. The performance was compared to that of a flow sensor by running potassium permanganate solutions on PCAT doped drop casted FLG films. The results of the experiment can be seen in Figure 2.9. The sensors were exposed to decreasingly low concentrations to test the resetting behaviour. It is apparent from the graphs that the dip sensor is more responsive to concentration changes and that the resetting is faster. This is a big improvement in performance, so the dip sensor geometry was used for most experiments.

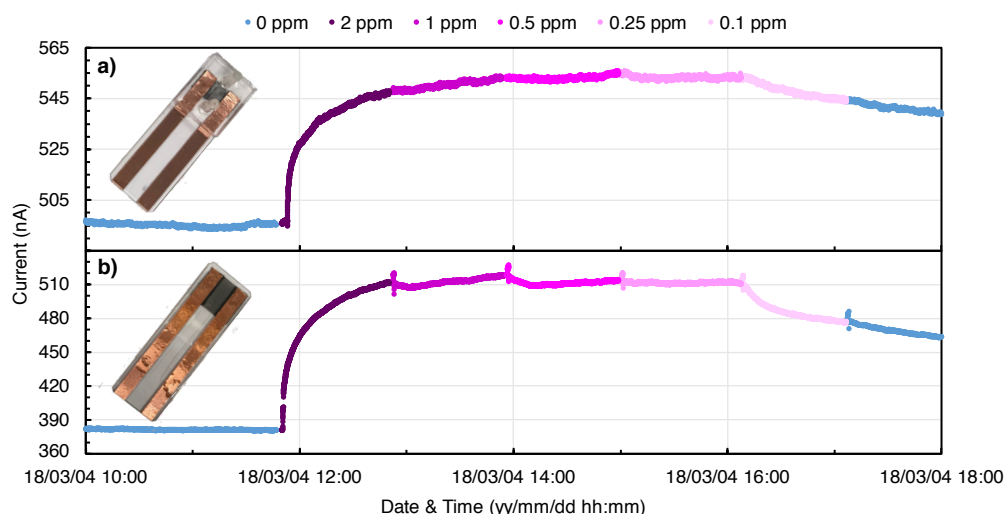


Figure 2.9. Sensing performance of two different sensing geometries: **a)** flow sensor and **b)** dip sensor. Insets: pictures of each type of device.

2.3. Analyte stability

2.3.1. pH of the solutions

When working with aqueous solutions, having a stable pH is very important. This parameter can affect the performance of the sensors, as

many of the molecules that are used to functionalize the transducing films have pH sensitive functional groups. The predominant chemical form of some analytes can also be affected by the pH of the solution. This can be solved with the addition of a buffer, but a lot of the preliminary testing needs to be done in ultrapure water to avoid interferences. Thus, it is important to know how stable the pH of ultrapure water is overtime. To study this a pH electrode (Van London Co. Tuff-Tip®) and a thermostat (eDAQ ET020) were connected to an eDAQ and they were immersed in an open beaker containing fresh ultrapure water. Figure 2.10 shows that the water started at a neutral pH but that it quickly dropped to 5.6 – 5.7, where it remained stable for the 5 consecutive days tested despite the changes in temperature. This pH value matches that of clean rain water perfectly.¹⁶ Ultrapure and rain water have low to negligible concentrations of ions. As a consequence, they have no buffering capacity and atmospheric CO₂ can dissolve in them, producing carbonic acid. Due to the stability of the pH in our measurements, it was decided that there is no need to monitor temperature or pH during the experiments. However, it is important to remember that the pH of the solutions is acidic when drawing conclusions about the performance of the sensors.

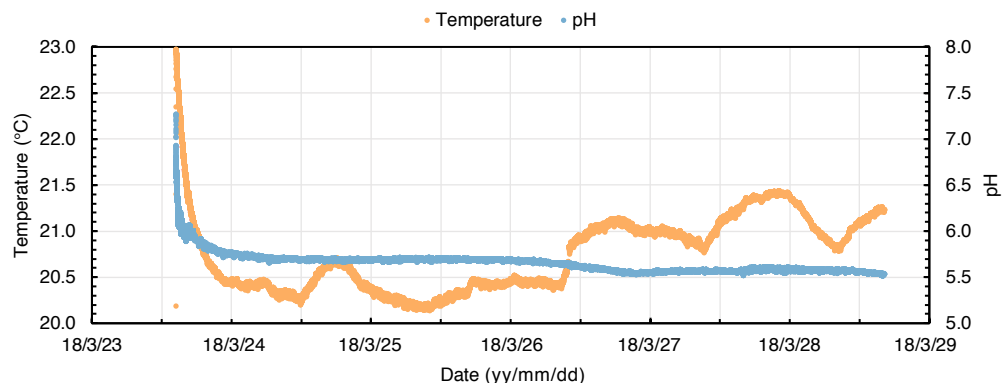


Figure 2.10. Long-term pH stability of ultrapure water when left in an open beaker. The temperature has no effect in the pH of the solution.

2.3.2. Free chlorine degradation

Chlorine solutions are known to be unstable and degrade through different mechanisms.^{5,16,112} This was found to be an issue while conducting long experiments with the dip sensors (Figure 2.11a), as the signal started to decay after less than one hour. The PDMS used to mask the copper tape has traces of platinum catalyst,¹⁴⁹ which can react with the analyte, lowering the concentration of free chlorine. In addition, the decay of the analyte was likely being exacerbated by the use of open vessels, which bring the solutions into contact with oxygen and do not renew the sample that is interacting with the sensors. This remained an issue despite having pretreated the glassware for chlorine demand by soaking it in diluted bleach for at least an hour.¹³⁶ In an attempt to solve the problem, flow sensors were tested. As it can be seen in Figure 2.11b, the solutions showed no sign of degradation even after 18 hours. This was confirmed by measuring the concentration of some fresh and old solutions with the DPD

method. Even though the samples do come into contact with PDMS, the surface area is smaller and the solutions only stay in the channel for less than a minute, so they do not have time to degrade. As a consequence, flow sensors were adopted as the standard device for experiments involving free chlorine.

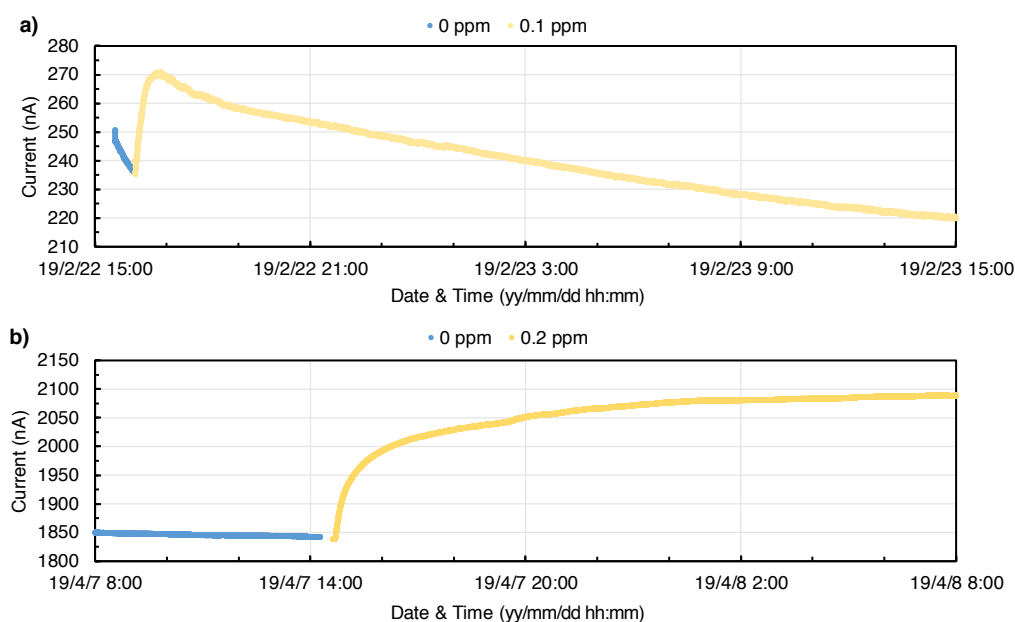


Figure 2.11. Long term stability of the concentration of free chlorine solutions using **a)** dip sensors and **b)** flow sensors. The time and amount of PDMS in contact with the solution affects the degradation of the solutions.

2.4. Summary

In this chapter the fundamentals of the characterization techniques used throughout the thesis have been summarized. These techniques are Raman spectroscopy, X-ray Photoelectron Spectroscopy and X-Ray induced Auger Electron Spectroscopy, the DPD colorimetric method, and conductance measurements of the chemiresistive sensors. Then, the fabrication processes

of different types of sensors have been outlined. The choice of transducing film (FLG or GLC), substrate (glass or PET), and sensor geometry (dip or flow) have been addressed. Finally, the stability of the analyte solutions has been discussed. The pH was found to reach a stable 5.6 value if unbuffered ultrapure water is used, and the free chlorine solutions were found to show minimal degradation if appropriately pretreated glassware is employed.

CHAPTER 3 — COPPER SENSORS

3.1. Introduction

In CHAPTER 1 the importance of monitoring copper was discussed, and our strategy for solving the problem was introduced. Following the idea of using dyes to functionalize the transducing film of chemiresistive sensors, 2,3-diaminophenazine (DAP) was used to dope the devices. DAP is a yellow molecule that turns colourless upon complexation with copper.¹⁵⁰ This specific compound was chosen because of its reported selectivity towards copper and its low solubility in water. In CHAPTER 2 the fabrication of different chemiresistive sensors was described. The design adopted here is a dip sensor geometry with a drop casted FLG transducing film. In this chapter we report and discuss the results obtained for the copper sensors.

3.2. Experimental details

3.2.1. Data acquisition

In order to study the changes in the conducting properties of the sensors a constant potential of 10 mV was applied across the FLG film. Higher voltages have been shown to cause electroplating of the metal on the surface of the nanocarbon film, which renders the sensors unresponsive to changes in concentration.⁴¹ Based on the anticipated signal amplitude, $\pm 2 \mu\text{A}$ was

chosen as the optimal sampling range. Every experiment began by dipping the sensors in methanol for about 10 minutes in order to clean and wet the FLG films, as well as to obtain a baseline signal. Functionalization was achieved by submerging the devices in a methanolic solution of DAP for about an hour, which leads to a drastic change in the signal as a result of the non-covalent bonding to the nanocarbon. They were then exposed to a blank solution overnight to get a baseline signal before running the analytes of interest. However, before dipping the sensors in the blank solution, they were rinsed with methanol followed by the blank. Finally, the sensors were exposed to the analyte solutions (after being rinsed with said solution). Figure 3.1 shows the raw data for the doping-sensing sequence described above and can be used as a proof of concept.

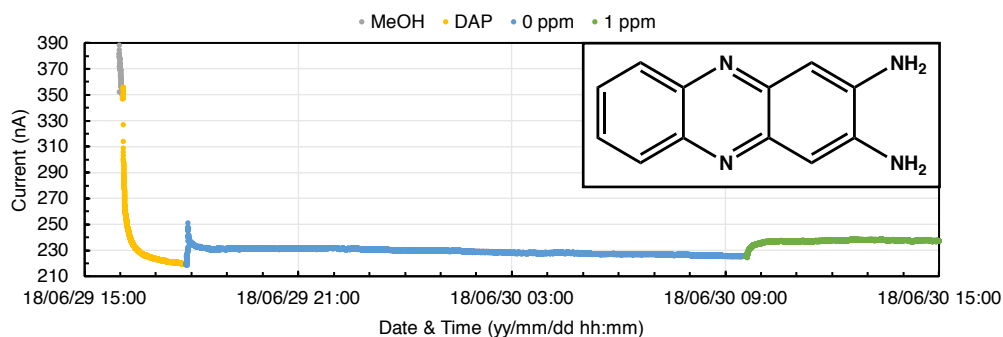


Figure 3.1. Doping-sensing sequence of a copper sensor (inset: structure of DAP).

3.2.2. Data quality

The quality of the signal was considered to be acceptable if the noise over a period of 10 minutes was similar to the noise inherent to the baseline. The standard deviation was used to estimate the noise because its value will be low on flat portions of the graph (i.e. stable measurement) but high on

portions that have not yet stabilized. For most sensors, the noise of the baseline was lower than ± 0.4 nA. The signal of the tested solutions was considered stable if the standard deviation was equal to or less than that value. In the few cases where that criterion was not met, the noise of the signal was no higher than the baseline noise + 15%.

3.2.3. Immersion mode: static or stirring and minimum concentration

One of the advantages of flow sensors is that the solution is continuously pumped into the system from a reservoir. This means that the solution that is in contact with the transducing film is always fresh, which minimizes local depletion and results in a signal that is more representative of the bulk sample. Equivalent experimental conditions could be achieved with dip sensors through the use of flow cells, but this was not a plausible option at this stage of the project. Thus, the sensors had to be immersed in vessels containing finite amounts of the solutions. However, if the amount of analyte needed to interact with the films is comparable to the amount of analyte in the vessel, the act of measuring the concentration could perturb the system and cause a non-representative result. This could be a concern at low concentrations, so the following calculation was run so as to determine whether or not 0.1 ppb of copper is an excessively low concentration.

There are 10^{15} atoms/cm² on the surface of a silicon wafer.¹⁵¹ Copper is about 1.2 times bigger, so it could be safe to assume that at least 10^{14} atoms/cm² would be required to cover the surface of the FLG film. If we take 1 mm³ as the volume of solution in immediate contact with the film, the number of copper atoms for a 0.1 ppb solution can be calculated as follows:

$$1 \text{ mm}^3 \text{ solution} \cdot \frac{0.1 \cdot 10^{-6} \text{ g Cu}}{(10^2 \text{ mm})^3 \text{ solution}} \cdot \frac{1 \text{ mol Cu}}{64 \text{ g}} \cdot \frac{6 \cdot 10^{23} \text{ atoms}}{1 \text{ mol Cu}} \approx 10^9 \text{ atoms/mm}^3$$

The size of the FLG film in a dip sensor is approximately 1 cm², so it would take 10^2 blocks of 1 mm³ to cover that area. Following our previous calculation, that volume would contain 10^{11} copper ions. Assuming that all the ions adsorb on the FLG film, we would get a 0.1% coverage:

$$\frac{10^{11} \text{ atoms in solution}}{10^{14} \text{ sites on film}} \cdot 100 = 0.1\% \text{ coverage}$$

According to the following calculation, we would need over 100 mL in order to get full coverage (i.e. adsorb copper ions on every available site on the film):

$$10^{14} \text{ atoms} \cdot \frac{1 \text{ mol Cu}}{6 \cdot 10^{23} \text{ atoms}} \cdot \frac{64 \text{ g Cu}}{1 \text{ mol Cu}} \cdot \frac{1000 \text{ mL}}{0.1 \cdot 10^{-6} \text{ g Cu}} = 107 \text{ mL}$$

Vessels with a capacity of 30 – 50 mL were being used, so a concentration of 0.1 ppb is too low to get a representative reading. Thus, the minimum concentration was increased to 10 ppb and vessels of 50 mL were used

exclusively. Under these conditions only 2% of the solute would be required to cover the entire FLG film, which was deemed an acceptable error.

$$50 \text{ mL solution} \cdot \frac{10 \cdot 10^{-6} \text{ g Cu}}{1000 \text{ mL solution}} \cdot \frac{1 \text{ mol Cu}}{64 \text{ g}} \cdot \frac{6 \cdot 10^{23} \text{ atoms}}{1 \text{ mol Cu}} \approx 5 \cdot 10^{15} \text{ atoms}$$

$$\frac{10^{14} \text{ sites on film}}{5 \cdot 10^{15} \text{ atoms in solution}} \cdot 100 = 2\% \text{ consumption}$$

In addition to increasing the lowest concentration, constant stirring was introduced as part of the experimental setup to enhance diffusion of the analyte to the film (i.e. minimize local depletion). This sped up the response of the sensors, which needed less time for the signals to stabilize (1 – 2 hours instead of 4 – 6).

3.3. Composition of the water

When studying a new system, it is advisable to start with the least possible unknown variables. This makes troubleshooting easier and helps understand the working mechanism. In the case of water quality sensors this would imply using solutions containing only the analyte. However, it might be necessary to add other chemicals in order to overshadow secondary processes or to stabilize the system. In this section we discuss the use of sodium chloride to increase the ionic strength of the solutions and the addition of sodium bicarbonate to stabilize the pH. The ultimate goal of these sensors is to monitor real water samples, which can have a rather complex matrix with a number of different ions dissolved in it. Thus, in this

section we also talk about testing the interfering power of ions commonly present in drinking water.

3.3.1. NaCl to control the ionic strength

The addition of small amounts of salt to ultrapure water will have a big effect on the ionic strength of the solution, which will affect its conductivity.^{152,153} A change in ionic strength will also result in a variation of the Debye length of the electric double layer that forms on the surface of the FLG films.^{153–155} The interdependence of these parameters can be seen on equations Equation 3.1 – Equation 3.3, where I is the ionic strength, c is the concentration of the ion, z is the charge of the ion, σ is the conductivity of the solution, F is the Faraday constant, μ is the mobility of the ion, and λ_D is the Debye length. Changes in any of these parameters could affect the conductance of the chemiresistive sensors, competing with the signal from the complexation of copper with DAP.¹⁵⁶ By introducing a constant background concentration of a salt that does not interfere with the sensing response, the changes in ionic strength due to the different concentrations of copper chloride can be made negligible. Sodium chloride at a concentration of 200 ppm (half the amount allowed in drinking water)¹⁷ was chosen for this. As it can be seen in Table 3.1, in the absence of sodium chloride, the change in copper concentration has a drastic effect on the ionic strength. However, after adding 200 ppm of NaCl, those changes become very small.

$$I = \frac{1}{2} \sum_i c_i z_i^2 \quad \text{Equation 3.1}$$

$$\sigma = \sum_i F \mu_i c_i z_i^2 = \sum_i F \mu_i 2I \quad \text{Equation 3.2}$$

$$\lambda_D \propto \frac{1}{\sqrt{2I}} \quad \text{Equation 3.3}$$

Table 3.1. Changes in the ionic strength of increasing concentration copper solutions before and after the addition of sodium chloride.

ppb (Cu)	I (μM)	% change	I (μM) + NaCl	% change + NaCl
10	0.47	—	3422.64	—
30	1.42	200	3423.59	0.03
100	4.72	233	3426.89	0.10
300	14.16	200	3436.33	0.28
1000	47.21	233	3469.38	0.96
3000	141.63	200	3563.80	2.72

In addition, the presence of sodium chloride significantly improved the resetting of the sensors (the resetting will be discussed in section 3.6). This can be appreciated in Figure 3.2, which shows that the magnitude of the response to 1 ppm of copper post-reset is closer to the initial response (pre-reset) when a background concentration of sodium chloride is used. Even though the NaCl does not seem to have a big impact on the magnitude of the initial response of the devices, in some cases it caused the signal to

stabilize faster. These observations could be a result of the decrease in the Debye length with increasing ionic strength. If the thickness of the electric double layer is smaller, it should be easier for the copper ions and the resetting agent to diffuse to and from the FLG film.

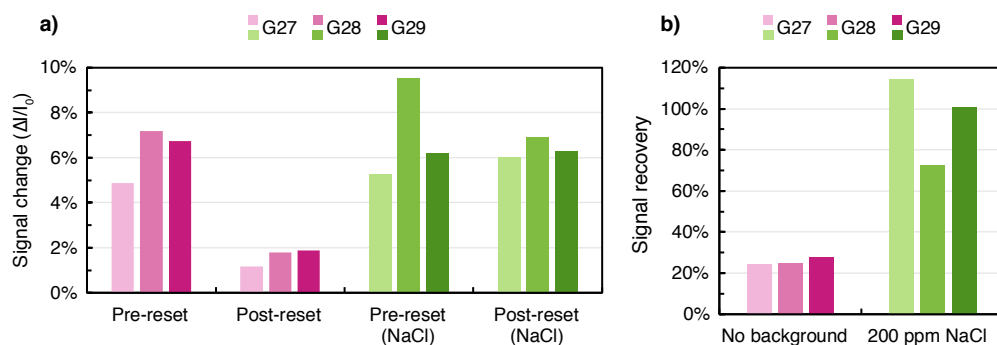


Figure 3.2. Effect of adding a 200 ppm NaCl background concentration on the resetting efficacy. **a)** Response of three sensors to 1 ppm of copper pre-reset and post-reset in the absence of NaCl (pink) and with 200 ppm of NaCl (green). **b)** Resetting efficacy given as the signal recovery (post-reset signal change to pre-reset signal change ratio).

3.3.2. NaHCO_3 to control the pH

The pH of the solutions is expected to impact the performance of the sensors due to its effect on the following aspects: the electric double layer,^{34,156,157} the protonation of defects in graphene,¹⁵⁸ the protonation of the amines in DAP,¹⁵⁰ and the solubility of copper.¹⁵⁹ Thus, keeping a stable pH throughout the experiments can significantly impact the results. Even though the pH of ultrapure water was found to maintain a reasonably constant value of 5.6 (see CHAPTER 2), it was decided to add carbonate to bring the pH of the samples closer to neutrality. This compound is naturally found in drinking water and it is sometimes used to increase its pH. Together with bicarbonate, it is the main source of alkalinity, which

measures the ability of water to withstand changes in pH due to the addition of an acid.¹⁶ There are no guideline values for this parameter, but it is usually found in the range of 10 – 300 ppm (expressed as calcium carbonate).¹⁶ An alkalinity of 50 ppm was targeted for the experiments, which is half the amount commonly found in Toronto drinking water.¹⁶⁰ Sodium bicarbonate and sodium carbonate were used to prepare solutions with that alkalinity value. However, a calculation error was made during the experimental design and 42 ppm sodium bicarbonate were used, which is equivalent to 25 ppm calcium carbonate. No mistakes were made for sodium carbonate and 53 ppm were used, which equals 50 ppm calcium carbonate. The pH of the solutions was measured with a pH meter and the values were compared to those of tap water (Table 3.2).

Table 3.2. pH of 42 ppm sodium bicarbonate and 53 ppm sodium carbonate solutions (fresh and overnight), and pH of different tap water samples.

Solution	pH (fresh)	pH (overnight)
42 ppm NaHCO ₃	7.7	7.5
53 ppm Na ₂ CO ₃	10.1	8.4
Lab tap water	7.5	—
Home tap water	7.7	—

The solution containing sodium bicarbonate was found to have the pH closest to tap water and it was able to maintain a stable pH over time, as opposed to sodium carbonate. The drop in pH observed for the latter could be a result of having the solution in an open vessel. The carbonate in solution will establish an equilibrium with the carbon dioxide in air, leading

to a partial neutralization of the solution. No evidence was found of sodium bicarbonate interfering with the sensor performance, so that salt was chosen for the experiments. Even though increasing the pH of the solutions can cause the precipitation of copper due to the formation of copper hydroxide and copper oxide, the presence of bicarbonate leads to the formation of water soluble carbonate complexes.^{159,161–163} Having a constant background concentration of NaCl and NaHCO₃ during the development of the sensors should have the advantage of making transitioning to real water samples easier.

3.4. Interferences

A big concern during the development of the sensors was their response to other ions commonly present in water. Bare graphene is known to be easily doped by a variety of molecules and atoms,^{61,63,64,164} and the literature is not conclusive on the selectivity of DAP towards copper.^{165,166} The effect of the following ions was planned to be studied: cations potassium, sodium, calcium, and magnesium; anions sulphate, nitrate, and phosphate; and trace metals iron, nickel, and zinc. The concentration of the cations and anions was set to 50 ppm and the trace metals were set to 1 ppm. Stock solutions were made using sodium or chloride salts, as these counterions have been shown to not interfere and are already present in the 200 ppm NaCl background concentration. The sensors were introduced in vessels containing the blank solution and they were spiked with each ion to a final concentration of 50 ppm or 1 ppm, finishing with 100 ppb of copper in order

to see whether or not the sensors could still detect the analyte at low concentrations. So as to simulate real water, this was done cumulatively, such that the final solution contained a mixture of all the ions.

Due to issues with the stability of the devices, the experiment outlined above could not be completed. Only the interferences from the cations could be studied and the response to copper was lower than expected. Figure 3.3a shows the signal change for two DAP functionalized sensors exposed to the aforementioned cations. All of them gave a response, with magnesium and calcium being the biggest interferences. The response of sensor G65 to the interferences is smaller than sensor G66, whereas the response to copper is bigger. This could be due to a non-optimized functionalization of the FLG films. If DAP was more uniformly deposited on sensor G65, the film would be better shielded from interferences and the response towards copper would be enhanced, whereas the opposite would be true for G66 if the functionalization was less uniform.

Owing to the scarcity of data, the results from some preliminary testing conducted on flow sensors have been included in Figure 3.3b. Sensors G2 and G3 were run as blanks, while G10 was functionalized with the ligand. The ions were run in series in the absence of sodium chloride and sodium bicarbonate, and the concentrations were slightly different: 58 ppm of magnesium, 96 ppm of calcium, and approximately 1 ppm (more specifically 20 μ M) of the trace metals including copper. All the ions studied decreased the conductance of the devices, except for iron and copper.

Overall, these experiments seem to indicate that the sensors have selectivity issues, and the similarities in behaviour between the functionalized and blank sensors raise the question of whether or not DAP is effectively shielding the FLG film. Thus, further experimenting needs to be done in order to optimize the selectivity of the devices. It is worth mentioning that the concentrations selected for the ions are below their guideline values (except for nitrate with a MAC of 45 ppm and iron with an AO of 0.3 ppm),¹⁷ but they are well above the concentrations usually found in drinking water.¹⁶⁰ As a consequence, the interferences are expected to be smaller in a real water sample.

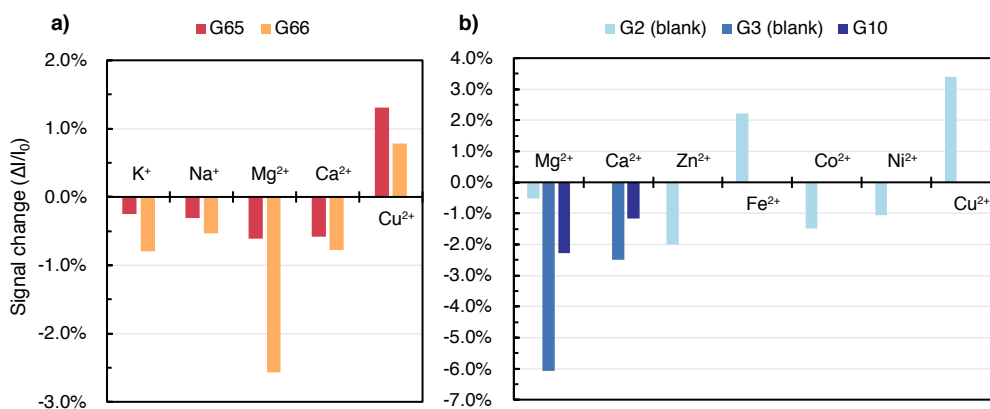


Figure 3.3. Interference study. **a)** Response of two doped dip sensors to the presence of cations commonly found in drinking water. The concentration of the cations is 50 ppm and copper is 100 ppb. All ions were added cumulatively. **b)** Response of three flow sensors to the presence of some cations and trace metals. The concentration of magnesium is 58 ppm, calcium is 96 ppm, and the trace metals including copper is 20 μ M (approximately 1 ppm). The devices were exposed to each ion in sequence. Sensors G2 and G3 were run as blanks while G10 was functionalized. The solutions contained no $NaHCO_3$ or $NaCl$ background.

3.5. Calibration curves

A calibration curve establishes the relationship between the concentration of the analyte and the output signal. Solutions of known concentration (standards) must be used for the calibration, so a single copper stock solution was used to make all dilutions in order to be as precise as possible. Then, the sensors were exposed to the standards in increasing concentration order and the output signal was recorded. The resulting curve can be used to determine the amount of copper in an unknown sample. In the early stages of the project, the calibration curves were obtained by dipping the sensors in different vessels containing the standards. However, due to issues with the mechanical stability of the films, the experimental design was changed to a step-up addition calibration curve, where the vessel is spiked with increasing concentrations of copper so that the sensors do not have to be removed from the solution at any point. A volumetric flask was used to add the same amount of blank solution to each vessel, and micropipettes were used to spike the solutions. Due to the fact that the vessels are open to the atmosphere, any evaporation of the solvent must be accounted for in order to report precise concentrations. This was achieved by using a control vessel, which was weighed before every copper addition and the mass lost was recorded. Then, that same mass of water was added to every vessel to restore the initial volume (assuming 1 g/mL density). The evaporation rate depends on the ambient humidity, so it should always be taken into consideration to ensure reproducibility of the

results. The concentration range tested was 10 ppb to 3 ppm, which includes the 1 ppm limit set by government regulations. Even though the quality of the signal was acceptable within 1.5 hours of being exposed to a new concentration, data was recorded for at least 2.5 hours. The raw data collected with one of the sensors is shown in Figure 3.4a.

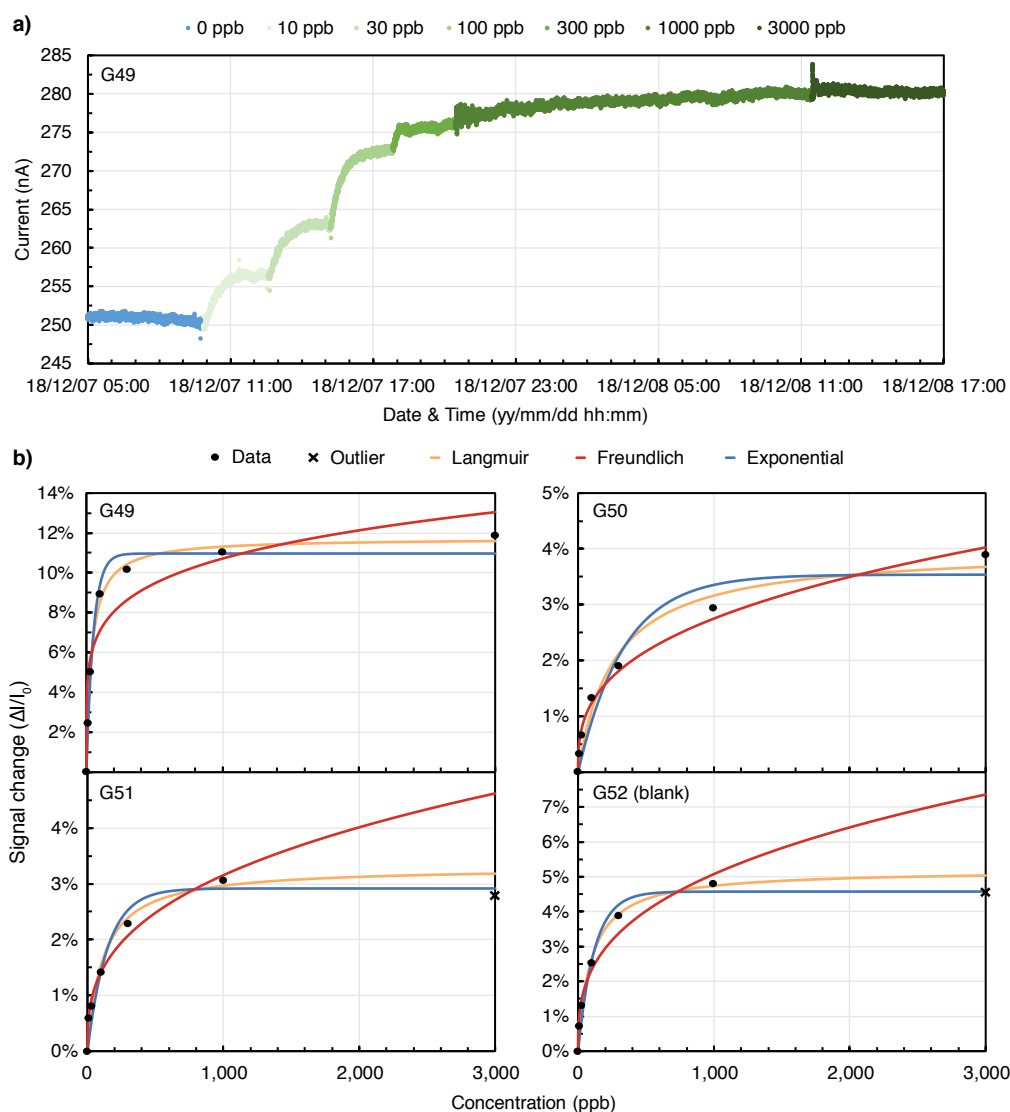


Figure 3.4. Calibration curves obtained with the copper sensors. Sensors G49, G50, and G51 were doped with DAP while G52 was run blank. **a)** Raw data collected with sensor G49. **b)** Curve fittings: Langmuir adsorption isotherm, Freundlich adsorption isotherm, and exponential decay.

Figure 3.4b shows the calibration curves obtained for each of the sensors (three functionalized and one blank). The percentage change was calculated by averaging a minute of data at the 2.5-hour mark and comparing it to the baseline. The following curve fittings were tested: a Langmuir adsorption isotherm, a Freundlich adsorption isotherm, and an exponential decay. These models were studied because they could provide a reasonable explanation for the sensing mechanism. The Langmuir isotherm (Equation 3.4) models the adsorption of a monolayer where the adsorbates do not interact with each other and in which the system reaches saturation at some point. In the equation, q is the amount of adsorbate adsorbed, C is the equilibrium concentration of adsorbate in solution, K_L is the Langmuir constant (indicative of the affinity of the binding sites), and q_M is the theoretical saturation point.¹⁶⁷ On the other hand, the Freundlich isotherm (Equation 3.5) models the adsorption mechanism of multilayers and heterogeneous surfaces. Similarly, q is the amount of adsorbate adsorbed, C is the equilibrium concentration of adsorbate in solution, and K_M and n are the Freundlich constants, where K_M is a measurement of the adsorption capacity and n indicates adsorption strength.¹⁶⁸ Finally, a formula for an exponential decay (Equation 3.6) was developed because it fulfils the conditions of going through zero (there should be no sensor response at concentration zero) and saturating at a specific concentration (represented by b in the equation). In the case of the Langmuir and Freundlich isotherms it has been assumed that the amount of adsorbate adsorbed is proportional

to the sensor response and that the adsorbate in solution is in excess such that the equilibrium concentration can be assumed to be the initial concentration (see section 3.2.3 for a calculation proving the latter assumption). In our curve fittings, y stands for sensor response, x stands for concentration in ppb ($\mu\text{g/L}$), and a ($\text{L}/\mu\text{g}$) and b are the curve parameters. The curve parameters obtained for each sensor are summarized in Table 3.3, as well as the coefficients of determination.

$$q = q_m \frac{K_L C}{1 + K_L C} \Rightarrow y = b \frac{ax}{1 + ax} \quad \text{Equation 3.4}$$

$$q = K_F C^{1/n} \Rightarrow y = ax^{1/b} \quad \text{Equation 3.5}$$

$$y = b(1 - e^{-ax}) \quad \text{Equation 3.6}$$

Table 3.3. Constants and coefficients of determination for the calibration curves.

Sensor	Langmuir			Freundlich			Exponential		
	a ($\text{L}/\mu\text{g}$)	b	R^2	a ($\text{L}/\mu\text{g}$)	b	R^2	a ($\text{L}/\mu\text{g}$)	b	R^2
G49	0.0266	0.1174	0.997	0.0311	5.5873	0.900	0.0194	0.1097	0.985
G50	0.0038	0.0400	0.976	0.0025	2.8850	0.988	0.0030	0.0354	0.943
G51	0.0088	0.0330	0.975	0.0029	2.8779	0.989	0.0068	0.0292	0.950
G52	0.0104	0.0520	0.996	0.0049	2.9604	0.967	0.0083	0.0458	0.980

The model that fits best changes from sensor to sensor. However, the difference is not very big, and the Langmuir adsorption isotherm seems to

provide the best fit overall. Similar systems have been shown to be described by a Langmuir isotherm,^{168–171} but the Freundlich isotherm is often included in the discussion and in some cases it provides a better or similar fit.^{172,173} The disparity between sensors can be due to inconsistencies in the film morphology or improper deposition of the ligand. Thus, further optimization and testing are required before settling on a model. The curves as presented in Figure 3.4 are not in a very friendly format to interpret the data, a linear regression is much preferred. The Langmuir adsorption isotherm can be linearized according to Equation 3.7. The resulting plots and equation parameters are shown in Figure 3.5 and Table 3.4 respectively. Resetting the devices and determining the concentration of a spiked blank using the calibration curves was attempted. However, the estimated concentrations were far from the actual ones. This could be due to the issues with the transducing films introduced earlier, so further optimization and testing are required.

$$\frac{C}{q} = \frac{1}{q_m K_L} + \frac{C}{q_m} \Rightarrow \frac{x}{y} = \frac{1}{ba} + \frac{x}{b} = A + Bx \quad \text{Equation 3.7}$$

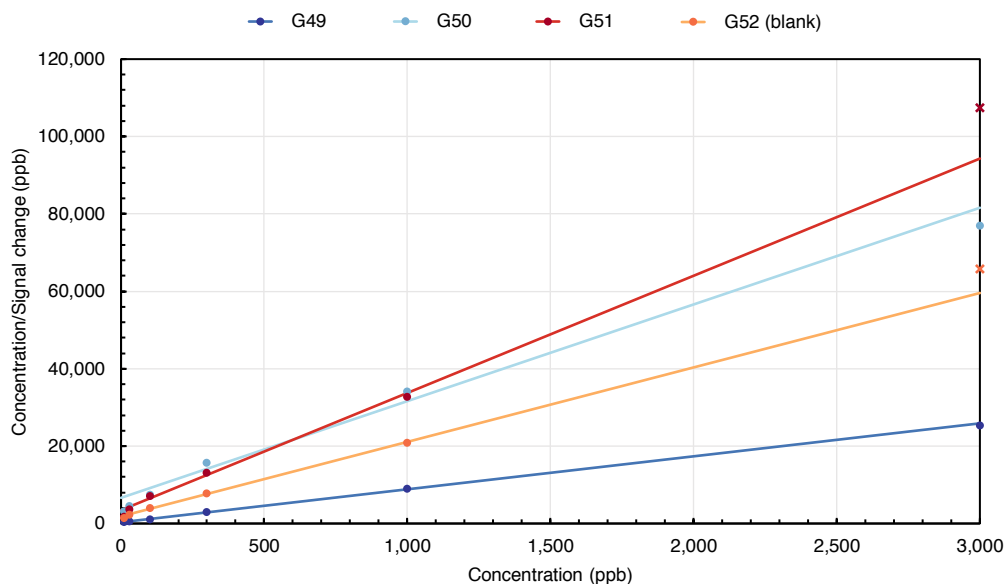


Figure 3.5. Linearized Langmuir adsorption isotherms of the copper sensors.

Table 3.4. Equation parameters for the linearized Langmuir adsorption isotherm.

Device	A ($\mu\text{g/L}$)	B
G49	320.26	8.52
G50	6631.23	24.99
G51	3451.29	30.28
G52	1854.79	19.24

It is worth mentioning that the data point for 3000 ppb was considered an outlier in sensors G51 and G52 due to the fact that the sensor response was lower than for the previous concentration. This could indicate saturation of the sensor. Interestingly, the degree of saturation seems to be correlated to the thickness of the FLG film. For films of similar dimensions, the thickness can be estimated from the resistance, with thicker films having a lower resistance due to the formation of an enhanced percolation network.

We hypothesize that thicker films should saturate at higher concentrations, as the surface area with which the analyte can interact is bigger (more FLG layers to diffuse through). The resistance values of the doped sensors increase in the sequence G50 (12.3 k Ω) < G49 (16.4 k Ω) < G51 (19.9 k Ω), which is in fact the trend observed in Figure 3.4 for the saturation points. The blank has a resistance of 14.4 k Ω , which according to this trend should lead to no saturation in the concentration range tested. However, it does saturate, which we hypothesize is a consequence of the absence of DAP. The presence of the ligand might be improving the working range of the devices. Due to previously discussed issues, further optimization and testing is required in order to study this hypothesis.

3.6. Resetting

In order to continuously monitor copper, the sensors need to be reset between measurements. Otherwise, they are limited to being single-use sensors. In section 3.3.2 we discussed that the pH of the solutions could impact the performance of the sensors. One of the mentioned reasons was that an acidic pH will protonate the amine functionalities of DAP. The binding of copper to DAP happens at the amine sites,¹⁵⁰ so their protonation should prevent them from forming complexes. Thus, by exposing the sensors to an acidic solution a reset could be achieved. In order to study this, multiple reset-sense cycles were performed on the sensors. Each cycle involved exposing the devices to an acidic solution to reset them, followed by a blank to restore the pH and get a baseline, and finishing with 1 ppm of

copper. The signal change was compared to the response obtained with the fresh sensor in order to study the efficacy of the reset. We found that multiple reset-sense cycles could be performed in a row with good reproducibility, and that the pH of the resetting solution impacts the efficacy of the reset. The raw data for two reset-sense cycles at different pH values is shown in Figure 3.6a, and the recovery of the signal for three doped sensors and a blank are shown in Figure 3.6b. The pH was lowered to 3 by adding hydrochloric acid, the pH 5.6 was obtained by letting ultrapure water equilibrate with the carbon dioxide in air, and the pH 7.5 solutions were made by adding 42 ppm of sodium bicarbonate. All the solutions were prepared with a background concentration of 200 ppm sodium chloride. The reset at pH 3 was found to work best, in agreement with the literature.¹⁷⁴ However, the data collected seems to indicate that the pH 5.6 solution could also work provided that the sensors are given more time to reset.

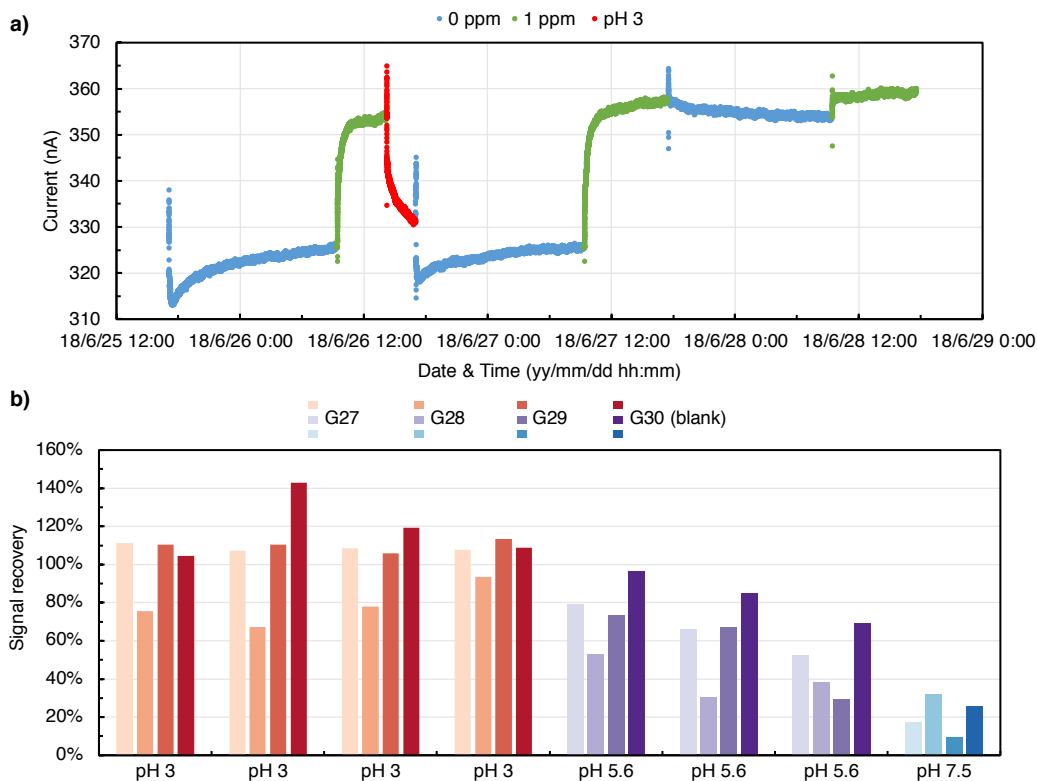


Figure 3.6. Reset-sense cycles. **a)** Raw data from two reset-sense cycles, the first one at pH 3 and the second one at pH 7.5. **b)** Resetting efficacy on four sensors given as the signal recovery (post-reset signal change to pre-reset signal change ratio). Each set of colours represents a different pH of the resetting solution.

Although here we acidified the solutions with hydrochloric acid, the reset could be made reagent-free by electrochemically splitting water, which could be optimized to locally acidify the solution close to the surface of the film.^{175–178} Other resetting strategies could be explored, such as copper sequestration with a chelating agent like EDTA.^{179,180} However, this could lead to unwanted functionalization of the FLG films and reagent-free approaches are much preferred.

3.7. Characterization of the sensors using XPS

A small amount of ligand and a set of sensors were sent for XPS analysis in order to confirm the functionalization of the films and to gain more insight into the sensing mechanism. The samples were analyzed using a Kratos AXIS Ultra X-ray photoelectron spectrometer. XPS survey spectra were obtained from an area of approximately $300 \times 700 \mu\text{m}$ using a pass energy of 160 eV. XPS high resolution spectra were obtained from an area of approximately $300 \times 700 \mu\text{m}$ using a pass energy of 20 eV. The devices sent for analysis were exposed to the same sequence of solutions. However, they were removed from the solutions at different stages in order to get a complete picture of the reset-sense cycle. The scheme is outlined in Figure 3.7. All the devices were rinsed with ultrapure water at the end and they were stored under an inert nitrogen atmosphere until the time of analysis.

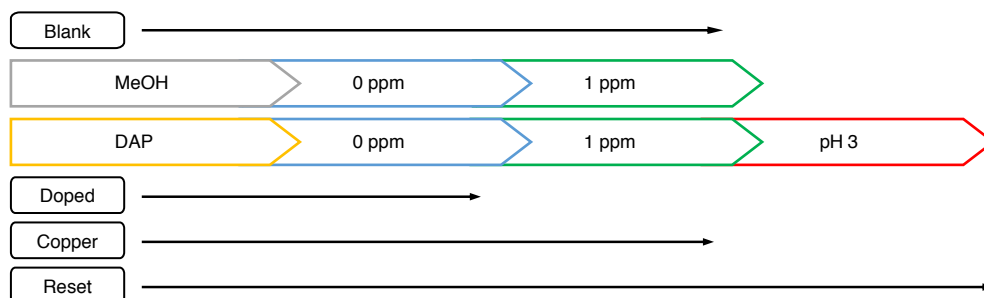


Figure 3.7. Scheme of what solutions the sensors were exposed to before XPS analysis.

First, a survey scan was collected in order to determine the elemental composition of the ligand and the sensor films. The atomic percent of each detected element can be seen in Table 3.5. The atomic makeup of the DAP sample reveals the presence of impurities. The ligand was used as

purchased, so we can only hypothesize the origin of those impurities. The high oxygen and silicon content could be explained by the use of column chromatography to purify the compound. The synthesis of DAP often involves the use of an organometallic catalyst with an iron centre, which would explain the trace amounts of iron, the unexpected carbon to nitrogen ratio (higher than the 3 to 1 predicted from the molecular structure), and some of the oxygen.^{181–183} In the case of the set of sensors, the high carbon content can be easily explained by the FLG films, while the oxygen and the silicon probably arise from the glass slides used as substrates for the sensors. The fact that oxygen and silicon are easily detected with XPS, a highly surface sensitive technique, suggests that the films do not uniformly cover the glass slides. All the sensors show small amounts of sodium and chloride, which could be explained by the 200 ppm NaCl background concentration used in every solution. Surprisingly, the blank sensor has small amounts of nitrogen. This could be a consequence of having stored the sensors under a nitrogen atmosphere (argon might have been better). The amount of nitrogen on the doped devices is significantly larger, indicating that the films were successfully functionalized. The percentage of nitrogen does not decrease in going from the doped sensor to the copper and reset sensors, suggesting that the ligand does not come off the FLG films after binding to copper or after being protonated. Finally, the fact that the concentration of copper is negligible in the doped sensor but increases significantly in the copper sensor and completely disappears in the reset

sensor provides proof that the reset-sense cycles work. It should be noted that the presence of copper on the blank sensor does not come as a total surprise as graphenic materials are easily doped.

Table 3.5. Elemental composition of the ligand and the transducing films. Obtained through XPS analysis and given as atomic percentage.

Sample	C	Cl	Cu	Fe	N	Na	O	Si
Ligand	73.4	—	—	0.1	15.7	—	8.1	2.7
Blank	79.1	0.4	1.0	—	0.7	0.5	14.8	3.5
Doped	79.6	tr.	0.1	—	2.0	0.6	13.7	3.8
Copper	76.2	0.1	0.9	—	2.4	0.7	15.4	4.3
Reset	79.5	0.1	—	—	1.9	0.6	13.9	4.0

Next, high resolution spectra of oxygen, copper, carbon, and nitrogen were collected. The oxygen spectra revealed that it was in the form of water, organic oxygen, silicon oxide, and hydroxide. In the case of copper, the shake-up line of the $2p_{3/2}$ peak indicates that it is Cu(+2).¹⁸⁴ Shake-up lines appear at higher binding energies than the main peak, and their intensities and chemical shifts are characteristic of the chemical state of the atom.¹³⁴ The shape and position of the Auger LMM peak also suggest that copper is in the (+2) oxidation state (for Ref. ¹⁸⁴ note that under our experimental conditions a binding energy of 572 eV equals approximately a kinetic energy of 915 eV).^{184,185} These observations were consistent for all the sensors, so the copper spectra of only one of them is provided as an example in Figure 3.8. The fact that copper keeps its oxidation state after being exposed to the sensor indicates that there are no electrochemical processes

happening. This was a problem when 100 mV were used to probe the sensors, which led to electroplating of the metal.⁴¹ However, it does not seem to be an issue when 10 mV are used. The carbon spectra reveal that around 40% of the carbon atoms do not participate in carbon-carbon double bonds. Instead, they show carbon-carbon and carbon-hydrogen single bonds, in addition to single and double bonds with oxygen. This suggests that defects were introduced during the production of the FLG suspensions, in agreement with the Raman data discussed in CHAPTER 2. However, no statements can be made on the nature and proportion of the defects, as the XPS signals will depend on the uniformity of the films and will also reflect the presence of adventitious carbon. It should also be mentioned that this particular set of sensors was fabricated with an airbrush, so outgassing from the hoses is also a possible explanation. For qualitative discussion purposes, the percentage areas of each carbon signal have been averaged for all sensors and they have been plotted in Figure 3.8d. Interestingly, it was observed that the area of the carbon-carbon double bond peak became smaller the longer the sensors were left in the solutions (blank \approx doped < copper < reset). This could indicate that carbon-based impurities are being deposited on the films (e.g. bicarbonate or VOCs). However, no final conclusions can be drawn at this time.

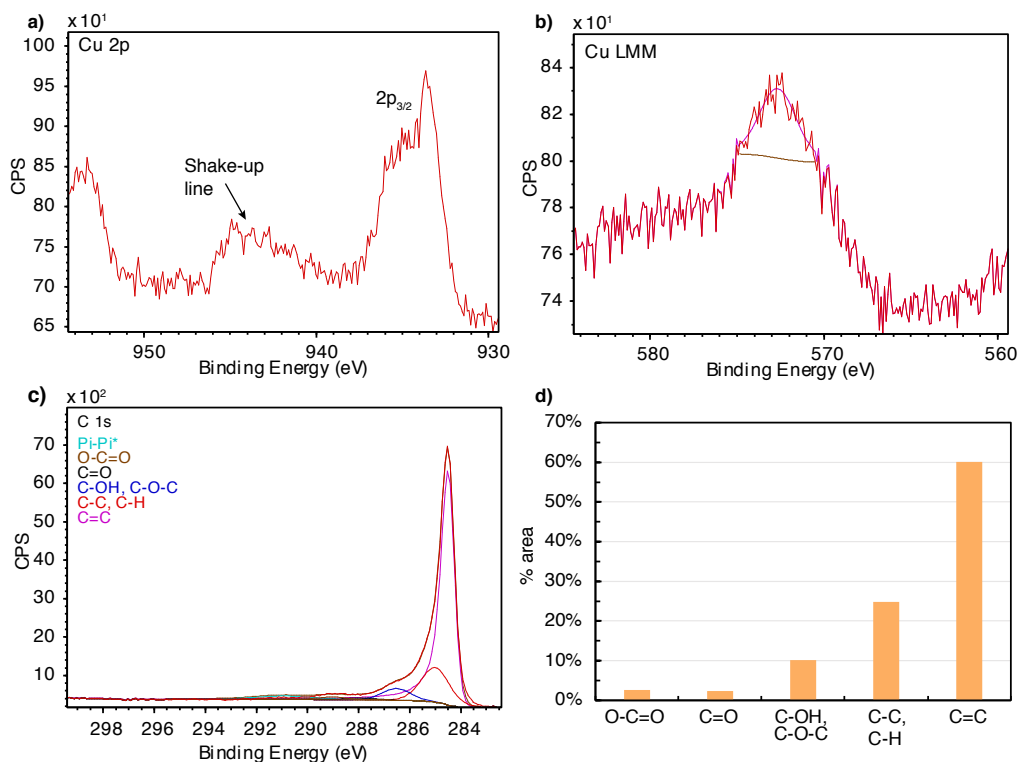


Figure 3.8. High resolution XPS spectra of copper and carbon. Only the spectra collected on the blank sensor are shown, but the results are consistent on all four sensors. **a)** Cu 2p spectrum. The 2p_{3/2} shake-up line indicates the presence of Cu(2+). **b)** Auger LMM line. Its position and shape confirms the presence of Cu(2+). **c)** C 1s spectrum (inset: colour code of the different types of carbon). **d)** Percentage area of the different types of carbon. The values shown are the average over all four sensors.

The high-resolution spectra of nitrogen provided good insight into the sensing mechanism. The 1s peak can be deconvoluted into two different signals: peak 1 at around 401.0 eV and peak 2 at around 399.4 eV. This energy range corresponds to organic nitrogen,¹³⁴ which could be explained by the functionalization of the films with 2,3-diaminophenazine. Interestingly, the area of the peaks is different for each sample. The spectra are shown in Figure 3.9, together with a bar graph of the percentage areas for easier visualization. The ligand and the doped sensor have an almost identical footprint, which suggests that DAP is unaffected by the deposition

onto the FLG films. After exposing the sensor to copper, peak 1 more than doubles in area. This seems to indicate that copper successfully binds to the ligand. The efficacy of the reset is supported by the absence of copper (Table 3.5) and the disappearance of peak 1. The fact that it does not drop back to 7% (as in the ligand and the doped sensor) could be explained by the presence of impurities in the DAP sample. It is possible that the reset removes those impurities, which would fit with some of the experiments where it was noticed that the second and subsequent sensor runs were slightly different than the first one. Thus, it might be advisable to always begin with a reset. The detection of copper results in an increase of the nitrogen signal with a higher binding energy, meaning that it is harder to abstract an electron. This will lead to p-doping of the FLG films, which modulates the conducting properties and in the case of our system increases the conductivity.

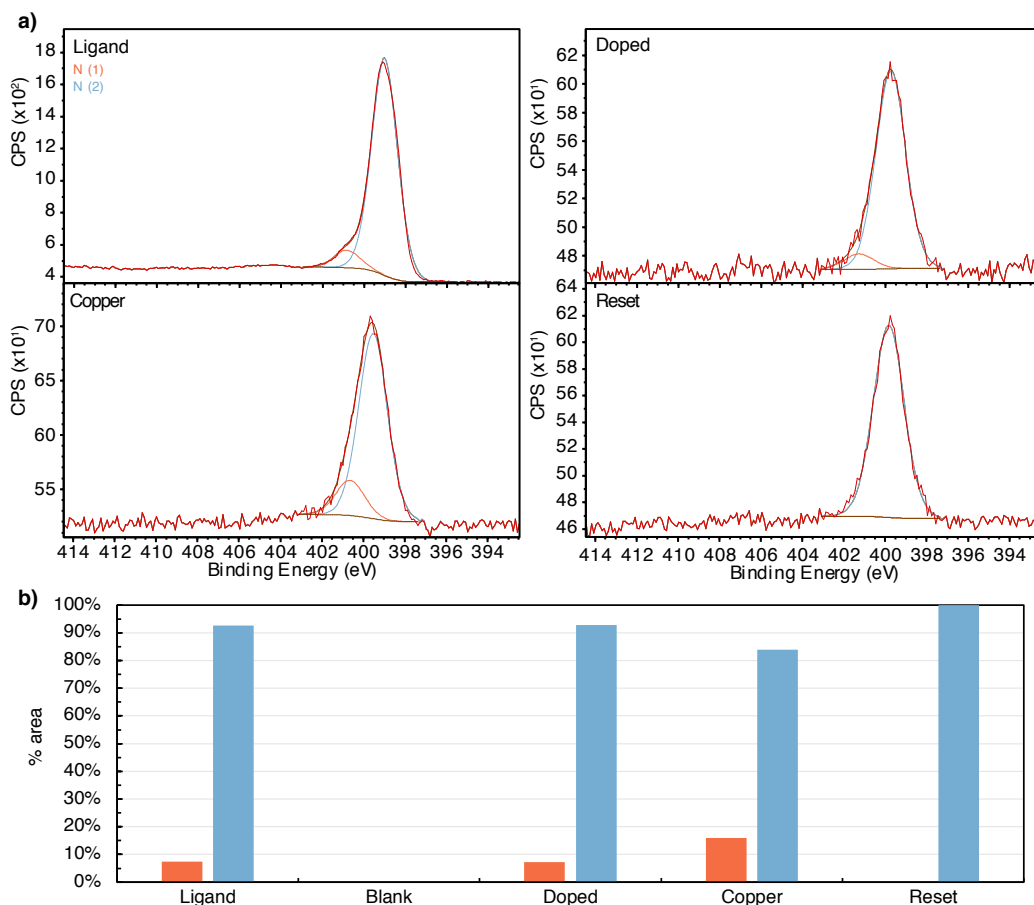


Figure 3.9. a) High-resolution spectra of nitrogen for the ligand and the sensors. b) Breakdown of the percentage area of the two nitrogens.

3.8. Summary

Exfoliated few layer graphene suspensions were produced and used to make sensors for the first time in the group. The dip sensor geometry was developed and successfully implemented. The use of sodium chloride and sodium bicarbonate to control the ionic strength and the pH of the solutions was introduced. Preliminary testing on interferences by other ions commonly present in drinking water was carried out. Two ways of obtaining calibration curves were explored, and it was found that the data

could be described by different models, including a Langmuir isotherm. The thickness of the films was found to be a possible cause for different saturation points of the devices. The sensors were reproducibly reset multiple times with a pH 3 solution, and the acidity of the solution was found to be related to the efficacy of the reset. XPS was used to further characterize the sensors, which provided information about the functionalization of the films, the sensing mechanism, and the presence of defects and impurities. Different weaknesses have been detected, which will be discussed and outlined in CHAPTER 5 as future work. Overall, we have shown that the development of a chemiresistive sensor for the continuous monitoring of metal cations is possible.

CHAPTER 4 — FREE CHLORINE SENSORS

4.1. Introduction

In CHAPTER 1 the importance of maintaining adequate free chlorine levels in drinking water in order to control the growth of harmful pathogens was highlighted. Chemiresistive sensors were introduced as a possible solution for the continuous monitoring of free chlorine concentrations. Transducing films fabricated with PCAT-functionalized single walled carbon nanotubes and pencil paths were presented as the state of the art. PCAT is readily oxidized by chlorine following the scheme depicted in Figure 4.1, which affects the electron transport properties of the carbon films and leads to a change in resistance. Substituting the aforementioned materials for graphene-like carbon (GLC) was suggested so as to overcome some limitations, such as the difficulty detecting fluctuations in concentration. In CHAPTER 2 we described the fabrication process of GLC flow sensors, and some comments were made regarding the stability of free chlorine solutions. In this chapter we report and discuss the data collected with GLC sensors.

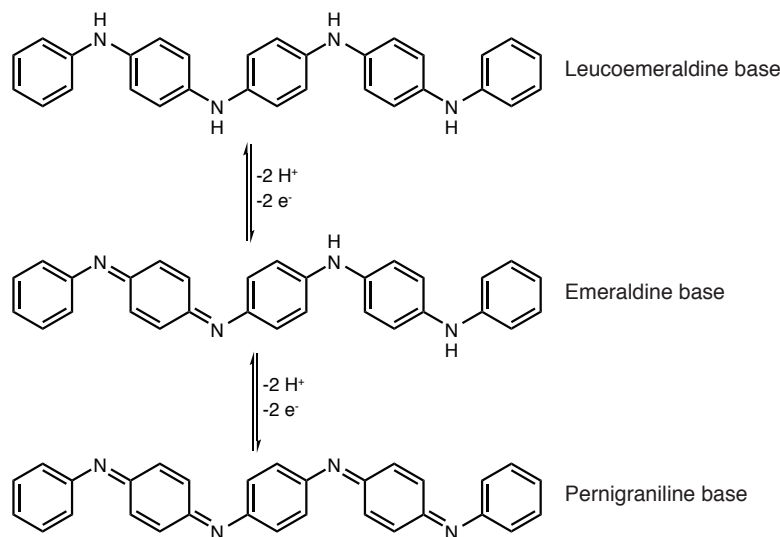


Figure 4.1. Reduction-oxidation reaction of PCAT. Exposure to free chlorine pushes the equilibrium towards the pernigraniline base.

4.2. Experimental details

4.2.1. Data acquisition

Conductance measurements were taken by applying a constant potential of 100 mV across the GLC film. Given the inherent resistance of the sensors, a sampling range of $\pm 2\ \mu\text{A}$ was determined to be optimal in most cases. For those sensors in the lower end of the resistance range it had to be increased to $\pm 20\ \mu\text{A}$. A two-channel peristaltic pump was used to flow the solutions through the devices at a 0.2 mL/min rate. In order to be able to study four sensors simultaneously, they were connected in series in sets of two (i.e. outlet of the first one turns into inlet of the second one). All experiments started with a 5-minute methanol run in order to clean and wet the channels, as well as to obtain a baseline signal. The set of doped sensors followed with a 30-minute run of a methanolic solution of PCAT, which

resulted in a dramatic change in signal due to the functionalization of the films. The set of blank sensors was exposed to methanol for the same amount of time. The last step in the doping protocol was a 5-minute methanol rinse. All sensors were exposed to fresh ultrapure water overnight in order to get a baseline before proceeding with the analyte solutions. Figure 4.2 shows the raw data for the doping-sensing sequence and provides proof of concept. The glassware used in the experiments was pretreated for chlorine demand as described in CHAPTER 2, and the tubing material was carefully chosen to avoid the presence of catalyst traces from the manufacturing process, which would cause depletion of the free chlorine solutions. The feed tube was replaced before switching to water in order to get rid of any PCAT that could have adsorbed onto the walls.

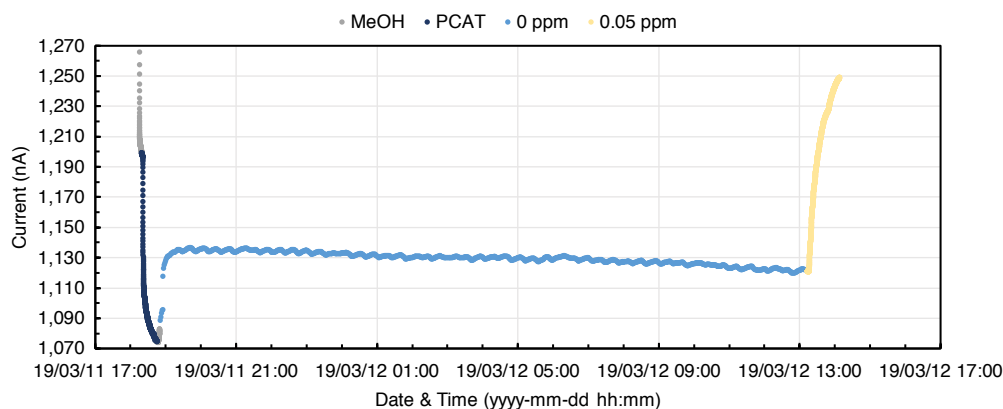


Figure 4.2. Doping-sensing sequence of a free chlorine sensor.

4.2.2. Data quality

The reproducibility of the signals is limited to ± 1 nA due to unexplained intermittent fluctuations. They had a periodicity of approximately 40

minutes and were synchronized between all four sensors, so they are caused by external factors in the experimental setup. However, we were unable to trace back their origin. The fluctuations can be clearly seen in the water signal in Figure 4.2. Regarding the stability of the signals, the noise after 25 minutes of data collection was found to be less than ± 0.5 nA. This was significantly smaller than 5% of the total response, so the signal was considered to be stable. Following a similar reasoning to that explained in CHAPTER 3, the noise was estimated by calculating the standard deviation of one minute of data.

4.2.3. Composition of the water

While having a background concentration of 200 ppm of sodium chloride was beneficial for the performance of the copper sensors, it was found to negatively impact the quality of the signal in free chlorine sensors. The addition of sodium chloride resulted in significantly smaller and noisier signals. This problem had already been encountered during the preliminary phase of the project, when potassium permanganate solutions were being used instead of free chlorine. The negative effect of adding sodium chloride can be clearly seen in Figure 4.3. Previous experiments carried out with lower voltages and different transducing materials did not show this behaviour. In acidic solutions, both hypochlorous acid and potassium permanganate degrade due to the oxidation of chloride ions.^{186,187} Even though the pH of our solutions (slightly acidic due to the use of unbuffered ultrapure water) was not low enough to make this a favourable process, it

is possible that the use of 100 mV facilitates it. Further investigation is needed to understand the effect of sodium chloride. It is worth mentioning that the presence of sodium chloride seems to improve the reset of the devices (Figure 4.3b). In light of these results, it was decided to use plain ultrapure water for the experiments.

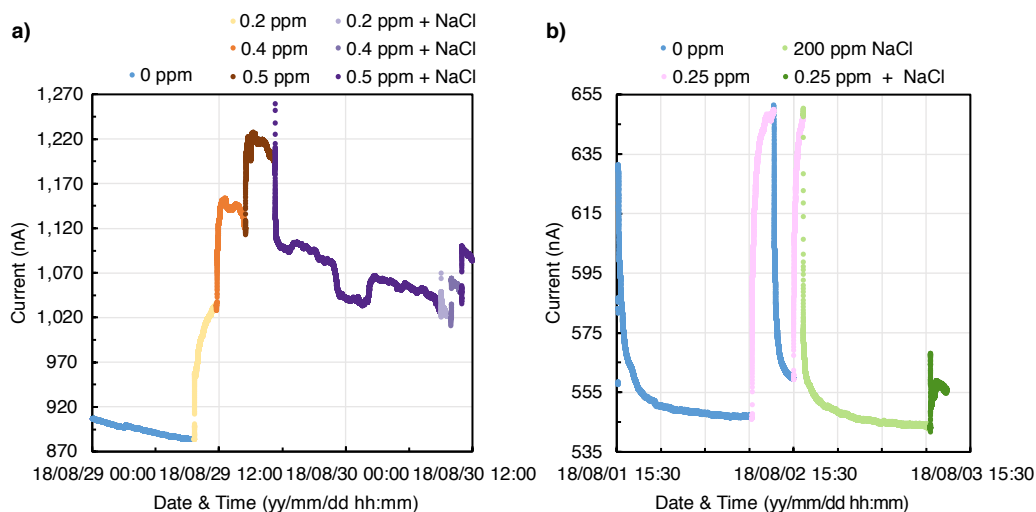


Figure 4.3. Raw data showcasing the negative effect of a 200 ppm NaCl background concentration on the performance of **a)** free chlorine sensors and **b)** permanganate sensors.

4.2.4. Determining the concentration of the solutions

Because free chlorine degrades over time, it is important to determine the concentration of the solutions before each experiment. This was done with the DPD colorimetric method. The Orion™ AC4P71 and AC2071 methods were used, which have a linear range of 0.02 – 2 ppm and 0.01 – 6 ppm respectively. The concentration of the sodium hypochlorite solution purchased from Sigma-Aldrich was too high, so a stock solution was prepared by diluting it. The actual concentration of the stock was unknown (the bottle gave it as a range), so it was further diluted to be approximately

1 ppm. The concentration of this solution was determined with the DPD method, which allowed us to calculate the real concentration of the stock. The solution was stored in a pretreated amber glass bottle, which minimizes degradation. Refrigerating the sample also helps to delay its decay. Even though the amount of free chlorine in the stock solution was now known, the concentration of every sample was verified before each experiment. It should be noted that the methods seemed to consistently underestimate low concentrations and overestimate high concentrations. It was observed that at low concentrations the DPD reagent did not completely dissolve, which could be introducing a systematic error. Nevertheless, the concentrations were overall in agreement with the values predicted after each dilution.

4.3. Performance at different concentration ranges

We were interested in studying the performance of the sensors in three concentration ranges based on different applications. Many households desire to remove chlorine from their tap water before consumption, which they achieve by using water filters. If these filters fail, small amounts of chlorine will leach into the water, so the sensors need to be able to detect very low levels of the analyte. Another potential application of the devices is the continuous monitoring of water quality, so they need to be capable of detecting fluctuations in a middle range of concentrations. Finally, the sensors might be used to quantify free chlorine in unknown samples. To do this, they must be able to work at higher concentrations. The range of

interest influenced the experimental design. The results are presented and discussed next.

4.3.1. Low range: detecting breaches in a chlorine filter

The sensors (two doped and two blank) were exposed to increasing concentrations of free chlorine in the range of 0.01 – 0.2 ppm for 30 minutes each. In order to evaluate the ability of the sensors to detect a sudden breach in a filter, they were reset between each concentration by running ultrapure water overnight. All devices gave a sharp signal as soon as they were exposed to free chlorine, even at the lowest concentration. The signal change was calculated by averaging a minute of data at the 25-minute mark and comparing it to the water baseline. The same curve fittings as in CHAPTER 3 were tested, and the response of the devices was found to vary with the concentration. The curve fittings are shown in Figure 4.4a, and their parameters are gathered in Table 4.1. According to the coefficients of determination, all models work at describing the data, but the Langmuir adsorption isotherm shows the best fit overall. The difference in fit quality is more noticeable in the case of the doped sensors. However, there is not enough evidence to make further claims. Finally, as it can be seen in Figure 4.4b, the response of the sensors to 0.01 ppm was sharp and big enough to suggest that the detection of even lower concentrations might be possible. The limit of detection was estimated by calculating 3 times the noise and it was found to be around 1 – 2 ppb.

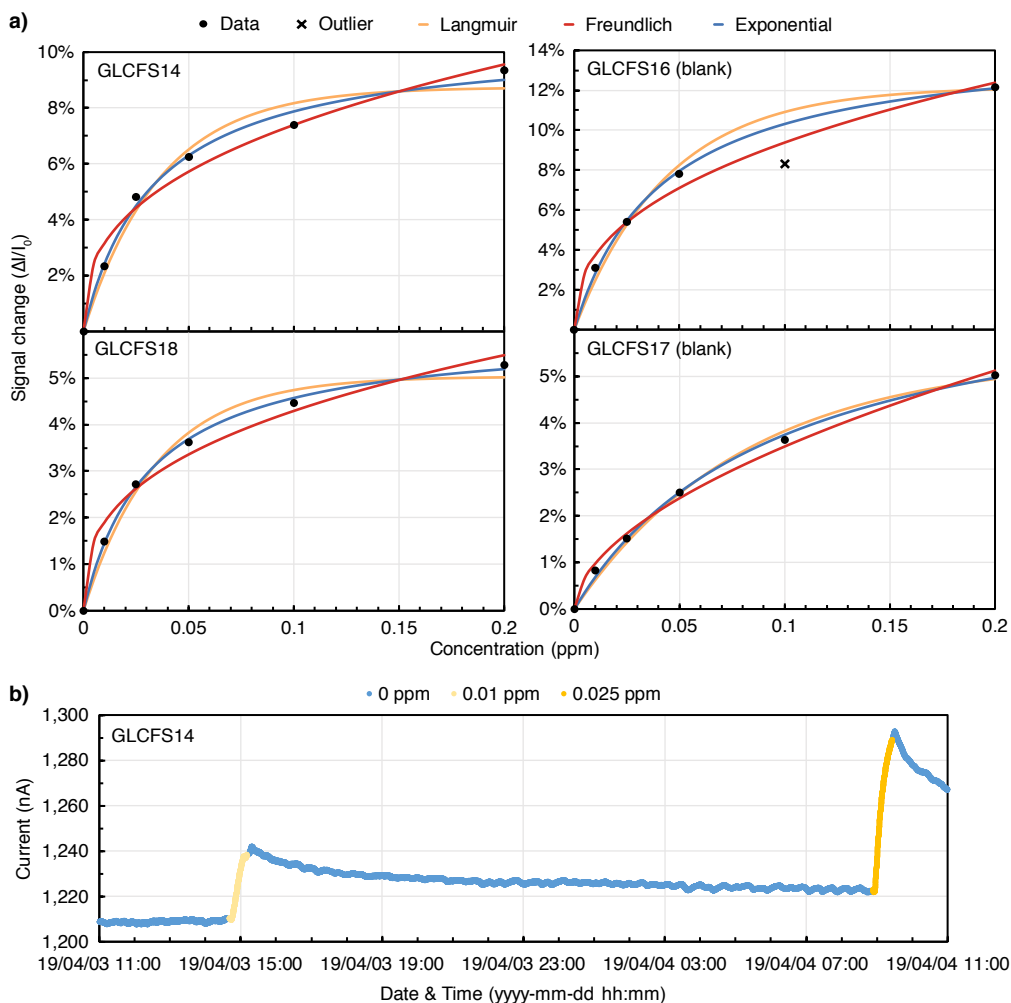


Figure 4.4. a) Curve fittings obtained for the low range concentrations (0.01 – 0.2 ppm). The curves shown are a Langmuir adsorption isotherm, a Freundlich adsorption isotherm, and an exponential decay. b) Raw data showing the response of sensor GLCFS14 to the lowest concentrations.

Table 4.1. Parameters of the curves that describe the response of the sensors to the low range concentrations.

Sensor	Langmuir			Freundlich			Exponential		
	a (L/mg)	b	R ²	a (L/mg)	b	R ²	a (L/mg)	b	R ²
GLCFS14	29.815	0.105	0.992	0.174	2.698	0.981	27.301	0.087	0.976
GLCFS18	31.806	0.060	0.998	0.097	2.817	0.983	28.514	0.050	0.986
GLCFS16	23.808	0.146	0.999	0.236	2.496	0.989	22.646	0.122	0.993
GLCFS18	10.278	0.074	0.998	0.125	1.809	0.996	12.308	0.054	0.994

4.3.2. Middle range: detecting fluctuations in the concentration

In order to study the ability of the sensors to detect fluctuations in the free chlorine levels, they were exposed to multiple cycles of increasing and decreasing concentrations. The raw data for two doped and two blank sensors is shown in Figure 4.5. Even though the response does not match perfectly for equal concentrations, it was within a small margin of error. Some sources of error might be the difficulty of higher concentrations to reset the devices and variability in the solution making process (all solutions were made fresh before running them through the sensors). These are things that can be optimized. For instance, it was determined that the solutions were stable for at least a day provided that pretreated glassware was used, so the same batch of solutions could be used for the entire experiment in order to avoid variability. No significant differences were detected between the performance of the doped sensors and the blank sensors. Overall, the devices were capable of detecting fluctuations in the concentration of free chlorine.

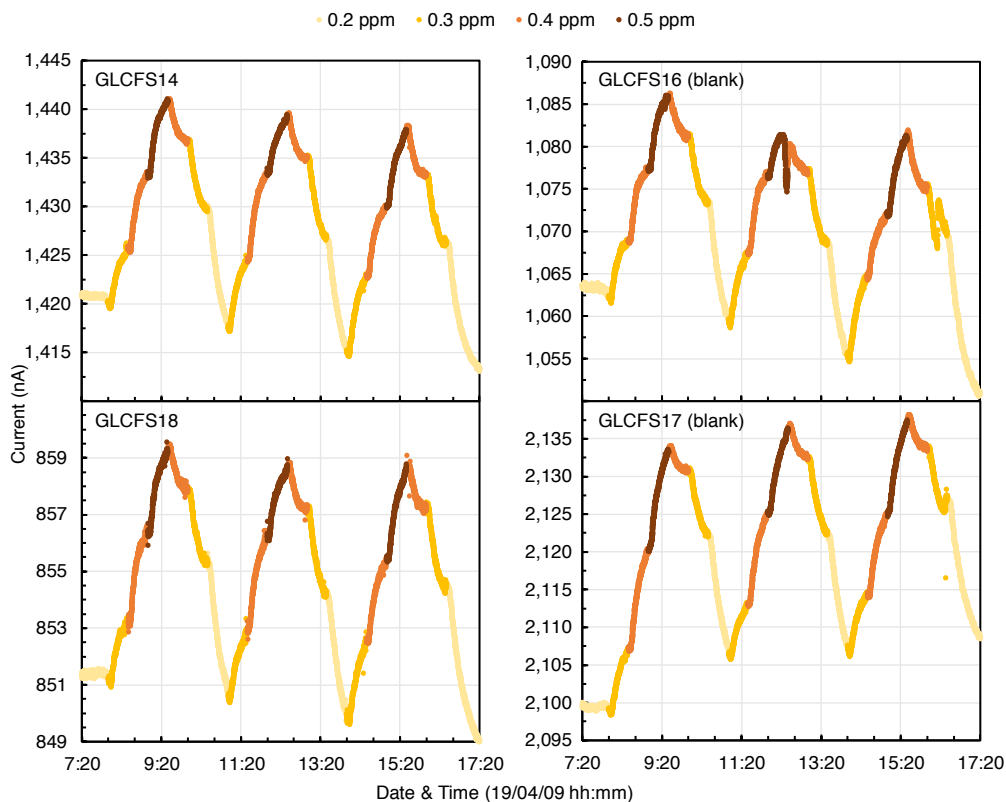


Figure 4.5. Detection of fluctuations in free chlorine concentration (0.2 – 0.5 ppm).

4.3.3. High range: quantifying free chlorine in unknown samples

The sensors were exposed to increasing concentrations of free chlorine in order to get calibration curves. The amount of free chlorine was increased until the response of the devices saturated. Each solution was run for 40 minutes, with no resetting in between. After saturation, the sensors were reset by running water for at least a day. The process was repeated until three calibration curves were obtained for each device. The signal change was calculated by averaging one minute of data at the 40-minute mark and comparing it to the water baseline. The curve fittings tested were a Langmuir adsorption isotherm, a Freundlich adsorption isotherm, and an

exponential decay. The curve parameters obtained with each model are shown in Table 4.2. They were all successful at describing the data, but the Langmuir adsorption isotherm and the exponential decay provided the best fits. The former was used for the discussion of the performance of the devices because it is a well-established surface chemistry model.¹⁶⁷ Even though it might not describe the sensing mechanism accurately, it goes through zero and shows an asymptotic behaviour for large concentrations. We theorize that those conditions should be fulfilled for the chemiresistive sensors.

Table 4.2. Calibration curve parameters for the three replicates performed at the high concentration range. GLCFS14 and GLCFS18 were functionalized with PCAT, while GLCFS16 and GLCFS17 were run as blanks.

Sensor	Langmuir			Freundlich			Exponential		
	a (L/mg)	b	R ²	a (L/mg)	b	R ²	a (L/mg)	b	R ²
GLCFS14	3.378	0.256	1.000	0.202	2.613	0.994	3.416	0.201	0.999
	2.185	0.312	0.999	0.214	2.227	0.989	2.438	0.235	1.000
	1.232	0.299	0.995	0.169	1.631	0.986	1.729	0.199	0.997
GLCFS18	3.756	0.143	1.000	0.116	2.767	0.997	3.633	0.114	0.997
	3.053	0.184	0.999	0.139	2.652	0.991	3.029	0.145	0.999
	1.941	0.161	0.999	0.109	1.974	0.991	2.370	0.116	1.000
GLCFS16	3.962	0.327	1.000	0.268	2.860	0.996	3.769	0.262	0.998
	3.254	0.383	0.999	0.294	2.748	0.992	3.147	0.306	0.998
	1.696	0.354	0.999	0.228	1.861	0.992	2.156	0.249	1.000
GLCFS17	1.806	0.245	0.999	0.158	2.041	0.993	2.122	0.180	0.999
	1.838	0.303	1.000	0.196	2.057	0.994	2.145	0.223	0.999
	1.655	0.229	0.998	0.143	1.960	0.990	2.011	0.165	0.999

The three calibration curves obtained with each sensor are shown in Figure 4.6. Even though they show similar trends in all sensors, the curves do not overlap. This reproducibility issue might be related to the quality of the reset. This is something that needs to be optimized before attempting to quantify free chlorine in unknown samples, as the current setup will likely lead to unprecise results. The saturation point of the devices was found to be around 1 ppm. Higher concentrations of free chlorine do not lead to an increase in signal. For reasons that are still not well understood, after the sensors saturate the signal becomes noisier and tends to decay. The 1.2 ppm point had to be excluded from most of the curve fittings because it had a lower signal than the 1 ppm. The concentration of free chlorine commonly found in drinking water is within the working range of our devices, so they could potentially be used for continuous monitoring. The performance of the doped and blank sensors did not differ significantly.

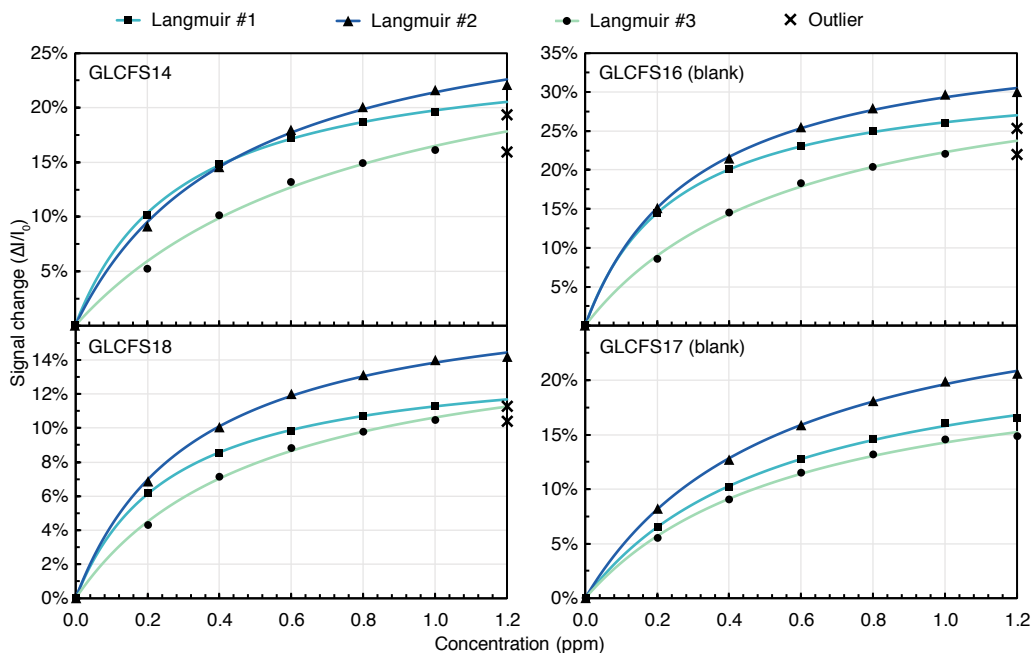


Figure 4.6. Three calibration curve replicates obtained with the same set of free chlorine sensors. Only the Langmuir adsorption isotherm curve fitting is shown.

4.4. Interferences

Before running real samples through the sensors, their response towards ions commonly present in drinking water must be studied. Thus, the effect of both anions and cations was tested. For the anionic interference experiment solutions containing 45 ppm of nitrate, 500 ppm of sulphate, and 0.03 ppm of phosphate were prepared. The concentrations were set based on water quality regulations.^{17,188} For the cationic interference study solutions containing 12 ppm of sodium, 10 ppm of potassium, 40 ppm of calcium, and 9 ppm of magnesium were prepared. These concentrations were chosen in order to mimic drinking water.^{160,189} The salts used to make the solutions had sodium or chloride as the counterions. The anionic and cationic experiments were run separately, but they followed the same

scheme. First, each individual ion was run through the sensors. Then, the devices were exposed to a solution containing all the ions. Finally, the mixture was spiked with 0.2 ppm of free chlorine in order to test the response in the presence of possibly interfering ions. The sensors were rinsed with water before each solution, and they were all run for 40 minutes.

The responses of both the doped and blank sensors have been plotted in Figure 4.7. Interestingly, the presence of chloride did not interfere with the free chlorine signal (see section 4.2.3). This might be due to the use of a lower concentration. Even though every ion gave a response, it is negligible in the presence of 0.2 ppm of free chlorine. It is worth mentioning that there was an inherent downwards drift in the water signal, so had the responses been corrected for it, they would have been even smaller. All the tested ions showed a negative signal, in agreement with the results discussed in CHAPTER 3. However, this is not consistent with previously reported results.^{36,38} We hypothesize that it could be a consequence of using a different material to fabricate the transducing films, but it requires further investigation. No significant differences were seen in the performance of the doped and blank sensors. Overall, the sensors were selective towards free chlorine in the presence of nitrate, sulphate, phosphate, sodium, potassium, magnesium, and calcium.

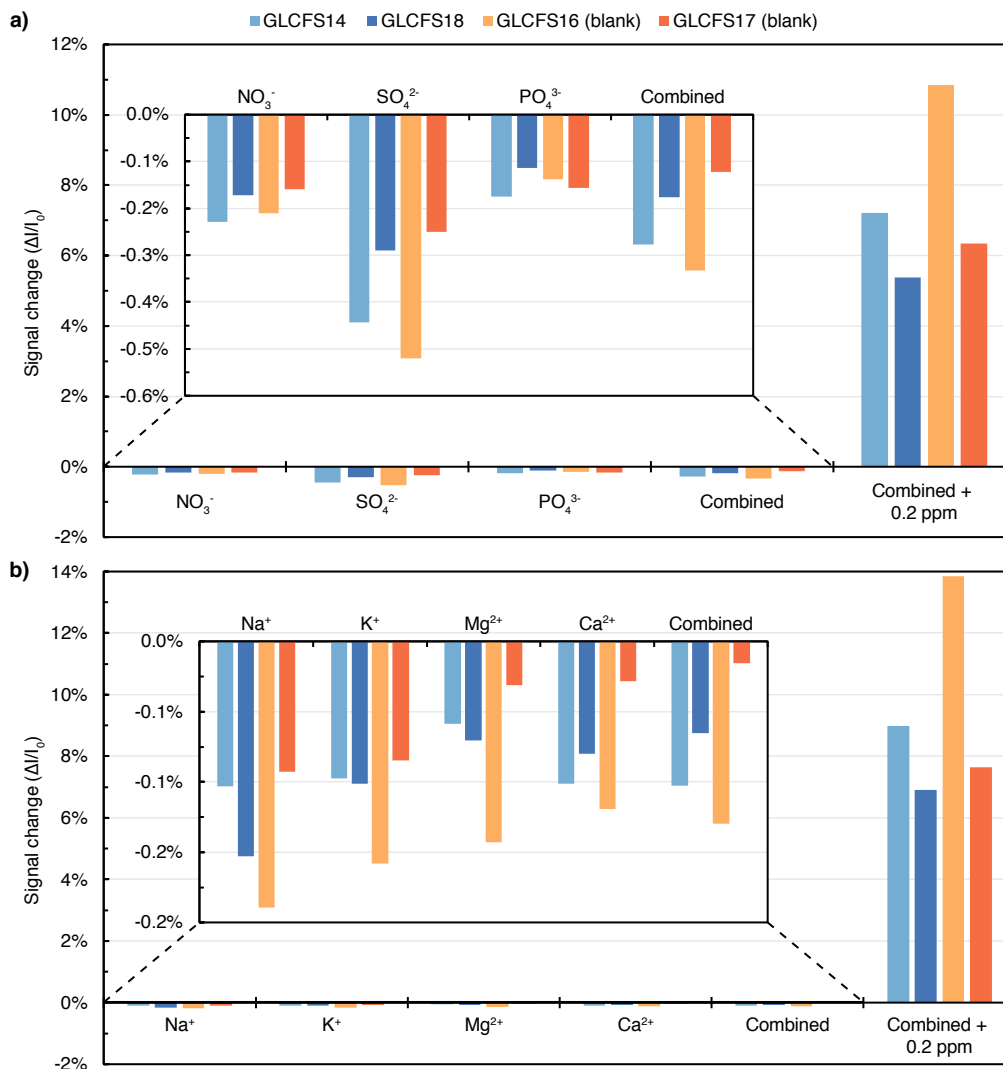


Figure 4.7. Interference study. Signal change of two doped sensors (blue) and two blank sensors (orange) when exposed to ions commonly found in drinking water. Inset: magnified portion of the graph. **a)** Response to anions. **b)** Response to cations.

4.5. Fouling resistance

The deterioration of sensor performance due to biofouling is a common problem.⁸⁵ To study the fouling resistance of the devices, the response of two doped and two blank sensors before and after exposure to humic acid was compared. They were first exposed to 0.2 ppm of free chlorine for 40

minutes in order to get the “before” response. Then, they were rinsed with ultrapure water for 1.5 hours before exposing them to 2 ppm of humic acid for 2.5 hours. Finally, they were rinsed with ultrapure water for 1.5 hours, followed by 40 minutes of 0.2 ppm of free chlorine in order to get the “after” response. The effect of the humic acid in the performance of the sensors is shown in Figure 4.8a. There is a response loss of at least 30% after humic acid is run through the sensors. Even though this could be a consequence of biofouling, poor resetting could be contributing as well. Further testing is required in order to determine what factor is the main cause for the deterioration of the signal. Surprisingly, the blank sensors showed slightly better fouling resistance. However, the difference is so minimal that no claims can be made until more experiments are run.

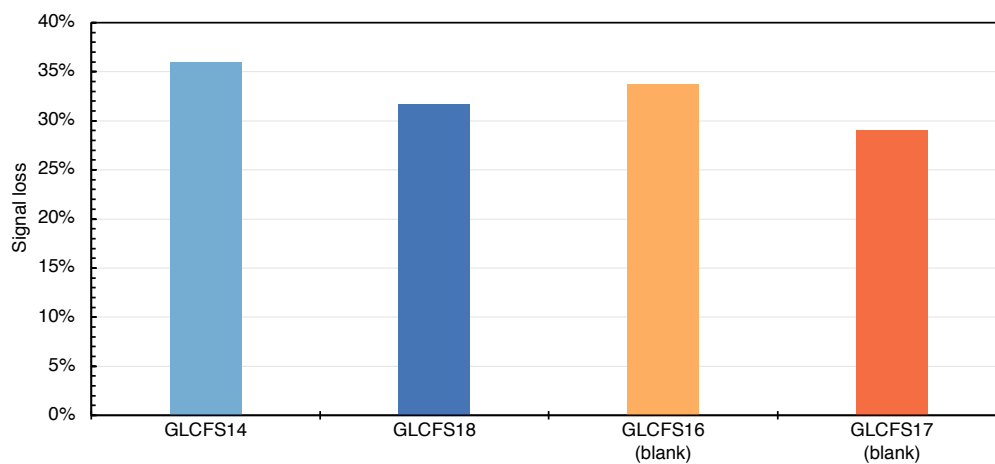


Figure 4.8. Signal loss due to exposure to 2 ppm of humic acid. The effect was studied on two doped sensors (blue) and two blank sensors (orange).

4.6. Summary

GLC was used to fabricate the transducing film of chemiresistive sensors and their performance measuring free chlorine in drinking water was studied. The ability of the devices to monitor free chlorine in three different concentration ranges was demonstrated. The sensors responded to both increases and decreases in free chlorine concentration, and they could be reset by running ultrapure water for long periods of time. However, the reproducibility of the data might improve by optimizing the resetting procedure. The sensors did not suffer from interferences in the presence of ions commonly found in drinking water. However, they might be prone to biofouling by humic acid. The performance of the doped and blank devices did not differ greatly, but this could be due to following an unoptimized PCAT deposition protocol. The same set of sensors was used for most of the experiments discussed in this chapter, demonstrating outstanding durability. Overall, we have shown that the sensors could potentially be used for the continuous monitoring of free chlorine in drinking water.

CHAPTER 5 — CONCLUSION

The aim of this final chapter is to summarize the main findings of the thesis and outline suggestions for future work. A brief commentary about some of the lessons learnt as a Chemistry graduate student is also included.

5.1. Summary

In CHAPTER 1 the need for water quality monitoring technology was introduced. Nanocarbon based chemiresistive sensors were presented as a possible solution to the problem and the motivation behind detecting copper ions and free chlorine was explained. The design, optimization, and fabrication of different types of sensors was described in CHAPTER 2. A method to obtain few layer graphene suspensions without the need for toxic solvents or expensive instrumentation was adapted from the literature, and it was used to produce transducing films. Raman spectroscopy was used to characterize the films. The stability of the analyte solutions was studied too. The pH of unbuffered ultrapure water was found to be stable after quickly equilibrating with carbon dioxide in air. The concentration of free chlorine solutions remained stable in the experimental timescale provided that properly pretreated glassware is used.

CHAPTER 3 focused on copper ion sensors. The use of FLG dip sensors was demonstrated for the first time. The importance of having a big enough

sample to ensure a representative measurement was shown. The addition of sodium chloride and sodium bicarbonate to control the ionic strength and pH of the solutions was studied. Using 200 ppm of NaCl and 42 ppm of NaHCO₃ was found to be optimal. The films were functionalized with 2,3-diaminophenazine, and the response of the sensors was found to be related to the concentration of copper ions, with a Langmuir adsorption isotherm describing the data best. Thicker FLG films were found to saturate at higher concentrations. The sensors were reproducibly reset multiple times in a row by exposing them to an acidified water solution. The sensing and resetting mechanisms were explained through XPS analysis. Even though the devices struggled with selectivity and testing on real water remains to be done, this chapter was overall a success as this is the first time that FLG suspensions have been produced and used to make chemiresistive sensors in the group. It also shows that chemiresistors can be used to detect ions in water samples.

CHAPTER 4 revolved around the results obtained with the free chlorine sensors. The transducing film was produced with GLC, and a flow sensor geometry was adopted. The durability of the devices was greatly improved, which had been a problem in the past. The films were functionalized with PCAT, but no significant differences were found in the performance of the doped and blank sensors. It was demonstrated that the devices can be used in three different concentrations ranges, which allows for the detection of breaches in chlorine filters, the detection of fluctuations in concentration,

and the quantification of free chlorine in unknown samples. In all cases, a Langmuir adsorption isotherm seemed to fit the data best. The devices were selective in the presence of ions commonly found in drinking water, and the problems with solution stability that had hindered free chlorine experiments in the past were overcome by using pretreated glassware.

5.2. Lessons learnt as a Chemistry graduate student

There are many things that I have learnt through this experience, many of which I wish someone had told me earlier. I have realized how incredibly important it is to have a well-defined action plan. I often did not and found myself conducting experiments that did not fit in the overall story. This can be exhausting, so every so often it is good to take a step back, reassess, and go back to the lab with a better view of the big picture. It is not necessary to be in the lab 24/7 as long as you are proactive and use time efficiently. I wish someone had warned me about how often things would not go as planned, and that they had reminded me that most times it is not the fault of the scientist. Not realizing that made me fear failure, and I would often be hesitant about starting an experiment simply because I thought it would not work. You will never regret spending a few hours each week organizing and analyzing your data, it is worth it down the road. I kept an updated electronic document with all my experimental designs, results, and conclusions and have been grateful every day that I have spent writing this thesis. As easy as it is to spend time working on urgent things, remember to focus on the important things. Finally, I cannot emphasize enough how

important it can be to socialize with other students from the department. For the longest time I did not do it, foolishly thinking that it was time better spent running experiments. Although our research topics might be totally different, we are all Chemistry graduate students and we face very similar struggles. There is no manual on how to do research, and you never know who will be able to offer useful advice.

5.3. Future work

Much of the hardship with the copper project was related to stability and reproducibility issues. In multiple occasions parts of the FLG films fell off the glass slides in the middle of an experiment. This really hindered progress, so work should be put into producing stable films. Further characterization of the FLG suspensions is also encouraged, as the number of layers and defects is unknown, which could impact sensor performance. A different fraction of the centrifugation might be better. An alternative to PDMS should also be found, as it clearly interferes with the concentration of the analytes. Finally, ways to scale up the fabrication should be explored.

The deposition of DAP onto the transducing film was never optimized, which could be playing a major role into the reproducibility issues. If the methanolic solution is too concentrated, the ligand could be aggregating through self-assembly. Thus, the concentration needs to be optimized in order to get a homogeneous monolayer on the surface of the FLG film. This could also improve the selectivity of the devices. The sensing and resetting

mechanism would be better understood if two extra sensors could be sent for XPS analysis: a blank after resetting in order to see whether or not the copper comes off the films, and a doped sensor that has been reset and exposed to copper again in order to see if the nitrogen signal reappears. Finally, the ability of the sensors to quantify copper in real water samples needs to be assessed.

In the case of the free chlorine sensors, the deposition of the PCAT needs to be optimized as well. The lack of optimization might explain why the results obtained with the doped and blank sensors were not significantly different. The resetting of the devices should be improved, which might minimize the reproducibility issues. The performance of the sensors on real water samples should also be tested. However, it is important to avoid the use of tap water containing chloramines. Finally, more experiments should be done in order to fully understand the effect of humic acid.

One of the main takeaways of this thesis is that any ion might be monitored with a chemiresistive sensor provided that the right molecule is used to functionalize the films. Thus, an important line of action moving forward should be developing sensors for other contaminants of concern, such as lead and arsenic. This would open the door to building sensor arrays. Lastly, spending more time trying to understand the sensing mechanism is encouraged. Complementary techniques (e.g. UV-Vis, AFM, Raman, NMR...) should be exploited in order to collect more evidence and have a stronger case.

REFERENCES

1. United Nations General Assembly. A/RES/64/292. The Human Right to Water and Sanitation. (2010).
2. World Health Organization (WHO) & United Nations Children's Fund (UNICEF). *Progress on Drinking Water, Sanitation and Hygiene: 2017 Update and SDG Baseline*. (WHO and UNICEF, 2017).
3. Prüss-Ustün, A. *et al.* Burden of disease from inadequate water, sanitation and hygiene in low- and middle-income settings: a retrospective analysis of data from 145 countries. *Trop. Med. Int. Heal.* **19**, 894–905 (2014).
4. World Health Organization. *Water for Health: Taking charge*. (2001).
5. World Health Organization. *Guidelines for drinking water-quality: Fourth edition incorporating first addendum, 4th ed + 1st add.* (World Health Organization, 2017).
6. Ministry of the Environment. Practices for the Collection And Handling of Drinking Water Samples. 37 (2009).
7. World Health Organization. *Guidelines for drinking-water quality. Vol. 3. Surveillance and control of community supplies*. (World Health Organization, 1997).
8. Office of the High Commissioner for Human Rights. The Right to Water: Fact Sheet No. 35. (2010).
9. Salvadori, M. I. *et al.* Factors that led to the Walkerton tragedy. *Kidney Int.* **75**, S33–S34 (2009).
10. Hrudey, S. E., Payment, P., Huck, P. M., Gillham, R. W. & Hrudey, E. J. A fatal waterborne disease epidemic in Walkerton, Ontario: comparison with other waterborne outbreaks in the developed world. *Water Sci. Technol.* **47**, 7–14 (2003).
11. Masten, S. J., Davies, S. H. & McElmurry, S. P. Flint Water Crisis: What Happened and Why? *J. Am. Water Works Assoc.* **108**, 22–34 (2016).
12. Pieper, K. J., Tang, M. & Edwards, M. A. Flint Water Crisis Caused By Interrupted Corrosion Control: Investigating “Ground Zero” Home. *Environ. Sci. Technol.* **51**, 2007–2014 (2017).

13. Hanna-Attisha, M., LaChance, J., Sadler, R. C. & Champney Schnepf, A. Elevated Blood Lead Levels in Children Associated With the Flint Drinking Water Crisis: A Spatial Analysis of Risk and Public Health Response. *Am. J. Public Health* **106**, 283–290 (2016).
14. Torrice, M. How lead ended up in Flint's tap water. *Chem. Eng. News* **94**, 26–29 (2016).
15. City of Hamilton. Corrosion Control. *Water & Sewer* (2018). Available at: <https://www.hamilton.ca/home-property-and-development/water-sewer/corrosion-control>. (Accessed: 20th June 2019)
16. Boyd, C. E. *Water Quality: An Introduction*. (Springer, 2015). doi:10.1007/978-3-319-17446-4
17. Health Canada. *Guidelines for Canadian Drinking Water Quality - Summary Table*. (Water and Air Quality Bureau, Healthy Environments and Consumer Safety Branch, 2017).
18. Council of the European Union. On the quality of water intended for human consumption. *Off. J. Eur. Communities* (1998).
19. Water Air and Climate Change Bureau & Healthy Environments and Consumer Safety Branch. Guidance for Issuing and Rescinding Drinking Water Avoidance Advisories in Emergency. (2009).
20. Ward, P. S. When is a standard not a standard? *Water Pollut. Control Fed.* **17**, 912–915 (1975).
21. HACH. Water Analysis Handbook. Available at: <https://www.hach.com/wah>. (Accessed: 24th June 2019)
22. International Organization for Standardization. ISO/TC 147 - Water quality. *Standards Catalogue* Available at: <https://www.iso.org/committee/52834/x/catalogue/>. (Accessed: 24th June 2019)
23. US Environmental Protection Agency. § 136. Guidelines establishing test procedures for the analysis of pollutants. *Code Fed. Regul.* **40**, (2016).
24. Ministry of the Environment. Protocol of Accepted Drinking Water Testing Methods. 58 (2010).
25. Mohtasebi, A. & Kruse, P. Chemical sensors based on surface charge transfer. *Phys. Sci. Rev.* **3**, 20170133 (2018).

26. Xinxia, C., Anna, S., Li, C. & Xiulan, H. A novel odour sensor coated with a lipid membrane. *Sensors Actuators B Chem.* **12**, 15–18 (1993).
27. Wohltjen, H., Barger, W. R., Snow, A. W. & Jarvis, N. L. A vapor-sensitive chemiresistor fabricated with planar microelectrodes and a Langmuir-Blodgett organic semiconductor film. *IEEE Trans. Electron Devices* **32**, 1170–1174 (1985).
28. Schedin, F. *et al.* Detection of individual gas molecules adsorbed on graphene. *Nat. Mater.* **6**, 652–655 (2007).
29. Yoon, H. J. *et al.* Carbon dioxide gas sensor using a graphene sheet. *Sensors Actuators B Chem.* **157**, 310–313 (2011).
30. Ko, G. *et al.* Graphene-based nitrogen dioxide gas sensors. *Curr. Appl. Phys.* **10**, 1002–1004 (2010).
31. Chen, G., Paronyan, T. M. & Harutyunyan, A. R. Sub-ppt gas detection with pristine graphene. *Appl. Phys. Lett.* **101**, 053119 (2012).
32. Cooper, J. S. *et al.* Performance of graphene, carbon nanotube, and gold nanoparticle chemiresistor sensors for the detection of petroleum hydrocarbons in water. *J. Nanoparticle Res.* **16**, 2173 (2014).
33. Myers, M. *et al.* Functionalized graphene as an aqueous phase chemiresistor sensing material. *Sensors Actuators B Chem.* **155**, 154–158 (2011).
34. Lei, N., Li, P., Xue, W. & Xu, J. Simple graphene chemiresistors as pH sensors: fabrication and characterization. *Meas. Sci. Technol.* **22**, 107002 (2011).
35. Raguse, B., Chow, E., Barton, C. S. & Wieczorek, L. Gold Nanoparticle Chemiresistor Sensors: Direct Sensing of Organics in Aqueous Electrolyte Solution. *Am. Chem. Soc. Anal. Chem.* **16**, 7333 (2004).
36. Hoque, E., Hsu, L. H. H., Aryasomayajula, A., Selvaganapathy, P. R. & Kruse, P. Pencil-Drawn Chemiresistive Sensor for Free Chlorine in Water. *IEEE Sensors Lett.* **1**, 4500504 (2017).
37. Hsu, L. H. H., Hoque, E., Kruse, P. & Ravi Selvaganapathy, P. A carbon nanotube based resettable sensor for measuring free chlorine in drinking water. *Appl. Phys. Lett.* **106**, 063102 (2015).
38. Mohtasebi, A., Broomfield, A. D., Chowdhury, T., Selvaganapathy, P. R. & Kruse, P. Reagent-Free Quantification of Aqueous Free Chlorine via Electrical Readout of Colorimetrically Functionalized Pencil

- Lines. *ACS Appl. Mater. Interfaces* **9**, 20748–20761 (2017).
39. Murphy, J. Anion Detection Utilizing Graphite Based Chemiresistive sensors. (McMaster University, 2018).
 40. Zubiarrain Laserna, A. Aqueous copper(II) ion chemiresistive sensors. (McMaster University, 2017).
 41. Benfield-Dexter, A. Optimization and characterization of chemiresistive sensors for the detection of copper(II) ions in drinking water. (McMaster University, 2018).
 42. Sareen, D., Kaur, P. & Singh, K. Strategies in detection of metal ions using dyes. *Coord. Chem. Rev.* **265**, 125–154 (2014).
 43. Miyaji, H. & Sessler, J. L. Off-the-Shelf Colorimetric Anion Sensors. *Angew. Chemie Int. Ed.* **40**, 154–157 (2001).
 44. Su, M., Zheng, B. & Liu, J. A scalable CVD method for the synthesis of single-walled carbon nanotubes with high catalyst productivity. *Chem. Phys. Lett.* **322**, 321–326 (2000).
 45. Dai, H. Carbon Nanotubes: Synthesis, Integration, and Properties. *Acc. Chem. Res.* **35**, 1035–1044 (2002).
 46. Colomer, J.-F. *et al.* Large-scale synthesis of single-wall carbon nanotubes by catalytic chemical vapor deposition (CCVD) method. *Chem. Phys. Lett.* **317**, 83–89 (2000).
 47. Cheng, H. M. *et al.* Large-scale and low-cost synthesis of single-walled carbon nanotubes by the catalytic pyrolysis of hydrocarbons. *Appl. Phys. Lett.* **72**, 3282–3284 (1998).
 48. Gorski, C. A. *et al.* Redox Properties of Structural Fe in Clay Minerals. 1. Electrochemical Quantification of Electron-Donating and -Accepting Capacities of Smectites. *Environ. Sci. Technol.* **46**, 9360–9368 (2012).
 49. Sousa, M. C. & Buchanan, J. W. Observational models of graphite pencil materials. *Comput. Graph. Forum* **19**, 27–49 (2000).
 50. Meier, L. P. & Kahr, G. Determination of the Cation Exchange Capacity (CEC) of Clay Minerals Using the Complexes of Copper(II) Ion with Triethylenetetramine and Tetraethylenepentamine. *Clays Clay Miner.* **47**, 386–388 (1999).
 51. Farkas, E., Elizabeth Anderson, M., Chen, Z. & Rinzler, A. G. Length

- sorting cut single wall carbon nanotubes by high performance liquid chromatography. *Chem. Phys. Lett.* **363**, 111–116 (2002).
52. Ghosh, S., Bachilo, S. M. & Weisman, R. B. Advanced sorting of single-walled carbon nanotubes by nonlinear density-gradient ultracentrifugation. *Nat. Nanotechnol.* **5**, 443–450 (2010).
53. Mourran, A. *et al.* Two Morphologies of Stable, Highly Ordered Assemblies of a Long-Chain-Substituted $[2 \times 2]$ -Grid-Type FeII Complex Adsorbed on HOPG. *Eur. J. Inorg. Chem.* **2005**, 2641–2647 (2005).
54. Henrion, O. & Jaegermann, W. Surface redox reactions of cobaltocene adsorbed onto pyrolytic graphite (HOPG). *Surf. Sci.* **387**, L1073–L1078 (1997).
55. Gao, A. *et al.* Two-Dimensional Self-Assembly of a Porphyrin-Polypyridyl Ruthenium(II) Hybrid on HOPG Surface through Metal-Ligand Interactions. *ChemPhysChem* **11**, 1951–1955 (2010).
56. Geim, A. K. & MacDonald, A. H. Graphene: Exploring carbon flatland. *Phys. Today* **60**, 35–41 (2007).
57. Partoens, B. & Peeters, F. M. From graphene to graphite: Electronic structure around the K point. *Phys. Rev. B - Condens. Matter Mater. Phys.* **74**, (2006).
58. Geim, A. K. Graphene: Status and Prospects. *Science* **324**, 1530–1534 (2009).
59. Khomyakov, P. A. *et al.* First-principles study of the interaction and charge transfer between graphene and metals. *Phys. Rev. B* **79**, 195425 (2009).
60. Chan, K. T., Neaton, J. B. & Cohen, M. L. First-principles study of metal adatom adsorption on graphene. *Phys. Rev. B* **77**, 235430 (2008).
61. Gierz, I., Riedl, C., Starke, U., Ast, C. R. & Kern, K. Atomic Hole Doping of Graphene. *Nano Lett.* **8**, 4603–4607 (2008).
62. Pinto, H., Jones, R., Goss, J. P. & Briddon, P. R. Unexpected change in the electronic properties of the Au-graphene interface caused by toluene. *Phys. Rev. B* **82**, 125407 (2010).
63. Georgakilas, V. *et al.* Functionalization of Graphene: Covalent and Non-Covalent Approaches, Derivatives and Applications. *Chem. Rev.* **112**, 6156–6214 (2012).

64. Dong, X. *et al.* Doping Single-Layer Graphene with Aromatic Molecules. *Small* **5**, 1422–1426 (2009).
65. Nigar, S., Zhou, Z., Wang, H. & Imtiaz, M. Modulating the electronic and magnetic properties of graphene. *RSC Adv.* **7**, 51546–51580 (2017).
66. Franklin, R. E. The structure of graphitic carbons. *Acta Crystallogr.* **4**, 253–261 (1951).
67. Lipson, H. & Stokes, A. R. The Structure of Graphite. *Proc. R. Soc. A Math. Phys. Eng. Sci.* **181**, 101–105 (1942).
68. Lui, C. H. *et al.* Imaging stacking order in few-layer graphene. *Nano Lett.* **11**, 164–169 (2011).
69. Stern, B. R. *et al.* Copper and Human Health: Biochemistry, Genetics, and Strategies for Modeling Dose-response Relationships. *J. Toxicol. Environ. Heal. Part B* **10**, 157–222 (2007).
70. Wang, Y. *et al.* The influence of soil heavy metals pollution on soil microbial biomass, enzyme activity, and community composition near a copper smelter. *Ecotoxicol. Environ. Saf.* **67**, 75–81 (2007).
71. World Health Organization. Copper in Drinking-water: Background document for development of WHO Guidelines for Drinking-water Quality. 23 (2004).
72. Health Canada. Guidelines for Canadian Drinking Water Quality: Guideline Technical Document - Copper. (1992).
73. Rushing, J. C. & Edwards, M. The role of temperature gradients in residential copper pipe corrosion. *Corros. Sci.* **46**, 1883–1894 (2004).
74. Federal-Provincial-Territorial Committee on Drinking Water. Copper in Drinking Water: Guideline Technical Document for public consultation. (2018).
75. Dudka, S. & Adriano, D. C. Environmental Impacts of Metal Ore Mining and Processing: A Review. *J. Environ. Qual.* **26**, 590–602 (1997).
76. Turner, A. Marine pollution from antifouling paint particles. *Mar. Pollut. Bull.* **60**, 159–171 (2010).
77. Hingston, J. A., Collins, C. D., Murphy, R. J. & Lester, J. N. Leaching of chromated copper arsenate wood preservatives: a review. *Environ. Pollut.* **111**, 53–66 (2001).

78. Yao, J. *et al.* Migration of Cu, Zn and Cr through municipal solid waste incinerator bottom ash layer in the simulated landfill. *Écol. Eng.* **102**, 577–582 (2017).
79. Olsen, S., Pessenda, L. C. R., Ružička, J. & Hansen, E. H. Combination of flow injection analysis with flame atomic-absorption spectrophotometry: determination of trace amounts of heavy metals in polluted seawater. *Analyst* **108**, 905–917 (1983).
80. Aceto, M. *et al.* Determination of metals in wine with atomic spectroscopy (flame-AAS, GF-AAS and ICP-AES); a review. *Food Addit. Contam.* **19**, 126–133 (2002).
81. Townsend, A. T. The accurate determination of the first row transition metals in water, urine, plant, tissue and rock samples by sector field ICP-MS. *J. Anal. At. Spectrom.* **15**, 307–314 (2000).
82. Avdeef, A., Zabronsky, J. & Stuting, H. H. Calibration of copper ion selective electrode response to pCu 19. *Anal. Chem.* **55**, 298–304 (1983).
83. HACH. Copper - Bicinchoninate Method 8506 and 8026. in *Water Analysis Handbook* (2017).
84. Lucia, M., Campos, A. M. & van den Berg, C. M. G. Determination of copper complexation in sea water by cathodic stripping voltammetry and ligand competition with salicylaldoxime. *Anal. Chim. Acta* **284**, 481–496 (1994).
85. Kruse, P. Review on water quality sensors. *J. Phys. D. Appl. Phys.* **51**, 203002 (2018).
86. Shan, Z. *et al.* Chloride accelerated Fenton chemistry for the ultrasensitive and selective colorimetric detection of copper. *Chem. Commun.* **52**, 2087–2090 (2016).
87. El-Zomrawy, A. A. Selective and sensitive spectrophotometric method to determine trace amounts of copper metal ions using Amaranth food dye. *Spectrochim. Acta Part A Mol. Biomol. Spectrosc.* **203**, 450–454 (2018).
88. Sareen, D., Kaur, P. & Singh, K. Strategies in detection of metal ions using dyes. *Coord. Chem. Rev.* **265**, 125–154 (2014).
89. Sasaki, Y., Minamiki, T., Tokito, S. & Minami, T. A molecular self-assembled colourimetric chemosensor array for simultaneous detection of metal ions in water. *Chem. Commun.* **53**, 6561–6564 (2017).

90. Wu, W. *et al.* Facile Synthesis of Fluorescent Conjugated Polyelectrolytes Using Polydentate Sulfonate as Highly Selective and Sensitive Copper(II) Sensors. *ACS Sensors* **2**, 1337–1344 (2017).
91. Chen, Y. & Rosenzweig, Z. Luminescent CdS Quantum Dots as Selective Ion Probes. *Anal. Chem.* **74**, 5132–5138 (2002).
92. Fan, C. *et al.* Silver Nanoclusters Encapsulated into Metal–Organic Frameworks with Enhanced Fluorescence and Specific Ion Accumulation toward the Microdot Array-Based Fluorimetric Analysis of Copper in Blood. *ACS Sensors* **3**, 441–450 (2018).
93. Gao, W. *et al.* Wearable Microsensor Array for Multiplexed Heavy Metal Monitoring of Body Fluids. *ACS Sensors* **1**, 866–874 (2016).
94. Wustoni, S. *et al.* Label-free detection of Cu(II) in a human serum sample by using a prion protein-immobilized FET sensor. *Analyst* **140**, 6485–6488 (2015).
95. Taillades, G. *et al.* ISE and ISFET microsensors based on a sensitive chalcogenide glass for copper ion detection in solution. *Sensors Actuators B Chem.* **59**, 123–127 (1999).
96. Kidgell, C. *et al.* *Salmonella typhi*, the causative agent of typhoid fever, is approximately 50,000 years old. *Infect. Genet. Evol.* **2**, 39–45 (2002).
97. Fields, B. S., Benson, R. F. & Besser, R. E. Legionella and Legionnaires' Disease: 25 Years of Investigation. *Clin. Microbiol. Rev.* **15**, 506–526 (2002).
98. Kaper, J. B., Nataro, J. P. & Mobley, H. L. T. Pathogenic Escherichia coli. *Nat. Rev. Microbiol.* **2**, 123–140 (2004).
99. Ramírez-Castillo, F. *et al.* Waterborne Pathogens: Detection Methods and Challenges. *Pathogens* **4**, 307–334 (2015).
100. LeChevallier, M. W. & Au, K.-K. *Water Treatment and Pathogen Control: Process Efficiency in Achieving Safe Drinking Water*. (World Health Organization, 2004).
101. Venkobachar, C., Iyengar, L. & Prabhakara Rao, A. V. S. Mechanism of disinfection: Effect of chlorine on cell membrane functions. *Water Res.* **11**, 727–729 (1977).
102. ASTM International. D1253 - 14: Standard test method for chlorine in water. in *Annual Book of ASTM Standards* (ASTM International, 2019).

doi:10.1520/D1253-14

103. Rice, E. W., Baird, R. B. & Eaton, A. D. 4500-Cl Chlorine (Residual). in *Standard Methods for the Examination of Water and Wastewater* (eds. Rice, E. W., Baird, R. B. & Eaton, A. D.) 61–74 (American Public Health Association, American Water Works Association, Water Environment Federation, 2017). doi:10.2105/SMWW.2882.078
104. International Organization for Standardization. 13.060.50 - Examination of water for chemical substances. *Standards Catalogue* Available at: <https://www.iso.org/ics/13.060.50/x/>. (Accessed: 26th June 2019)
105. Palin, A. T. *The Determination of Free and Combined Chlorine in Water by the Use of Diethyl-p-phenylene Diamine*. *American Water Works Association* **49**, (1957).
106. Moberg, L. & Karlberg, B. An improved N,N'-diethyl-p-phenylenediamine (DPD) method for the determination of free chlorine based on multiple wavelength detection. *Anal. Chim. Acta* **407**, 127–133 (2000).
107. Gordon, G., Sweetin, D. L., Smith, K. & Pacey, G. E. Improvements in the N,N-diethyl-p-phenylenediamine method for the determination of free and combined residual chlorine through the use of FIA. *Talanta* **38**, 145–149 (1991).
108. Pinkernell, U., Nowack, B., Gallard, H. & von Gunten, U. Methods for the photometric determination of reactive bromine and chlorine species with ABTS. *Water Res.* **34**, 4343–4350 (2000).
109. Zenki, M., Komatsubara, H. & Tōei, K. Determination of residual chlorine in tap water by flow-injection spectrophotometry. *Anal. Chim. Acta* **208**, 317–320 (1988).
110. Bauer, R. & Rupe, C. O. Use of syringaldazine in a photometric method for estimating 'free' chlorine in water. *Anal. Chem.* **43**, 421–425 (1971).
111. Hallaj, T., Amjadi, M., Manzoori, J. L. & Shokri, R. Chemiluminescence reaction of glucose-derived graphene quantum dots with hypochlorite, and its application to the determination of free chlorine. *Microchim. Acta* **182**, 789–796 (2015).
112. Marino, D. F. & Ingle, J. D. Determination of chlorine in water by luminol chemiluminescence. *Anal. Chem.* **53**, 455–458 (1981).

113. Ballesta Claver, J., Valencia Mirón, M. C. & Capitán-Vallvey, L. F. Determination of hypochlorite in water using a chemiluminescent test strip. *Anal. Chim. Acta* **522**, 267–273 (2004).
114. Fang, Q. *et al.* High photoluminescent TPA and the ratiometric sensor for free chlorine. *Sensors Actuators B Chem.* **244**, 771–776 (2017).
115. Dong, Y. *et al.* Graphene Quantum Dot as a Green and Facile Sensor for Free Chlorine in Drinking Water. *Anal. Chem.* **84**, 8378–8382 (2012).
116. Jović, M. *et al.* Electrochemical detection of free chlorine at inkjet printed silver electrodes. *J. Electroanal. Chem.* **756**, 171–178 (2015).
117. Seymour, E. H., Lawrence, N. S. & Compton, R. G. Reaction with N,N-Diethyl-p-phenylenediamine: A Procedure for the Sensitive Square-Wave Voltammetric Detection of Chlorine. *Electroanalysis* **15**, 689–694 (2003).
118. Salazar, P., Martín, M., García-García, F. J., González-Mora, J. L. & González-Elipe, A. R. A novel and improved surfactant-modified Prussian Blue electrode for amperometric detection of free chlorine in water. *Sensors Actuators B Chem.* **213**, 116–123 (2015).
119. Pan, S., Deen, M. J. & Ghosh, R. Low-Cost Graphite-Based Free Chlorine Sensor. *Anal. Chem.* **87**, 10734–10737 (2015).
120. van den Berg, A. *et al.* On-wafer fabricated free-chlorine sensor with ppb detection limit for drinking-water monitoring. *Sensors Actuators B Chem.* **13**, 396–399 (1993).
121. Ferraro, J. R., Nakamoto, K. & Brown, C. W. *Introductory Raman Spectroscopy*. (Academic Press, 2002).
122. Ferrari, A. C. & Basko, D. M. Supplementary Information for ‘Raman spectroscopy as a versatile tool for studying the properties of graphene’. *Nat. Nanotechnol.* **8**, 1–13 (2013).
123. Ferrari, A. C. & Basko, D. M. Raman spectroscopy as a versatile tool for studying the properties of graphene. *Nat. Nanotechnol.* **8**, 235–246 (2013).
124. Ferrari, A. C. *et al.* Raman Spectrum of Graphene and Graphene Layers. *Phys. Rev. Lett.* **97**, 187401 (2006).
125. Hao, Y. *et al.* Probing layer number and stacking order of few-layer graphene by Raman Spectroscopy. *Small* **6**, 195–200 (2010).

126. Dong, X., Shi, Y., Chen, P., Ling, Q. & Huang, W. Aromatic Molecules Doping in Single-Layer Graphene Probed by Raman Spectroscopy and Electrostatic Force Microscopy. *Jpn. J. Appl. Phys.* **49**, 01AH04 (2010).
127. Das, A. *et al.* Monitoring dopants by Raman scattering in an electrochemically top-gated graphene transistor. *Nat. Nanotechnol.* **3**, 210–215 (2008).
128. Iqbal, M. W., Singh, A. K., Iqbal, M. Z. & Eom, J. Raman fingerprint of doping due to metal adsorbates on graphene. *J. Phys. Condens. Matter* **24**, (2012).
129. Eckmann, A. *et al.* Probing the nature of defects in graphene by Raman spectroscopy. *Nano Lett.* **12**, 3925–3930 (2012).
130. Dresselhaus, M. S., Jorio, A., Souza Filho, A. G. & Saito, R. Defect characterization in graphene and carbon nanotubes using Raman spectroscopy. *Philos. Trans. R. Soc. A Math. Phys. Eng. Sci.* **368**, 5355–5377 (2010).
131. Cançado, L. G. *et al.* Quantifying defects in graphene via Raman spectroscopy at different excitation energies. *Nano Lett.* **11**, 3190–3196 (2011).
132. Khrapach, I. *et al.* Novel highly conductive and transparent graphene-based conductors. *Adv. Mater.* **24**, 2844–2849 (2012).
133. Watts, J. F. & Wolstenholme, J. *An Introduction to Surface Analysis by XPS and AES*. (Wiley, 2003). doi:10.1002/0470867930
134. Moulder, J. F., Stickle, W. F., Sobol, P. E. & Bomben, K. D. *Handbook of X-ray Photoelectron Spectroscopy*. (Perkin-Elmer, 1992).
135. Stephenson, R. J. X-ray fluorescence yields. *Phys. Rev.* **51**, 637–642 (1937).
136. Harp, D. L. Current Technology of Chlorine Analysis for Water and Wastewater. **30** (2002).
137. Capasso, A. *et al.* Ink-jet printing of graphene for flexible electronics: An environmentally-friendly approach. *Solid State Commun.* **224**, 53–63 (2015).
138. Georgakilas, V. *et al.* Organic functionalisation of graphenes. *Chem. Commun.* **46**, 1766–1768 (2010).

139. Hernandez, Y. *et al.* High-yield production of graphene by liquid-phase exfoliation of graphite. *Nat. Nanotechnol.* **3**, 563–568 (2008).
140. Lotya, M., King, P. J., Khan, U., De, S. & Coleman, J. N. High-Concentration, Surfactant-Stabilized Graphene Dispersions. *ACS Nano* **4**, 3155–3162 (2010).
141. Lotya, M. *et al.* Liquid Phase Production of Graphene by Exfoliation of Graphite in Surfactant/Water Solutions. *J. Am. Chem. Soc.* **131**, 3611–3620 (2009).
142. Yi, M., Shen, Z., Zhang, X. & Ma, S. Achieving concentrated graphene dispersions in water/acetone mixtures by the strategy of tailoring Hansen solubility parameters. *J. Phys. D: Appl. Phys.* **46**, 025301 (2013).
143. Halim, U. *et al.* A rational design of cosolvent exfoliation of layered materials by directly probing liquid–solid interaction. *Nat. Commun.* **4**, 2213 (2013).
144. Khan, U. *et al.* Size selection of dispersed, exfoliated graphene flakes by controlled centrifugation. *Carbon N. Y.* **50**, 470–475 (2012).
145. Bauld, R., Choi, D.-Y. W., Bazylewski, P., Divigalpitiya, R. & Fanchini, G. Thermo-optical characterization and thermal properties of graphene–polymer composites: a review. *J. Mater. Chem. C* **6**, 2901–2914 (2018).
146. Ezugwu, S., Ahmed, M. S., Bauld, R., Divigalpitiya, R. & Fanchini, G. Influence of the addition of graphene-like materials on the thermophysical properties of poly(3,4-ethylenedioxythiophene):poly(styrenesulfonate) thin film nanocomposites. *Thin Solid Films* **534**, 520–528 (2013).
147. Lee, J. N., Park, C. & Whitesides, G. M. Solvent Compatibility of Poly(dimethylsiloxane)-Based Microfluidic Devices. *Anal. Chem.* **75**, 6544–6554 (2003).
148. Mark, J. E. *Polymer Data Handbook*. (Oxford University Press, 1999).
149. Fawcett, A. S., So, H. Y. & Brook, M. A. Silicone foams stabilized by surfactants generated in situ from allyl-functionalized PEG. *Soft Matter* **6**, 1229 (2010).
150. Udhayakumari, D., Velmathi, S., Sung, Y.-M. & Wu, S.-P. Highly fluorescent probe for copper (II) ion based on commercially available compounds and live cell imaging. *Sensors Actuators B Chem.* **198**, 285–293 (2014).

151. Franssila, S. *Introduction to Microfabrication*. (John Wiley & Sons, Ltd, 2010). doi:10.1002/9781119990413
152. Alva, A. K., Sumner, M. E. & Miller, W. P. Relationship between ionic strength and electrical conductivity for soil solutions. *Soil Sci.* **152**, 239–242 (1991).
153. Kim, D. R., Lee, C. H. & Zheng, X. Probing Flow Velocity with Silicon Nanowire Sensors. *Nano Lett.* **9**, 1984–1988 (2009).
154. Stern, E. *et al.* Importance of the Debye Screening Length on Nanowire Field Effect Transistor Sensors. *Nano Lett.* **7**, 3405–3409 (2007).
155. Pennathur, S. & Santiago, J. G. Electrokinetic Transport in Nanochannels. 1. Theory. *Anal. Chem.* **77**, 6772–6781 (2005).
156. Heller, I. *et al.* Influence of Electrolyte Composition on Liquid-Gated Carbon Nanotube and Graphene Transistors. *J. Am. Chem. Soc.* **132**, 17149–17156 (2010).
157. Ang, P. K., Chen, W., Wee, A. T. S. & Loh, K. P. Solution-Gated Epitaxial Graphene as pH Sensor. *J. Am. Chem. Soc.* **130**, 14392–14393 (2008).
158. Shih, C.-J., Lin, S., Sharma, R., Strano, M. S. & Blankschtein, D. Understanding the pH-Dependent Behavior of Graphene Oxide Aqueous Solutions: A Comparative Experimental and Molecular Dynamics Simulation Study. *Langmuir* **28**, 235–241 (2012).
159. Clement, J. A., Schock, M. R. & Lytle, D. A. Effect of pH, DIC, Orthophosphate and Sulfate on Drinking Water Cuprosolvency. 107 (1995).
160. City of Toronto. Drinking Water Analysis Summary. 8–9 (2016).
161. Zuehlke, R. W. & Kester, D. R. Ultraviolet spectroscopic determination of the stability constants for copper carbonate and bicarbonate complexes up to the ionic strength of seawater. *Mar. Chem.* **13**, 203–226 (1983).
162. Arnold, R. B., Griffin, A. & Edwards, M. Controlling copper corrosion in new construction by organic matter removal. *J. Am. Water Works Assoc.* **104**, E310–E317 (2012).
163. Stiff, M. J. Copper/bicarbonate equilibria in solutions of bicarbonate ion at concentrations similar to those found in natural water. *Water*

Res. **5**, 171–176 (1971).

164. Dan, Y., Lu, Y., Kybert, N. J., Luo, Z. & Johnson, A. T. C. Intrinsic Response of Graphene Vapor Sensors. *Nano Lett.* **9**, 1472–1475 (2009).
165. Liu, S., Qin, X., Tian, J., Wang, L. & Sun, X. Photochemical preparation of fluorescent 2,3-diaminophenazine nanoparticles for sensitive and selective detection of Hg(II) ions. *Sensors Actuators B Chem.* **171–172**, 886–890 (2012).
166. Yong, B. R. *et al.* Highly selective and sensitive chemosensor based on 2,3-diaminophenazine hydrochloride for the detection of cyanide in pure water and its application in plant seed samples. *New J. Chem.* **42**, 14766–14771 (2018).
167. Langmuir, I. The adsorption of gases on plane surfaces of glass, mica and platinum. *J. Am. Chem. Soc.* **40**, 1361–1403 (1918).
168. Wu, C. H. Studies of the equilibrium and thermodynamics of the adsorption of Cu²⁺ onto as-produced and modified carbon nanotubes. *J. Colloid Interface Sci.* **311**, 338–346 (2007).
169. Liu, T. *et al.* Adsorption of methylene blue from aqueous solution by graphene. *Colloids Surfaces B Biointerfaces* **90**, 197–203 (2012).
170. Huang, Z.-H. *et al.* Adsorption of Lead(II) Ions from Aqueous Solution on Low-Temperature Exfoliated Graphene Nanosheets. *Langmuir* **27**, 7558–7562 (2011).
171. Awual, M. R., Hasan, M. M., Khaleque, M. A. & Sheikh, M. C. Treatment of copper(II) containing wastewater by a newly developed ligand based facial conjugate materials. *Chem. Eng. J.* **288**, 368–376 (2016).
172. Özcan, A. S., Erdem, B. & Özcan, A. Adsorption of Acid Blue 193 from aqueous solutions onto Na-bentonite and DTMA-bentonite. *J. Colloid Interface Sci.* **280**, 44–54 (2004).
173. Meena, A. K., Mishra, G. K., Rai, P. K., Rajagopal, C. & Nagar, P. N. Removal of heavy metal ions from aqueous solutions using carbon aerogel as an adsorbent. *J. Hazard. Mater.* **122**, 161–170 (2005).
174. Udhayakumari, D., Velmathi, S., Sung, Y. M. & Wu, S. P. Supporting Information - Highly fluorescent probe for copper (II) ion based on commercially available compounds and live cell imaging. *Sensors Actuators, B Chem.* **198**, 285–293 (2014).

175. Kao, L. T.-H., Hsu, H.-Y. & Gratzl, M. Reagentless pH-stat for Microliter Fluid Specimens. *Anal. Chem.* **80**, 4065–4069 (2008).
176. Hagedorn, R., Korlach, J. & Fuhr, G. Amperometric pH regulation - A flexible tool for rapid and precise temporal control over the pH of an electrolyte solution. *Electrophoresis* **19**, 180–186 (1998).
177. May, E. L. & Hillier, A. C. Rapid and Reversible Generation of a Microscale pH Gradient Using Surface Electric Fields. *Anal. Chem.* **77**, 6487–6493 (2005).
178. Morimoto, K., Toya, M., Fukuda, J. & Suzuki, H. Automatic Electrochemical Micro-pH-Stat for Biomicrosystems. *Anal. Chem.* **80**, 905–914 (2008).
179. Yang, F. *et al.* Controllable and eco-friendly synthesis of P-riched carbon quantum dots and its application for copper (II) ion sensing. *Appl. Surf. Sci.* **448**, 589–598 (2018).
180. Liu, Y., Zhao, Z. & Liu, Q. Preparation of Macrometallocycle and Selective Sensor for Copper Ion. *Sci. Rep.* **8**, 10943 (2018).
181. He, D., Wu, Y. & Xu, B. Q. Formation of 2,3-diaminophenazines and their self-assembly into nanobelts in aqueous medium. *Eur. Polym. J.* **43**, 3703–3709 (2007).
182. Tyagi, N. & Mathur, P. Iron(III) complexes of bis (benzimidazol-2-yl) methyl) thiophene-2,5-dicarboxamide: Synthesis, spectral and oxidation of o-phenylenediamine. *Spectrochim. Acta Part A Mol. Biomol. Spectrosc.* **96**, 759–767 (2012).
183. Tarcha, P. J., Chu, V. P. & Whittern, D. 2,3-diaminophenazine is the product from the horseradish peroxidase-catalyzed oxidation of o-phenylenediamine. *Anal. Biochem.* **165**, 230–233 (1987).
184. Biesinger, M. C. Advanced analysis of copper X-ray photoelectron spectra. *Surf. Interface Anal.* **49**, 1325–1334 (2017).
185. Biesinger, M. C. Cu LMM Peak Shapes (unpublished data). (2013). Available at: <http://www.xpsfitting.com/2012/04/cu-lmm-peak-shapes.html>. (Accessed: 15th July 2019)
186. Liu, K. J., Lester, H. & Peterson, N. C. Kinetics of the Permanganate Ion-Chloride Ion Reaction. *Inorg. Chem.* **5**, 2128–2130 (1966).
187. Lister, M. W. The decomposition of hypochlorous acid. *Can. J. Chem.* **30**, 879–889 (1952).

188. Canadian Council of Ministers of the Environment. *Canadian Environmental Quality Guidelines for the protection of Aquatic life - Phosphorus: Canadian Guidance Framework for the Management of Freshwater Systems. Canadian Environmental Quality Guidelines* (2004).
189. Azoulay, A., Garzon, P. & Eisenberg, M. J. Comparison of the Mineral Content of Tap Water and Bottled Waters. *J. Gen. Intern. Med.* **16**, 168–175 (2001).